SLAC-PUB-1878
January 1977

HIGH ENERGY PHOTOPRODUCTION: DIFFRACTIVE PROCESSES.*

D.W.G.S. Leith

Stanford Linear Accelerator Center
Stanford University, Stanford, California 94305

(to appear in Electromagnetic Interactions of Hadrons;
ed. A. Donnachie and G. Shaw, Plenum Publishing Corp.)

*Work supported by the Energy Research and Development Administration.

Contents

1 INTRODUCTION

The interaction of photons with nucleons in the energy range (2.0 - 30) GeV is observed to have many of the features of purely hadronic processes (i.e., πN, KN, pN collisions). More specifically, the total cross section is almost independent of energy, and the elastic scattering amplitude is mainly imaginary with a sharp t-dependence and almost no energy-dependence. These features find a natural explanation in the Vector Dominance Model of photoprocesses [Sakurai, 1960], in which the photon is pictured as a superposition of vector mesons which mediate the interaction of the photon with other hadrons. This implies that the photoproduction of vector mesons should be a favored process in γp reactions, and indeed it is observed to account for ~20% of the total cross section. The vector meson production process, the elastic γ-nucleon scattering (Compton scattering), and, through the optical theorem, the total γ-nucleon cross section—all display the characteristics of diffractive processes. But before continuing on a detailed review of the properties of these reactions, we first review the general phenomenological features of diffractive scattering.

Diffraction scattering can be discussed in terms of two pictures representing the t-channel or the s-channel points of view. In the t-channel (or exchange channel) picture the scattering is thought to proceed through the exchange of a singularity called the Pomeron. The basis for this picture is that of Regge exchange models. The s-channel (or direct channel) picture is seen in geometric or optical terms, where diffraction is generated by the absorption due to the competition among the many open inelastic channels. The target nucleon is seen as an absorbing disc (black or grey), with a specific radius and a specific opacity. From this viewpoint the diffractive reactions are merely the shadow of all the inelastic processes taking place. In both pictures, measurements of the energy and momentum-transfer dependence of the diffractive reactions provides information either on the Pomeron amplitude or on the size and opacity of the scatter.

Unfortunately beyond these two pictures we have no good theoretical description of the dynamics of diffractive processes and no basic understanding of the Pomeron singularity. Rather we have a set of phenomenological rules which allows us to identify what we mean by diffraction. Below we list the features which we expect from a diffractive process:

- energy independent cross sections, or at most increasing no faster than logarithms of the energy;
- sharp forward peak in the differential cross section, $\frac{d\sigma}{dt}$;
- mainly imaginary scattering amplitude;
- particle cross sections equal to antiparticle cross sections;
- factorization—i.e., the strength of a given subprocess (e.g., $a \rightarrow A$ or $b \rightarrow B$ in the reaction $ab \rightarrow AB$), is independent of which other particles are participating in the reaction;
- exchange process characterized by the quantum numbers of the vacuum (in the t-channel);
- change in parity in the scattering process follows the natural spin-parity series $(-1)^J$ or $P_0=P_i \cdot (-1)^J$ where ΔJ is the spin change and P_0, P_i are the intrinsic parities of the outgoing and incoming particles;

- the spin structure of the scattering process is dominantly s-channel helicity conserving (SCHC).

Photoproduction is a particularly interesting process for the study of diffractive reactions since, although it probes the same s-channel quantum numbers as πN scattering (i.e., S=0, B=1), the photon has both an isoscalar and an isovector component and has spin J=1. Therefore it brings an unusual variety to the study of the scattering processes. Furthermore, since polarized beams are relatively easy to prepare, vector meson photoproduction allows a detailed study of the spin characteristics of diffractive reactions. It has also been pointed out [Freund, 1967] that vector meson photoproduction, especially of the ϕ meson, should be a particularly suitable laboratory for study of diffraction since, in these reactions, the other exchanges (f, A_2, π --) are suppressed.

In the following sections we review the experimental results on high energy diffractive photoproduction. In the preparation of this review, I have extensively used the following excellent articles: [Wolf, 1971], [Moffeit, 1973] and [Silverman, 1975]. Data on the total cross section and on Compton scattering are presented and discussed in section 2, followed by a detailed look at vector meson photon-production of ρ, ω, and ϕ in section 3 and of higher mass states in section 4. The vector dominance model is discussed in section 5, together with a review of the measurements of the photovector meson coupling strengths. Section 6 contains some concluding remarks.

2 THE TOTAL PHOTON-NUCLEON CROSS SECTION, AND COMPTON SCATTERING

2.1 Total Cross Sections

The total photon-nucleon cross section has been measured from threshold up to ~30 GeV on both proton and neutron targets, using a variety of techniques. The most extensive measurements come from counter setups in tagged photon beams at NINA [Armstrong et al., 1972], DESY [Meyer et al., 1970], SLAC (UCSB) [Caldwell et al., 1973], and SERPUKOV (Lebedev) [Belousov et al., 1973]. Other measurements have been obtained with monochromatic photon beams at SLAC—both from e^+e^- annihilation in flight and from the back scattered laser beams—using hydrogen or deuterium filled bubble chambers as a detector [Ballam et al., 1972]. All the above measurements are in good agreement. Early measurements of the total γp cross section were also obtained from an analysis of extensive inelastic electron [Bloom et al., 1969] and muon scattering data [Lakin et al., 1971] where the one photon exchange approximation was used and the total cross section extracted by extrapolating the inelastic scattering to $q^2=0$. These measurements agree with the directly measured total cross section to within 10-20%. The energy dependence of the total cross section exhibits the well known resonant structure from N* formation at low energy, followed by a very slow, smooth falloff as the photon energy increases above 2 GeV. The photon cross sections show very similar behavior to the πN cross sections, but are much smaller. Figure 1 shows 1/200 of the average π^+p and π^-p cross sections compared to an average of the photon measurements. The similarity is striking.

At high energies, the forward Compton scattering amplitude and, via the optical theorem, the total cross section, are expected to be dominated by the following C=+1 exchanges— $\mathbb{P}$, f, A_2. The Pomeron (P) is expected to give rise to an energy independent contribution, while the meson exchange contributions (f, A_2) fall off like $E^{-1/2}$. This leads to an expected energy dependence of the form

$$\sigma(\gamma N) = a_0 + a_1 \cdot E^{-1/2} \tag{2.1}$$

where E is the photon energy. The isoscalar and isovector exchange contributions (T_0 and T_1 respectively) couple with opposite sign to the Compton scattering on protons and neutrons:

$$A_{\gamma p} = T_0 + T_1 \tag{2.2}$$

$$A_{\gamma n} = T_0 - T_1 \tag{2.3}$$

Identifying the isospin of the various exchange terms, we may write the cross section on protons and neutrons, as

$$\sigma^T(\gamma p) = C_{\mathbb{P}} + \left(C_f + C_{A_2}\right) \cdot E^{-1/2} \tag{2.4}$$

$$\sigma^T(\gamma n) = C_{\mathbb{P}} + \left(C_f - C_{A_2}\right) \cdot E^{-1/2} \tag{2.5}$$

Taking the sum and difference of the total cross sections then allows the isolation of the isoscalar and isovector exchange contributions.

$$\frac{1}{2}\left[\sigma^T(\gamma p) + \sigma^T(\gamma n)\right] = \mathrm{Im}\ T_0 = C_{\mathbb{P}} + C_f \cdot E^{-1/2} \tag{2.6}$$

$$\frac{1}{2}\left[\sigma^T(\gamma p) - \sigma^T(\gamma n)\right] = \mathrm{Im}\ T_1 = C_{A_2} \cdot E^{-1/2} \tag{2.7}$$

In fig. 2, all the data on direct measurement of the total cross section on protons is shown. A best fit to the form of eqn. (2.1) yields

$$\sigma^T(\gamma p) = (98.7 \pm 3.6) + (65 \pm 10.1) \cdot E^{-1/2} \ \mu b \qquad (2.8)$$

The measurements of the total cross section on deuterium are given in fig. 3.

The neutron cross sections are obtained from the deuterium data using the relationship

$$\sigma^T(\gamma n) = K \cdot \sigma^T(\gamma d) - \sigma^T(\gamma p) + \sigma_S + \sigma_W \qquad (2.9)$$

where K is a kinematic factor which takes into account the Fermi motion of the nucleon, σ_S is the screening correction [Franco and Glauber, 1966] to account for the shadowing of one nucleon by the other, and σ_W is a smearing term [West, 1971] which corrects for the fact that the nucleons in the deuterium are slightly off the mass shell and moving. Around 5 GeV the two corrections (σ_S, σ_W), are of comparable size, and together amount to ~3% adjustment to the measured cross sections, with an estimated uncertainty of ~0.5%. These corrections are very important since they are of the same magnitude as the difference in the proton and neutron cross sections for energies around 10 GeV. The neutron cross sections, obtained in this manner, are shown in fig. 4. The best fit to the energy dependence of eqn. (2.1) yields

$$\sigma^T(\gamma n) = (103.4 \pm 6.7) + (33.1 \pm 19.4) \cdot E^{-1/2} \ \mu b \qquad (2.10)$$

The difference between the neutron and proton cross sections is also shown in fig. 4. A best fit to the SLAC (UCSB) cross sections yields

$$\sigma^T(\gamma p) - \sigma^T(\gamma n) = (18.3 \pm 6.1) \cdot E^{-1/2} \ \mu b \qquad (2.11)$$

However, it is also clear from fig. 4, that the Serpukov measurements are compatible with no difference between the proton and neutron cross sections. Therefore the result given in eqn. (2.11) should be regarded as an upper limit.

An analysis of the isospin composition of the total cross sections using eqns. (2.6) and (2.7), yields the following estimates for the I=0 and 1 exchange contributions [Caldwell et al., 1973; Dominguez et al., 1972]:

$$\begin{aligned} I = 0 \text{ exchange:} & \quad \begin{cases} C_P = (101.9 \pm 2.9)\ \mu b \\ C_f = (50.9 \pm 8.5)\ \mu b \cdot GeV^{1/2} \end{cases} \\ I = 1 \text{ exchange:} & \quad C_{A_2} = (9.1 \pm 3)\ \mu b \cdot GeV^{1/2} \quad . \end{aligned} \tag{2.12}$$

From these results we may derive the isovector exchange contribution to the forward Compton amplitudes, and find:

$$\frac{\mathrm{Im}\ T_1}{\mathrm{Im}\ T_0} = \begin{cases} (3 \pm 1)\% \text{ at } 6 \text{ GeV} \\ (1.6 \pm 0.5)\% \text{ at } 25 \text{ GeV} \end{cases} \tag{2.13}$$

In summary, the total photon-nucleon cross section is observed to behave like the πN total cross section, reduced by a factor ~ 200; the energy dependence exhibits a slow decrease above 2 GeV. The proton cross section is slightly larger than the neutron cross section implying a small but probably nonzero contribution for isovector exchange to the Compton amplitude ($\lesssim 3\%$ around 6 GeV).

2.2 Compton Scattering

Compton scattering (i.e., elastic photon-nucleon scattering), is not only one of the basic reactions between photons and nucleons, but is also interesting due to its relation to the total hadronic cross section, σ_T, via the optical theorem, and to the photoproduction of vector mesons through the vector dominance model [Sakurai, 1960]. The process is expected to be diffractive and exhibit strong forward peaking in the scattering angular distribution. Furthermore, the comparison of the forward cross section, $\left.\frac{d\sigma}{dt}\right)_0$, and σ_T allows a test of forward dispersion relations not possible from πN data, since γp scattering may have extra contributions to the real part of the diffractive amplitude which are not present in πN collisions [Damashek and Gilman, 1970].

The Compton scattering reaction has been well studied over a wide range of energies and momentum transfers, and there is good agreement between the different experiments [Buschorn et al., 1970; Anderson et al., 1970; Boyarski et al., 1971]. The results of these measurements are shown in fig. 5. The differential cross sections show a sharp forward peak with very little energy dependence of the forward cross section or of the shape of the scattering distribution. The differential cross sections are fit to the forms

$$\frac{d\sigma}{dt} = \left.\frac{d\sigma}{dt}\right)_0 \cdot \exp(At) \tag{2.13a}$$

$$\frac{d\sigma}{dt} = \left.\frac{d\sigma}{dt}\right)_0 \cdot \exp(At + Bt^2) \tag{2.13b}$$

For momentum transfers less than 0.6 GeV^2, the simple exponential form (eqn. (2.13a)) describes the data well, but the quadratic form of eqn. (2.13b) is required to fit the data out to $t=1$ GeV^2. The results of these fits are summarized in table 1. The Compton scattering differential cross sections show very similar behavior to those of πN elastic scattering.

The forward amplitude in Compton scattering may be written [Gell-Mann, Goldberger and Thirring, 1954; Damashek and Gilman, 1970],

$$f^{o}_{\gamma p} = (\underset{\sim}{\epsilon}_f \times \underset{\sim}{\epsilon}_i) \cdot f_1 + i\sigma \cdot (\underset{\sim}{\epsilon}_f \times \underset{\sim}{\epsilon}_i) \cdot f_2 \tag{2.14}$$

where $\underset{\sim}{\epsilon}_i$, $\underset{\sim}{\epsilon}_f$ are the polarization vectors of the photon before and after the scattering, σ is the Pauli spin matrix of the recoil proton, and f_1 and f_2 are the amplitudes for parallel and perpendicular polarization vectors. Now, applying the optical theorem $\left(\mathrm{Im}\, f_1 = \frac{k}{4\pi}\sigma_T\right)$, the forward Compton cross section, $\left.\frac{d\sigma}{dt}\right)_0(k)$, as a function of photon momentum, k, may be written as

$$\left.\frac{d\sigma}{dt}\right)_0 (k) = \frac{\sigma_T^2}{16\pi} + \frac{\pi}{k^2} \cdot |\mathrm{Re}\, f_1|^2 + \frac{\pi}{k^2} \cdot |f_2|^2 \tag{2.15}$$

The real part of f_1 can be evaluated using the measured total cross sections and a dispersion relation, assuming Regge behavior for $f_1(k)$;

$$\mathrm{Re}\, f_1(k) = -\frac{\alpha}{M} + \frac{k^2}{2\pi^2} \int \sigma^T(k')\, dk' \tag{2.16}$$

The calculated ratio of the real part to the imaginary part of f_1 is shown in fig. 6 [Damashek and Gilman, 1970]. The calculation implies that the ratio of real to imaginary amplitudes in the forward direction is ~ 0.2 at 5 GeV, and ~ 0.1 at 20 GeV.

A comparison of both sides of eqn. (2.15) is shown in fig. 7 where the total cross section data discussed above are compared to the measured forward Compton cross section. Good agreement is obtained assuming $f_2=0$, and using f_1 from the dispersion calculation. An estimated upper limit of the f_2 contribution to the forward cross section of 10% is obtained from this comparison.

An estimate of the isovector contribution to Compton scattering may be obtained from a comparison of the cross section on hydrogen and deuterium targets. An example of such a measurement, for photon energies of 8 and 16 GeV, is shown in fig. 8 [Boyarski et al., 1971]. The data show a sharp forward peak from the coherent deuteron scattering with a flatter incoherent contribution at larger t. The deuterium cross section, ignoring spin effects, is given by

$$\left.\frac{d\sigma}{d\Omega}\right)_D = 2\,|T_0|^2\left\{1 + F(t) + 2G(t)\right\} + 2\,|T_1|^2\left\{1 - F(t)\right\} \qquad (2.17)$$

where T_0, T_1 are the isoscalar and isovector t-channel exchange amplitudes on nucleons, F(t) is the deuterium form factor and G(t) is the Glauber scattering term. The cross section on hydrogen is written;

$$\left.\frac{d\sigma}{d\Omega}\right)_H = |T_0+T_1|^2 = |T_0|^2 + |T_1|^2 + 2\mathrm{Re}\;T_0\cdot T_1^* \qquad (2.18)$$

Then,

$$\left[\left.\frac{d\sigma}{dt}\right)_D\Big/\left.\frac{d\sigma}{dt}\right)_H\right] = 2\left[1 - \frac{2\mathrm{Re}\;T_0\cdot T_1^*}{|T_0+T_1|^2}\cdot\left\{1 + F(t) + 2G(t)\right\} - \frac{2\,|T_1|^2}{|T_0+T_1|^2}\cdot\left\{F(t) + G(t)\right\}\right] \qquad (2.19)$$

The deuterium form factor, F(t), is taken from the electron scattering data, as $F(t) = \exp(56t)$, † and the screening correction term from the calculations of Ogren [Ogren, 1970],

$$G(t) = -0.069\,\exp(-At/4) + 0.007\,\exp(-At/2)$$

with $A = 7.8\ \mathrm{GeV}^{-2}$.

---

†This parametrization of the form factor is known to fall off too steeply. A more accurate parametrization is given by Franco, V. and Varma, G. K. (1974), Phys. Rev. Letters 33, 44;

$$F(t) = 0.34\,e^{141.5\,t} + 0.58\,e^{26.1\,t} + 0.08\,e^{15.5\,t}\ .$$

The ratio of deuterium and hydrogen cross sections, given in eqn. (2.19), was fit as a function of t (for $0.014 < t < 0.17\ \mathrm{GeV}^2$), using the combined 8 and 16 GeV data, and the following ratios determined:

$$\frac{\mathrm{Re}\, T_0 \cdot T_1^*}{|T_0 + T_1|^2} = -0.049 \pm 0.012$$

$$|T_1|^2 / |T_0 + T_1|^2 = 0.03 \pm 0.10 \qquad (2.20)$$

A literal interpretation of this result implies that the neutron Compton cross section is larger than the proton cross section, and that the isovector amplitude is purely real. However, a more probable interpretation of this data together with that on the difference between the neutron and proton total cross sections would be that the isovector exchange contribution in Compton scattering is small, near the forward direction.

3 PHOTOPRODUCTION OF VECTOR MESONS—ρ, ω, ϕ

3.1 Introduction

In this section we discuss the photoproduction of the lowest lying vector meson states—the ρ, ω and ϕ mesons. These processes have been extensively studied using a variety of techniques, on both proton and deuteron targets. The experimental situation is summarized in table 2. The various techniques each have their own peculiar experimental problems. The track chamber experiments allow a clean isolation of the exclusive reactions with very little background and they measure the full decay angular distribution. However, they have difficulty measuring the cross section near the forward direction, due to scanning losses (typically for $t < 0.02 - 0.05\ \mathrm{GeV}^2$). The counter experiments either detect the decay products of the photoproduced meson, or the recoil nucleon system and then identify the meson production in the missing mass distribution. The former method detects only part of the decay angular distribution and the observed angular correlations have to be corrected for the geometrical efficiency of the apparatus. The recoil experiments clearly have no information on the decay correlations. Both counter techniques are also vulnerable to inelastic vector meson production being included as background in the data, since they do not, in general, detect the complete final state. However, the counter experiments are high statistics, good resolution measurements with data all the way in to the forward direction.

Since the vector mesons have spin-parity 1^- like the photon, one might expect these processes to have large cross sections and be diffractive in character (i.e., to exhibit the properties listed in section 1 above). Indeed, the production rates are found to be large and decrease slowly with energy above 2 GeV, and with scattering distributions that falloff with an exponential slope. An analysis of the decay distributions of the photoproduced vector mesons, especially from polarized photons, provides a powerful tool for the study of the spin dependence of diffraction scattering.

3.2 Rho Production

3.2.1 Cross sections

Rho production is the dominant process in the reaction $\gamma N \rightarrow \pi^+\pi^- N$. The $\pi^+\pi^-$ mass distribution is shown in fig. 9 for the 9.3 GeV hydrogen and 4.3 GeV deuterium bubble chamber experiments [Ballam et al., 1973; Eisenberg et al., 1976]. The ρ^o peak dominates the $\pi^+\pi^-$ mass spectrum, and what little background exists under the peak is observed to get smaller, the higher the photon energy. The ρ^o shape is clearly skewed, in that there are too many low mass events and too few high mass events when compared to a p-wave Breit-Wigner resonance shape. The skewing, and resultant ρ^o mass shift, are observed to be dependent on momentum transfer, and are most pronounced in the forward direction. Since this effect is not fully understood, and since the ρ^o is a broad object, defining an absolute cross section is rather difficult. Further, since the backgrounds are energy dependent and the skewing of the ρ^o shape is t-dependent, it is very difficult to compare cross sections from different experimental techniques, measuring different fractions of the decay distribution, over different t-ranges, at different energies. The typical spread in the reported cross sections due to these uncertainties is of order (10-30)%.

The above behavior of the $\pi^+\pi^-$ mass spectrum may be described by several models. We describe the most successful one—the Söding model [Söding, 1966]—which explains the phenomena in terms of an interference between ρ^o production and the production of pion pairs through the Drell mechanism [Drell, 1961]. The model is shown diagramatically in fig. 10; diagram (a) refers to the ρ^o production process while (b) and (c) are the Drell terms; diagram (d) and (e) are rescattering terms introduced to avoid problems with double counting [Bauer and Yennie, 1970; Pumplin, 1970]. They ensure that at the ρ^o mass, the ρ^o amplitude saturates the unitarity bound. The mass skewing results from the interference of diagram (a) with the other four diagrams. This interference term changes sign from positive to negative in passing through the ρ^o mass. The various contributions to the cross section are shown in fig. 11. While the interference term contributes little to the integrated cross section, it does account for the observed ρ^o mass shift and skewing of the $\pi^+\pi^-$ spectrum. (This model also provides a good description of the t-dependence and angular correlation of the photoproduced pion pairs, as we will discuss below.)

Yennie has used this picture in proposing a simple recipe to determine the ρ^o cross sections free from the problems discussed above, of having to understand the details of the $\pi^+\pi^-$ mass shape for different experiments measuring in different regions of the kinematic variables. He suggests taking the yield of $\pi^+\pi^-$ pairs at the rho mass (i.e., $M_{\pi\pi} = M_\rho$), where the interference term is zero, and then the cross section is given by:

$$\frac{d\sigma}{dt} = \frac{\pi}{2} \cdot \Gamma_\rho \cdot \frac{d^2\sigma}{dM_{\pi\pi} \cdot dt} \tag{3.1}$$

where Γ_ρ is the rho width.

There are problems with this recipe; the mass and width of the rho meson are not precisely known quantities and they influence strongly the determination of the cross section; the presence of ω-ρ interference effects are ignored and can introduce ~10% differences in the estimated cross section. However, it is a standard method and has served to bring some degree of order in an area of great confusion. We shall use this definition in comparing the various ρ^o photoproduction experiments discussed below.

The total ρ^o production cross section is shown in fig. 12 from the track chamber experiments. There is good agreement among the different measurements. The energy dependence of the cross section closely resembles that of the average of the elastic π^+p and π^-p cross sections. More specifically from the quark model we expect the (ρ^op) system to behave like the average of π^+p and π^-p scattering, while from vector dominance we expect the $\gamma \to \rho^o$ transition to be the same as $\rho^o \to \rho^o$ multiplied by a constant, $\sqrt{\alpha\pi}/\gamma_\rho$ which measures the strength of the photon-rho meson coupling (see section 5 below). We then may write

$$\sigma(\gamma p \to \rho^o p) = \frac{\alpha\pi}{\gamma_\rho^2}\, \sigma^{el}\, (\rho^o p \to \rho^o p)$$

$$= \frac{\alpha\pi}{\gamma_\rho^2}\, \frac{1}{2}\left[\sigma^{el}(\pi^+ p) + \sigma^{el}(\pi^- p)\right] \quad . \qquad (3.2)$$

The solid line in fig. 12 represents the above relation with $\left(\gamma_\rho^2/4\pi\right) = 0.65$ and using the measured $\pi^\pm p$ cross sections [Giacomelli, 1969]. The agreement is good.

Typical differential cross sections for $\gamma p \to \rho^o p$ are shown in fig. 13 for 9 and 16 GeV. The agreement between the different experiments is fairly good, with all measurements typically lying within a ±15% band at each energy. The shape of the scattering distribution, for $t < 0.5$ GeV^2, is well fit by an exponential form

$$\frac{d\sigma}{dt} = \left.\frac{d\sigma}{dt}\right)_0 \exp(At) \tag{3.3}$$

Experiments measuring over a wide range of momentum transfers [e.g., Anderson et al., 1970; $0.1<t<1.2$ GeV^2] find they require a quadratic term in the exponential. A summary of the forward cross section, $\left.\frac{d\sigma}{dt}\right)_0$, and slope parameter, A, for those experiments using the Söding model analysis, is given in table 3, and the data plotted in figs. 14 and 15 respectively.

The measured forward ρ^o cross section data in fig. 14 show good agreement among the different experiments, and exhibit a slow falloff with energy similar to that observed for diffractive hadronic reactions. More specifically, we may relate the forward ρ^o cross section to the measured π^+p and π^-p total cross sections using the quark model and vector dominance (see eqn. (5.5), and the discussion of the vector dominance model in section 5). The solid line in fig. 14 is the result of such a calculation, and provides a good representation of the forward ρ^o production cross sections which are measured to be $\approx 125\ \mu b/GeV^2$ at 4 GeV, and falls to $\sim 100\ \mu b/GeV^2$ at 10 GeV, with an estimated uncertainty of $\sim$(10-15)%.

The slope of the forward ρ^o cross section is shown in fig. 15. It shows very little energy dependence and is in good agreement with the average of the measured $\pi^{\pm}p$ elastic slopes, shown as the solid line. It is important to note the different t-ranges measured in the various experiments (see table 3). Recent studies of hadron elastic scattering distributions at the CERN-ISR [Barbiellini et al., 1972] and at SLAC [Carnegie et al., 1975] have shown that the slope of the scattering distribution for

$t \lesssim 0.2$ GeV^2 can be 1 to 2 units larger than for the region $0.2 \leq t \leq 0.5$ GeV^2. Examples of this are shown in fig. 16 where the forward slopes in $\pi^{\pm}p$, $K^{\pm}p$ and $p^{\pm}p$ elastic scattering at 10 GeV, are shown as a function of momentum transfer. For ρ^0 photoproduction, we compare data from the very forward direction ($0 < t < .2$ GeV^2) to larger t-measurements ($0.05 < t < 1$ GeV^2) in fig. 13, and observe that although the cross sections agree where the data overlap the measurements of the slope differ by 1 to 2 units. The situation is summarized in table 4. This is an indication that forward steepening is present in the ρ^0 photoproduction cross section, just as for other diffractive elastic processes.

3.2.2 Angular correlation studies

The systematics of the ρ^0 decay angular distribution have been most beautifully studied in a series of experiments using a linearly polarized photon beam at energies of 2.8, 4.7 and 9.3 GeV [Ballam et al., 1973]. The definition of the angles used for these studies is shown in fig. 17, and depending on the coordinates system the Z-axis is defined as

- γ direction in ρ^0 rest frame, for Gottfried-Jackson
- ρ^0 direction in total center of mass system, for Helicity
- γ direction in total center of mass system, for Adair

The full information of the ρ^0 decay angular distribution is contained in nine independent density matrix elements [Schilling et al., 1971];

$$\begin{aligned} W(\cos\theta, \phi, \Phi) = \frac{3}{4\pi} \Big\{ & \frac{1}{2}\left(1 - \rho^0_{00}\right) + \frac{1}{2}\left(3\rho^0_{00} - 1\right)\cos^2\theta - \sqrt{2}\,\mathrm{Re}\,\rho^0_{10}\sin 2\theta\cos\phi \\ & - \rho^0_{1-1}\sin^2\theta\cos 2\phi - P_\gamma\cos 2\Phi\Big[\rho^1_{11}\sin^2\theta + \rho^1_{00}\cos^2\theta \\ & - \sqrt{2}\,\mathrm{Re}\,\rho^1_{10}\sin 2\theta\cos\phi - \rho^1_{1-1}\sin^2\theta\cos 2\phi\Big] \\ & - P_\gamma\sin 2\Phi\Big[\sqrt{2}\,\mathrm{Im}\,\rho^2_{10}\sin 2\theta\sin\phi + \mathrm{Im}\,\rho^2_{1-1}\sin^2\theta\sin 2\phi\Big]\Big\} \end{aligned} \tag{3.4}$$

where P_γ is the degree of linear polarization, and the density matrix of the rho has been split into three parts

$$\rho_{ik} = \rho^0_{ik} - P_\gamma \cos 2\phi \cdot \rho^1_{ik} - P_\gamma \sin 2\phi \cdot \rho^2_{ik} \quad .$$

P_γ varies from 95% at 2.8 GeV to 77% at 9.3 GeV.

The photon, due to its zero rest mass, can only have helicities $\lambda_\gamma = \pm 1$, while the ρ^o meson may have helicities $\lambda_\rho = \pm 1$ and 0. A study of the decay distribution allows a separation of the various helicity amplitudes, since for $\lambda_\rho = \pm 1$ the decay angular distribution will have the form $\sin^2\theta$, and for $\lambda_\rho = 0$, it would follow $\cos^2\theta$. The decay angular distributions also allow a separation of the natural† and unnatural parity t-channel exchange amplitudes to leading order in the photon energy [Schilling et al., 1971]. The natural parity exchange process has the pions from ρ^o decay emerging preferentially in the plane of photon polarization ($\Psi \sim 0^o$), and the unnatural exchange processes have the pions emerging perpendicular to it ($\Psi \sim 90^o$).

Figure 18 shows the distribution of $\cos\theta$ against Ψ in the helicity system, for $\gamma p \rightarrow \rho^o p$ at 4.7 GeV. The data show a beautiful $\sin^2\theta \cos^2\Psi$ correlation, implying the ρ^o takes over the photon's polarization with no helicity flip and that the process is dominated by natural parity exchanges.

The relative contribution from natural parity exchange (σ^N) in the t-channel is measured by the parity asymmetry

$$P_\sigma \equiv \frac{\sigma^N - \sigma^u}{\sigma^N + \sigma^u} = 2\rho^1_{1-1} - \rho_{00} \qquad (3.5)$$

†Natural parity exchanges have the property $P = (-1)^J$, where J is the intrinsic spin of the object being exchanged. Unnatural parity exchanges have $P = -(-1)^J$.

P_σ is shown in fig. 19 as a function of momentum transfer, for the three energies 2.8, 4.7 and 9.3 GeV. Rho production is completely dominated by natural parity exchange. The fraction of unnatural parity exchange is found to be $<5\%$ and consistent with the contribution expected from one-pion-exchange calculations. Similar conclusions were obtained from counter experiment studies using linearly polarized photons at DESY [Criegee et al., 1970] and CORNELL [Diambrini-Palazzi et al., 1970]. These experiments were able to show that unnatural exchange contributions were small (i.e., $<10\%$), right down close to threshold for the reaction.

The nine density matrix elements describing the ρ^o decay distributions are presented in fig. 20 as a function of t for the 4.7 GeV study, as evaluated in each of the three coordinate systems—Gottfried-Jackson, Helicity and Adair. Substantial spin flip or t-channel helicity flip contributions are seen in the Gottfried-Jackson and Adair system density matrix elements while in the helicity system the density matrix elements are consistent with no flip contributions (i.e., they are consistent with s-channel helicity conservation). The SLAC streamer chamber [Davier et al., 1970] and wire chamber spectrometer [Giese, 1974] confirm this behavior up to the highest energies available (i.e., $E_\gamma = 16$ GeV) and for $t \lesssim .5$ GeV^2. These results imply that in the center of mass the rho behaves like a photon with its spin along its direction of flight.

This tidy picture in which s-channel helicity conservation (SCHC) was a property of the rho production amplitudes (and perhaps all diffractive amplitudes [Gilman et al., 1970]) was not to be; it certainly is the dominant contribution to the process but careful and systematic study discovered small helicity-flip amplitudes. The density matrix elements for the

9.3 GeV experiment are shown in fig. 21, for the helicity system. The parity asymmetry P_{σ}, is close to 1 showing the rho meson is predominantly produced by natural parity exchange, and the elements ρ^1_{1-1} and $-\mathrm{Im}\,\rho^2_{1-1}$ are close to 0.5 and all other elements close to zero, as required by SCHC. However, there are small but systematic deviations from zero in the interference terms between helicity-flip and nonflip amplitudes. The relevant elements are:

$$\left.\begin{array}{l}
\text{intensity of } \Delta\lambda=\pm1 \text{ amplitude: } \rho^0_{00} \\
\text{intensity of } \Delta\lambda=\pm2 \text{ amplitude: } \rho^1_{1-1} + \mathrm{Im}\,p^2_{1-1} \\
\text{interference between } \Delta\lambda=\pm1 \text{ and } \Delta\lambda=0 \text{ amplitudes:} \\
\qquad\qquad \mathrm{Re}\,\rho^1_{10} - \mathrm{Im}\,\rho^2_{10} \\
\qquad\qquad \mathrm{Re}\,\rho^0_{10} \\
\text{interference between } \Delta\lambda=\pm2 \text{ and } \Delta\lambda=0 \text{ amplitudes:} \\
\qquad\qquad \rho^0_{1-1}
\end{array}\right\} \qquad (3.6)$$

In the forward direction these elements must go to zero from kinematics, but in the range $(0.2<t<0.8)$ GeV^2 they appear to be systematically nonzero.

Similar studies have been performed for rho production in deuterium, where they find the same angular correlations. Figure 22 indicates that the process is mainly SCHC and natural parity exchange and further detailed analysis of the density matirx elements confirms such a conclusion. This indicates that rho production on protons and neutron has the same spin dependence. Since I=1 exchange amplitudes will couple with opposite sign in the proton and neutron reactions (see eqn. (3.11)), and the density matrix elements for the γp and γn reactions are the same (even for those implying helicity flip), it would appear that the isovector contributions must be small and do not account for the helicity flip behavior. The I=1 exchange amplitudes are discussed more fully in the next section.

Using the linearly polarized γ beam data, the density matrix elements, and the cross sections, can be separated (to leading order in energy), into natural and unnatural parity exchange contributions [Schilling et al., 1971]

$$\rho_{ik}^{\substack{N\\U}} = \frac{1}{2}\left[\rho_{ik}^{0} \mp (-1)^{i} \cdot \rho_{ik}^{1}\right] \tag{3.7}$$

Analysis of the hydrogen and deuterium laser beam experiments [Ballam et al., 1973; Eisenberg et al., 1976] for example, shows that the ρ_{ik}^{U} are close to zero, confirming once more the dominance of natural parity exchange. (See fig. 23.) The deviations from SCHC in fig. 21 may now be observed to originate in the natural parity exchange density matrix elements, ρ_{ik}^{N}, of fig. 23.

In order to check for instrumental bias the density matrix elements were separately evaluated for data with the photon polarization parallel and normal to the camera axis in the bubble chamber. Since the ρ^{o} decays preferentially in the polarization plane, this effectively rotates the asymmetry of the angular distribution by 90^{o} in the chamber. No difference was observed in the two results.

Given the observation of helicity flip behavior in the data, it may be identified with either the rho production or the nonresonant π-π background. This question was studied in detail using the Söding model [Söding, 1966] to describe the mass and t-dependence of the dipion angular correlations. Figure 24 shows two of the helicity flip moments, as examples, with the expected behavior of the nonresonant π-π background subtracted out. One plainly sees that the s-channel helicity flip effect is associated with the rho production.

Assuming that the rho production is natural parity exchange, that the helicity flip amplitudes are small and that the nonflip amplitude is imaginary, the measured density matrix elements may be used to estimate the ratio of single and double helicity flip to the dominant nonflip amplitude. The results are shown in table 5. The different estimations of the strength of the flip term are in fair agreement with each other, and imply that the single flip amplitude is of same sign as the nonflip amplitude and ~10-15% in magnitude, while the double flip is roughly the same size but opposite in sign. Both helicity flip amplitudes are dominantly natural parity exchange.

There are two facts that argue for the isospin of the helicity flip amplitude being zero;

(a) if the exchange were I=1 the sign of the helicity flip amplitude on neutrons and protons would be opposite, while it is observed to be the same

(b) if the exchange were I=1 we would expect a much bigger effect for helicity flip in $\gamma p \to \omega p$, since

$$\frac{\mathrm{Re}\,\rho^{N}_{10}(\gamma\to\omega)}{\mathrm{Re}\,\rho^{N}_{10}(\gamma\to\rho)} \sim \frac{\gamma^2_\omega}{\gamma^2_\rho} = 7\pm1 \quad .$$

Therefore, we would expect very large Re ρ^{o}_{10} and ρ^{o}_{1-1} in the natural parity exchange part of omega production. Instead one observes (see table 5) an amplitude similar in size to that found for rho production, as one would expect for I=0 exchange.

The magnitude of the helicity-flip amplitude does not change much from 4 to 9 GeV, although an $s^{-1/2}$ behavior cannot be ruled out due to the large errors. It is tempting to relate the helicity-flip behavior to the diffractive Pomeron exchange amplitude, especially as similar features have been identified in elastic πN scattering, for the nucleon vertex.

A Saclay group [Cozzika et al., 1972] studying the A and R polarization parameters in πN elastic scattering have shown that the t-channel, I=0 nucleon helicity-flip amplitude F^{o}_{+-} is of order ~10% of the nonflip F^{o}_{++} amplitude for $0.2 < t < 0.8$ GeV^2 and is roughly independent of energy. The ratio of flip to nonflip amplitude as a function of momentum transfer, is shown in fig. 25 for both the $\gamma \rightarrow \rho^o$ and $p \rightarrow p$ analysis. The similarity is strong, indicating that helicity flip is a common property of diffractive processes and that it has the same characteristic for the meson or the nucleon vertex.

In summary, ρ^o photoproduction is dominated by natural parity exchanges in the t-channel and the $\gamma \rightarrow \rho^o$ transition mainly conserves the s-channel helicity of the incoming photon. A small helicity flip amplitude is observed, also dominated by natural parity exchanges, and is ~10% of the nonflip term. The angular correlations are found to be the same for ρ^o production on neutron or proton targets.

3.2.3 Amplitude structure in $\gamma N \rightarrow \rho^o N$—isolation of I=1 exchanges

The contribution of isovector t-channel exchange to the process $\gamma N \rightarrow \rho^o N$ may be estimated by comparing the production cross sections from deuterium and hydrogen targets. Four separate methods for extracting the I=1 exchange amplitude are summarized below.

i) Comparison of forward cross sections

The forward cross section, $\left.\frac{d\sigma}{dt}\right)_0$, for rho production on deuterium or hydrogen may be written:

$$\left.\frac{d\sigma}{dt}\right)_0 (\gamma d \rightarrow \rho^o d) = 4\,|T_0|^2\,(1-G) \quad , \tag{3.8}$$

where G is the shadowing correction [Franco and Glauber, 1966], and

$$\left.\frac{d\sigma}{dt}\right)_0 (\gamma p \rightarrow \rho^o p) = |T_0 + T_1|^2 \tag{3.9}$$

For no I=1 exchange, the ratio of expressions (3.8) and (3.9) should be 3.72. Otherwise, for an I=1 exchange contribution one may obtain from R the following:

$$\frac{2T_1 \cdot T_0^*}{|T_0|^2} + \left|\frac{T_1}{T_0}\right|^2 = 2\left|\frac{T_1}{T_0}\right| \cdot \cos\Delta\phi + \left|\frac{T_1}{T_0}\right|^2 \tag{3.10}$$

where $\Delta\phi$ is the relative phase between the isoscalar and isovector amplitudes at t=0.

Given that ρ^o production is dominated by natural parity exchange in the t-channel we can identify the isoscalar amplitude with (P+f) exchange, and the isovector amplitude with A_2 exchange. The absolute phase of T_0 has been measured experimentally by DESY-MIT [Alvensleben et al., 1970] and NINA [Biggs et al., 1971] groups by observing the interference between Bethe-Heitler production and leptonic decay of the rho meson. They find the phase of T_0 to be 102^o–106^o. If T_1 were taken to have the phase of the A_2 Regge trajectory it would be $\sim 135^o$, and hence $\cos\Delta\phi = 0.84$. If, however, we assume that absorption or other effects may alter this phase we might still expect T_1 to lie in the second quadrant and hence $\cos\Delta\phi > 0.2$. Applying these assumptions on $\Delta\phi$ to eqn. (3.10) we can estimate $|T_1/T_0|$.

Table 6 shows the results of such a calculation for the three bubble chamber and two counter experiments studying rho production on deuterium. For the counter experiments only the highest energy data (i.e., those near the end point of the bremsstrahlung spectrum) were used in order to remove possible confusion due to inelastic background contributions. The ratio of the deuterium to hydrogen cross sections near the forward cross section is shown in fig. 26 from the highest energy SLAC experiment [Giese, 1974]. The data from all five experiments are in fair agreement, and imply that the isovector exchange amplitude, T_1, is small.

ii) Comparison of closure and coherent cross sections

We may write the helicity nonflip amplitude for rho production on protons and neutrons as

$$\left.\begin{aligned} f(\gamma p \rightarrow \rho^o p) &= T_0 \exp(At/2) + T_1(t) \\ f(\gamma n \rightarrow \rho^o u) &= T_0 \exp(At/2) - T_1(t) \end{aligned}\right\} \qquad (3.11)$$

where T_0, T_1 are the isoscalar and isovector exchange amplitudes, as before. The Glauber multiple scattering theory then gives the differential cross section for coherent production from deuterium, following [Eisenberg et al., 1976]:

$$\frac{d\sigma}{dt}(\gamma d \rightarrow \rho^o d) = 4\,|T_0|^2\,[S(t/4)\exp(At) - S(t/4)\cdot G\cdot \exp(3At/4)] \qquad (3.12)$$

where G is the shadowing correction [Franco and Glauber, 1966], and S(t) is the deuteron form factor.

The total closure cross section for rho production, including both coherent and breakup contributions, is written

$$\frac{d\sigma}{dt}(\gamma d \rightarrow \rho^o pn) = 4\,|T_0|^2 \exp(At)\cdot\frac{1}{2}\cdot(1+S(t)) + 4\,|T_1|^2\cdot\frac{1}{2}\cdot(1-S(t)) - 4\,|T_0|^2\cdot G\cdot\exp(3At/4) \qquad (3.13)$$

Knowing $|T_0|^2$ from the forward coherent deuteron cross section, the total rho production data may be fit to eqn. (3.13) and an estimate of $|T_1/T_0|^2$ obtained. The closure and coherent cross sections from the 4.3 GeV γd bubble chamber experiment [Eisenberg et al., 1976] are shown in fig. 27 together with their fit to eqn. (3.13). The results of these calculations are given in table 6 for experiments at 4.3 and 16 GeV, and also indicate that the isovector contribution is small.

iii) Neutron-proton cross section difference

Another method of estimating the isovector contributions is to compare the production cross section on neutrons and on protons, as we did for Compton scattering and the total photon cross section in section 2 above. Here, we have

$$\frac{\sigma(\gamma p \to \rho^o p) - \sigma(\gamma n \to \rho^o n)}{\sigma(\gamma p \to \rho^o p) + \sigma(\gamma n \to \rho^o n)} \approx \frac{2\mathrm{Re}\ T_1 \cdot T_0^*}{|T_0|^2} \quad . \tag{3.14}$$

The comparison may be performed from the data of the deuterium bubble chamber experiments [Eisenberg et al., 1976], but have to be done at a value of momentum transfer where the recoil nucleon can be clearly kinematically separated from the spectator nucleon. The analysis is done for recoil momenta greater than 280 MeV/c. The results are shown in table 6, and again show that T_1 is small.

iv) Exchange contribution to $\gamma n \to \rho^- p$

Yet another independent limit on the isovector contribution may be obtained from the cross section for the charge-exchange process, $\gamma n \to \rho^- p$.

The principal t-channel exchanges contributing to this reaction are π^+, ρ^+, A_2^+. If we assume that the natural parity exchanges do not interfere destructively, we can obtain an upper limit for the A_2^+ contribution, and from SU(2), a limit on the A_2^o contribution to ρ^o photoproduction. The cross section data are summarized in fig. 28 and the resulting limits recorded in table 6.

In summary, all the methods in table 6 imply that the isovector contribution to $\gamma N \rightarrow \rho^o N$ is small and less than (5 - 10)% of the isoscalar amplitude. This is in good agreement with the estimates obtained in section 2 for the isovector contribution to the related reaction of Compton scattering and the total hadronic cross section, of ≈3% at 6 GeV and ≈1.5% at 20 GeV.

3.2.4 Amplitude structure in $\gamma n \rightarrow \rho^o N$—isolation of f and P exchanges

The rho production process may be considered dominated by f^o-meson and Pomeron exchanges in the t-channel, since both unnatural parity exchanges and I=1 natural parity exchanges have been shown to be small (see sections 3.2.2 and 3.2.3). Further, since there is substantial energy dependence of both the total rho cross section and the forward differential cross section in the 2-5 GeV range, it may be expected that the meson exchange amplitude is appreciable.

A separation of the f and $\mathbb{P}$ amplitudes has been performed [Chadwick et al., 1973] utilizing the Dual Absorption Model [Harari, 1971] as a guide to the structure of the exchange amplitudes. A more detailed description of this work may be found in the thesis of Kogan [Kogan, 1975]. This analysis followed a similar separation of the f and $\mathbb{P}$ exchange amplitudes in πN scattering [Davier, 1972].

The rho production is parametrized in terms of two components—a central Pomeron term and a peripheral f exchange term:

$$\mathbb{P}(s,t) = iC_p \exp\left[A_p(s)\,t\right]$$

$$\mathrm{Im}\ f(s,t) = (C_f/\sqrt{s})\ \exp\left[A_f(s)\ t\right] \cdot J_0(R\sqrt{-t}) \tag{3.14}$$

and the cross section at a given energy is written

$$\begin{aligned} \frac{d\sigma}{dt}(\gamma p \to \rho^o p) &= |\mathbb{P}(t) + f(t)|^2 \\ &= |\mathbb{P}(t)|^2 + 2\mathbb{P}(t) \cdot \mathrm{Im}\ f(t) \end{aligned} \tag{3.15}$$

neglecting the $|f(t)|^2$ term which decreases like 1/s.

The rho production and Compton scattering cross sections may be well represented with this model as shown in fig. 29. The logarithmic slope of the Pomeron contribution to the ρ^o differential cross section as a function of energy, as determined from this analysis is given in fig. 30 together with the Pomeron slope from Davier's πN analysis. For comparison the slope of the differential cross section for the reaction $\gamma p \to \phi p$ is also shown.

It is interesting to note that the lack of energy dependence in the shape of the ρ^o differential cross section (fig. 15) is the result of a conspiracy between the falling energy dependence of the steep peripheral f-exchange amplitude the rapid shrinking of the Pomeron amplitude. This is the same result as found for πN scattering.

It is also interesting to note that the ratio of f-exchange to Pomeron exchange required for these fits [Chadwick et al., 1973] is the same for Compton scattering, rho photoproduction and for the πN elastic scattering.

3.2.5 Summary

In summary, the rho photoproduction reaction is observed to be diffractive, dominantly isoscalar natural parity exchange and with a spin structure which is mainly s-channel helicity conserving. The small (10-15)%, helicity flip contribution stems from I=0, natural parity exchanges and is probably associated with Pomeron exchange.

3.3 Omega Production

Omega production is experimentally much more difficult to study than the rho, since in addition to the problem of lack of precise knowledge of the incoming photon beam energy, one has to deal with the three-body ($\pi^+\pi^-\pi^o$) decay mode of the vector meson. The various experiments studying ω production on proton and neutron targets are listed in table 2. The ω mass distribution from two experiments—the 9.3 GeV bubble chamber experiment [Ballam et al., 1973], and a counter experiment [Gladding et al., 1973], are shown in fig. 31, where a rather clean signal is observed in each case. Typical backgrounds are estimated to be ~(10-15)%.

The cross section, as a function of energy, for ω production in the reaction

$$\gamma p \rightarrow \omega p$$

is shown in fig. 32. There is good agreement among the different measurements. Unlike the rho cross section, the ω data show a very rapid decrease of the cross section in the energy range from 2 to 5 GeV and then become almost constant above 5 GeV. The linearly polarized photon experiment [Ballam et al., 1973] allows a separation into the contributions from natural (σ^N), and unnatural (σ^U), parity exchanges in the t-channel

$$\sigma^{\substack{N\\U}} = \frac{1}{2}(1 \pm P_\sigma)\cdot\sigma \tag{3.16}$$

where P_σ is the parity asymmetry defined in eqn. (3.5) above. The rapid fall is almost entirely accounted for by the σ^U component of the cross section which has essentially disappeared by 10 GeV. The natural parity cross section, by contrast, is almost constant, decreasing by only 20% from 2 to 10 GeV.

The behavior of the ω cross section can be understood as a superposition of a strong pion exchange part and a diffractive part. The pion exchange contribution is about half the total ω cross section for energies $\sim$4 GeV, but due to the steep energy dependence this term is negligible by 10 GeV.

The differential cross sections are sharply forward peaked, with a slight steepening near the forward direction (see fig. 33). The cross sections from different experiments agree within $\sim$(10-15)% except for the new CORNELL data [Abramson et al., 1976], which appears to be systematically $\sim$30% lower than the other measurements. When the differential cross section is separated into the natural $\left(\frac{d\sigma^N}{dt}\right)$, and unnatural $\left(\frac{d\sigma^U}{dt}\right)$ components, using a t-dependent form of (3.16), the natural parity exchange component is found to be well represented by a simple exponential form

$$\frac{d\sigma^N}{dt} = \left.\frac{d\sigma}{dt}\right)_0 \exp At \quad .$$

The slope of the ω cross section at small t agrees well with that found for ρ^o photoproduction in section (3.2), namely $\sim$7-8 GeV^{-2}. The forward cross section measurements are summarized in table 7, where data from both hydrogen and coherent deuterium experiments are included. We quote, where possible, forward cross sections evaluated using the same assumption for the slope of $\frac{d\sigma^N}{dt}$ $(\gamma p \rightarrow \omega p)$ when fitting the measured differential cross section. As discussed above in section (3.2) for the ρ^o, the hydrogen data measure $|T_0 + T_1|^2$ while the coherent deuterium cross section determines $|T_0|^2$, where T_0, T_1 are the t-channel isoscalar and isovector exchange amplitudes respectively. Also included in table 7 are estimates of $|T_0|^2$ from optical model analyses of ω production on complex nuclei [Behrend et al., 1970, 1971; Braccini et al., 1970].

An independent estimate of $|T_0|^2$ may be obtained from the quark model and vector dominance model. Anticipating section 5 below, in which these relations are fully discussed, we take eqn. (5.4) and insert $\sigma^T(\omega N)$ and η_ω as 27 mb and -0.2 respectively (using the quark model and our knowledge of $\rho^o N$ scattering), and the measured photon-omega coupling strength, $\gamma_\omega^2/4\pi = 4.6$ from the storage ring experiments. Such a calculation results in $|T_0|^2 = 15.3\ \mu b/GeV^2$, and is entered on the bottom line of table 7. Except for the Cornell-Rochester measurement, all other data are in tolerable agreement with each other and with this VDM estimate of the ω forward cross section, $|T_0|^2$.

The ω decay angular distributions at low energy (<5 GeV) show none of the beautiful polarization correlations observed for the rho, due to the large pion exchange contribution to the production process. However, by 9.3 GeV the familiar $\sin^2\theta \cos^2\psi$ pattern for the ω decay distribution is observed (see fig. 34) indicating that at this energy the ω is produced mainly by natural parity exchange and that the process approximately conserves the s-channel helicity of the photon. The ω density matrix elements, ρ_{ik}^N, are consistent with those obtained for ρ^o production, although more poorly determined due to the smaller production cross section. They indicate that the same production and decay properties pertain for the ω reaction as for the ρ^o, even to the presence of a small helicity flip contribution to the $\gamma \to \omega$ transition.

The cross sections, differential cross sections and angular distributions for the reaction

$$\gamma N \rightarrow \omega N$$

are well represented by a model which describes the natural parity exchange in terms of the $\rho^0 N$ data and the unnatural parity exchange by a one-pion-exchange calculation [Wolf, 1969; Benecke-Dürr, 1968] in which the ω radiative width was taken to be $\Gamma_{\omega\pi\gamma} = 0.9$ MeV [Barash-Schmidt et al., 1974]. The solid lines in figs. 32 and 34 are the result of this fit.

The isospin decomposition for the reaction $\gamma N \rightarrow \omega N$ is specially interesting, as was first pointed out by Harari [Harari, 1969], since any I=1 contribution to the forward Compton amplitude gets amplified by a large factor in the ω production process. More precisely, Δ, the isovector contribution to $\gamma N \rightarrow \omega N$ may be written

$$\Delta = 2\left[\frac{\sigma(\gamma p \rightarrow \omega p) - \sigma(\gamma p \rightarrow \omega n)}{\sigma(\gamma p \rightarrow \omega p) + \sigma(\gamma n \rightarrow \omega n)}\right] = 2\left[\frac{\mathrm{Im}\, T^1_{\gamma p \rightarrow \omega p}}{\mathrm{Im}\, T^0_{\gamma p \rightarrow \rho p}}\right]$$

$$= \frac{\gamma_\omega^2}{\gamma_\rho^2}\, \frac{\mathrm{Im}\, T^1_{\gamma p \rightarrow \gamma p}}{\mathrm{Im}\, T^0_{\gamma p \rightarrow \gamma p}} \qquad (3.17)$$

$$= \frac{\gamma_\omega^2}{\gamma_\rho^2}\left[\frac{\sigma^T(\gamma p) - \sigma^T(\gamma n)}{\sigma^T(\gamma p) + \sigma^T(\gamma n)}\right]$$

and

$$\frac{\gamma_\omega^2}{\gamma_\rho^2} \approx 7 \quad .$$

In section (2.1) we estimated, with some reservation, that the isovector amplitude contribution is of order $(3 \pm 1)\%$ at energies around 6 GeV, implying a large isoscalar-isovector interference in ω photoproduction, with a value of $\Delta \sim 0.21$. However, as we mentioned in section 2.1, this result is very sensitive to the subtraction procedure and the deuterium model used.

We may estimate Δ from the ω photoproduction data through the relations:

$$\left.\frac{d\sigma^N}{dt}\right)_0 (\gamma p \to \omega p) = |T_0^N + T_1^N|^2 \tag{3.18}$$

(which excludes the pion exchange contribution), and

$$\left.\frac{d\sigma}{dt}\right)_0 (\gamma d \to \omega d) = 4(1-G)\,|T_0^N|^2 \tag{3.19}$$

where G is the shadowing correction [Franco and Glauber, 1966] and is equal to 0.068. We may then find limits on Δ from

$$\Delta \leq \frac{|T_0^N + T_1^N|^2 - |T_0^N|^2}{|T_0^N|^2} \quad . \tag{3.20}$$

Using the data summarized in table 7, the Weizmann group [Eisenberg et al., 1976] find

$$\Delta \leq -0.3 \pm 0.3$$

while the Rochester-Cornell group Abramson et al., 1976 find

$$\Delta = 0.20 \pm 0.12$$

The difference between these estimates stems from the different measured forward cross sections, and as shown in table 7 the Rochester-Cornell experiment find a much lower cross section than all other experiments. However, neither experiment is sufficiently precise to allow a good determination of the I=1 exchange amplitude, independent of the relative normalization question, and an answer to this interesting question awaits a new experiment.

In summary, the ω photoproduction experiments indicate that at low energies (<5 GeV) one pion exchange is an important part of the production process, but that by energies of ~10 GeV the ω reaction behaves very much like ρ^0 production, with a cross section ~7 times smaller. At these energies the ω is produced via natural parity exchange and is mainly s-channel helicity conserving. The intriguing possibility of using ω production to measure the I=1 exchange contribution to forward Compton scattering, since it is ~7 times enhanced in $\gamma N \rightarrow \omega N$, has not been achieved due to the smallness of the amplitude and the lack of precision in the current experimental measurements.

3.4 ϕ Production

The phi photoproduction reaction has been studied in the counter and track chamber experiments listed in table 2. The ϕ signal is very clean as shown in fig. 35, where the K^+K^- mass distribution from the 9.3 GeV bubble chamber experiment [Ballam et al., 1973] is given. The cross section for ϕ photoproduction as a function of photon energy is shown in fig. 36 and is about 0.5 μb and rather constant, perhaps rising a little as the energy increases.

The differential cross section is sharply forward peaked and well described by the usual exponential form

$$\frac{d\sigma}{dt} = \left.\frac{d\sigma}{dt}\right)_0 \exp(At)$$

A compilation of the published differential cross sections prior to Spring 1975 is shown in fig. 37a where fair agreement among the different experiments is observed. There is little indication of any s-dependence of the shape or magnitude of the ϕ differential cross section. In fig. 37b, the above data is combined with the new small momentum transfer, high statistics DESY experiment [Behrend et al., 1975], (the previous data are only plotted for $t > .4$ GeV^2). Again agreement between the various experiments is apparent where the data overlap. However, the small momentum transfer measurements exhibit a much steeper falloff of the differential cross section than the larger t measurements, indicating that the cross section is not well described by a simple exponential form.

The energy dependence of the slope of the ϕ differential cross section (i.e., the shrinkage) was studied, prior to the Behrend experiment by fitting the combined data in fig. 37a [Moffeit, 1973], to the usual Regge form for the slope, A,

$$A = A_0 + 2\alpha' \ln s \tag{3.21}$$

(where s is the total center of mass energy squared), and yielded the following value for the shrinkage parameter, α',

$$\alpha' = 0.14 \pm 0.09 \quad .$$

This is in good agreement with the results obtained from a SLAC-Wisconsin experiment [Anderson et al., 1973] studying ϕ production at a fixed t-value of 0.6 GeV^2. The measured cross sections from this experiment are shown in fig. 38, and an analysis of the s-dependence indicates

$$\alpha' = -0.03 \pm 0.13$$

(i.e., these measurements confirm the lack of energy dependence of the slope of the ϕ production cross section.)

A new fit to the energy dependence of all the available measurements on the ϕ differential cross section [Silverman, 1975], finds, for $t < 0.4$ GeV^2

$$\alpha' = 0.22 \pm 0.27 \quad .$$

The slope of the forward cross section as a function of energy, and the result of this new fit to the energy dependence, are shown in fig. 39. We will return to the question of the energy dependence of the shape of the ϕ differential cross section later in this section.

The decay angular distribution of the ϕ from the linearly polarized laser beam experiment, although limited in statistics, shows the now familiar $\sin^2\theta \cos^2\Psi$ correlation implying natural parity exchange dominance and s-channel helicity conservation in the production process (see fig. 40). Indeed the density matrix elements are compatible with those measured in rho photoproduction. A similar conclusion is obtained from measurements of the asymmetry in yield of $K^{\pm}$'s (from ϕ decay), counted in the plane of photon polarization and normal to that plane, by the Wisconsin-SLAC group using polarized photons of energy ~8 GeV [Halpern et al., 1972]. They find the asymmetry parameter, Σ, is close to unity,

$$\Sigma = 0.985 \pm 0.12 \quad ,$$

implying natural parity exchange and no spin-flip in the ϕ production.

Photoproduction of ϕ mesons from complex nucleii has been studied by DESY-MIT and CORNELL groups [Alvensleben et al., 1972; McClellan et al., 1971]. The ϕ is observed to be coherently produced and an analysis of the (K^+K^-) decay distribution is consistent with the SCHC production hypothesis. The photoproduction of ϕ mesons from deuterium and hydrogen targets has been measured for photon energies ~8 GeV [McClellan et al., 1971], and the ratio, R, of the cross sections at t=0 is found to be

$$R = 3.6 \pm 0.6$$

compatible with the expected ratio of 3.89 for no I=1 exchange.

Thus the ϕ photoproduction experiments indicate that the ϕ is diffractively produced, with natural parity, I=0 t-channel exchanges and with mainly SCHC.

These observations are in agreement with our expectations for ϕ photoproduction. It has been pointed out on very general grounds that ϕp elastic scattering should proceed only by Pomeron exchange [Freund, 1967]. This follows directly from the quark model in which the ϕ is described in terms of two strange quarks $(\lambda\bar{\lambda})$, and is supported by experimental evidence showing the ϕ to be decoupled from nonstrange hadrons. Then a measurement of ϕp elastic scattering should determine the parameters of the Pomeron trajectory rather clearly in comparison to other elastic scattering processes which usually involve additional exchange contributions. Since the ϕ-meson photoproduction cross section is related to the elastic scattering of transversely polarized ϕ mesons on protons through VDM via the relation

$$\frac{d\sigma}{dt}(\gamma p \rightarrow \phi p) = \left(\frac{\alpha\pi}{\gamma_\rho^2}\right) \cdot \frac{d\sigma}{dt}(\phi p \rightarrow \phi p) \qquad (3.22)$$

then measurements of the energy dependence of the photoproduction cross section, $\frac{d\sigma}{dt}(\gamma \rightarrow \phi)$, should also allow a good understanding of the Pomeron amplitude.

There is one caveat on this picture. The DESY/MIT group [Alvensleben et al., 1971] have measured the real part of the forward amplitude for the $\gamma p \rightarrow \phi p$ process by observing the interference between the resonant ϕ production and the Bethe-Heitler process in $\gamma C \rightarrow \phi C$, with $\phi \rightarrow e^+e^-$, at 7 GeV. They find that the ϕ amplitude differs from being purely imaginary by $25^{\circ} \pm 15^{\circ}$, or in terms of the amplitudes;

$$\frac{\mathrm{Re}\, T_{\phi}}{\mathrm{Im}\, T_{\phi}} = -0.48 \begin{smallmatrix} +.33 \\ -.45 \end{smallmatrix} \quad .$$

This may be an indication that the $\gamma \to \phi$ process is not purely due to Pomeron exchange. Unfortunately the above phase measurement is a difficult experiment and the errors do not allow a firm conclusion.

How do we accommodate our expectations for the behavior of a purely diffractive process with the experimental results on the s- and t-dependence of the ϕ cross section? Let us consider the two regions of momentum transfer with $t < 0.4\ \mathrm{GeV}^2$, and $t > 0.4\ \mathrm{GeV}^2$, separately.

First, the larger t region with $t > 0.4\ \mathrm{GeV}^2$: ϕ photoproduction shows no s-dependence over the energy range $s \sim 4$ to $40\ \mathrm{GeV}^2$. The value of α' obtained from an analysis of the cross sections in this region was

$$\alpha'_{\phi} = -0.03 \pm 0.13$$

The s-dependence for the elastic cross section at $t \sim 0.6\ \mathrm{GeV}^2$ for two hadronic processes (pp and K^+p elastic scattering), are shown in fig. 41 for comparison. These processes have exotic quantum numbers in the s-channel, and are therefore expected to be dominated by Pomeron exchange (i.e., to be mainly diffractive in character). For energies corresponding to $s > (10\text{-}15)\ \mathrm{GeV}^2$ they also exhibit little energy dependence. In fact, the Wisconsin-SLAC value of α'_{ϕ} agrees well with the shrinkage parameter of other hadronic processes evaluated for $s > 10\ \mathrm{GeV}^2$, and in the same t-range [Leith, 1975],

$$\alpha'_{\pi^- p} = -0.04 \pm 0.03\ \mathrm{GeV}^{-2}$$

$$\alpha'_{K^- p} = 0.00 \pm 0.04\ \mathrm{GeV}^{-2}$$

$$\alpha'_{K^+p} \sim 0.1 \text{ GeV}$$

$$\alpha'_{pp} = 0.10 \pm 0.06 \text{ GeV}^{-2}$$

Therefore the main difference between these purely hadronic processes and the $\gamma \rightarrow \phi$ reaction is that at low energies (i.e., $s < 10 \text{ GeV}^2$) the hadronic reactions begin to show strong shrinkage (see again fig. 41), while the photoprocess maintains the high energy behavior. In this same energy region, the total hadronic cross sections exhibit a rapidly falling energy dependence (see fig. 42), rather than the typical constant or slowly rising cross section characteristic of our picture of a Pomeron dominated process. The ϕ cross section, however, is quite constant—see fig. 36. The low energy hadron total cross section behavior is usually explained in terms of absorptive corrections or cuts [Barger and Phillips, 1971], and perhaps these effects also modify the elastic t-dependence. It is entirely possible that the photoproduction of ϕ meson does provide a good picture of the Pomeron at low energies, and that the photoproduction and hadron-hadron scattering data agree at high energies when nondiffractive contribution to the hadronic processes have become small.

The small t-region (i.e., $t < 0.4 \text{ GeV}^2$), is more complicated. In this region the ϕ differential cross section displays a steepening in the forward direction and is not well described by a simple exponential form. However, recent high statistics studies of elastic K^+p and pp scattering around 10 GeV have shown similar behavior in these classically "Pomeron dominated" reactions [Carnegie et al., 1975]. High energy pp elastic scattering experiments at the ISR, also observe this feature [Barbiellini et al., 1972; Leith, 1975a]. In fact, for both K^+p and pp the slope of the forward scattering cross section shows qualitatively the same behavior as the ϕ photoproduction; the larger t region shrinks slowly, while the forward direction has a steeper slope and shrinks more rapidly. This data is summarized in fig. 43. The small t differential cross sections are characterized by a shrinkage factor α'

$$\alpha'_{pp} = 0.28 \pm 0.03$$

$$\alpha'_{K^+p} \sim 0.5$$

and the analysis of the small t ϕ photoproduction cross section finds

$$\alpha_{\phi} \sim 0.22 \pm 0.27 \quad .$$

To summarize, the ϕ photoproduction experiments find

- the production cross section independent of energy.
- the differential cross section sharply peaked, with indication of steepening near the forward direction; the energy dependence for the change of the shape of the production angular distribution is poorly determined but quite consistent with that observed for other diffractive dominated processes like K^+p and pp elastic scattering.
- the production process involves natural parity exchanges and conserves s-channel helicity; there is very little I=1 exchange.
- there may be a substantial real part to the forward ϕN scattering amplitudes; measurement of the interference of $\phi \to e^+e^-$ decays with the Bethe-Heitler process yielded $\eta_{\phi} = -0.48^{+0.33}_{-0.45}$, while the ϕ photoproduction on complex nuclei measurements become consistent with the storage ring data on $(\gamma_{\phi}^2/4\pi)$ if η_{ϕ} is around 0.5.

- assuming the $\gamma \to \phi$ reaction is dominated by Pomeron exchange, the slope is around 4 GeV^{-2} and implies that the ϕ-nucleon interaction radius is much smaller than the nucleon-nucleon or, pion-nucleon radii. This is just what we expect from the quark model and find experimentally in a study of ϕ production from complex nucleii (i.e., $\phi(\phi N) \sim 8$-13 mb). (These experiments will be discussed in section 5 below.) Indeed, the measured ϕN slope agrees well with that expected from the ratio of the total cross sections and the measured πN, $K^{+}N$, pp forward slopes.
- finally, ϕ photoproduction may well be the way to a better understanding of the diffractive mechanism, but it will require much better experiments over a larger range of momentum transfers, and especially, over a wider range of energies.

4 HIGHER MASS VECTOR MESONS

4.1 Introduction

The existence of higher mass vector meson states (than the ρ^o, ω and ϕ), has long been predicted by the Veneziano model [Veneziano, 1968], and from analysis of the nucleon form factor [Schumacher and Engle, 1971]. An example of such states are the ρ' at 1300 MeV and ρ'' at 1700 MeV [Shapiro, 1969]. There is now experimental support for two isovector states with mass around 1250 MeV and 1600 MeV, and their existence implies that, one must also find the associated isoscalar ω', ϕ' states. Below we discuss the evidence for the existence of higher mass vector states, and review the characteristics of the photoproduction reactions.

4.2 ρ' (1250)

The first experimental report for such states comes from a study of the missing mass distribution in the reaction

$$\gamma p \rightarrow p + (\text{missing mass})$$

for photon energies up to 17 GeV [Anderson et al., 1970]. An enhancement was observed at a missing mass of 1230 MeV. The SLAC-Berkeley bubble chamber group [Ballam et al., 1974], the SLAC streamer chamber group [Davier et al., 1973], and the DESY streamer chamber collaboration [Rabe et al., 1971] found an enhancement in ($\pi^+\pi^-$ + missing mass) at around the same mass value, when studying the process

$$\gamma p \rightarrow p\pi^+\pi^- + MM$$

for missing mass, MM, greater than or equal to, two pion masses (i.e., not the final state $p\pi^+\pi^-\pi^o$).

The ($\pi^+\pi^-$MM) spectrum is shown in fig. 44, for the three energies of the bubble chamber experiment (viz. 2.8, 4.7 and 9.3 GeV). The bump around 1240 MeV is strongly enhanced when $\pi^+\pi^-$ masses in the region (330-660) MeV are selected, as indicated by the shaded region in fig. 44. This would be characteristic of $\pi^+\pi^-$ from ω decays. From this observation, and from a study of other final states, the bubble chamber group conclude that the 1240 MeV bump represents an $\omega\pi^0$ decay mode of a resonant state.

The cross section for the production of this object is shown in fig. 45, where it is observed to be about 1 μb and quite independent of the energy. The differential cross section (see fig. 46), is found to be sharply peaked, and well represented by an exponential form.

These observations suggests that the $\omega\pi^0$ system is produced diffractively. The absence of any $\omega\pi^-$ enhancement at the same mass for the charge exchange reaction

$$\gamma n \rightarrow p\omega\pi^-$$

is a confirmation that nondiffractive contributions are small [Benz et al., 1973].

The isospin, charge conjugation and G-parity of any $\omega\pi^0$ system must be $I^{CG} = 1^{-+}$. The spin and parity have been studied through analysis of the decay angular correlations in the SLAC-Berkeley experiment [Ballam et al., 1973] and both $J^P = 1^-$ and 1^+ assignments are found to be compatible with the data.

Preliminary studies of $e^+e^- \rightarrow \omega\pi^0$ from Frascati show indications of an enhancement in the cross section at a center of mass energy of ~1250 MeV [Conversi et al., 1973]. This would be further confirmation of the existence of a $J^P = 1^-$ object of mass 1250 MeV decaying into $\omega\pi^o$, since e^+e^- reactions proceed through one photon exchange.

We call this object the ρ' (1250).

4.3 ρ'' (1600)

The region above the rho meson was initially scanned for effects in $(\pi^+\pi^-)$ by several counter and track chamber experiments [Ballam et al., 1972, 1973; Park et al., 1972; Eisenberg et al., 1972; Hicks et al., 1969; McClellan et al., 1969; Bulos et al., 1971; Alvensleben et al., 1971] and no clear sign of vector meson production observed. A broad structure, about 200 MeV wide, around 1600 MeV was seen in two of the experiments on complex nucleii [Alvensleben et al., 1971; Bulos et al., 1971], but the effect was difficult to interpret since the high mass tail of the ρ^o mesons is not well understood (see fig. 47). The 4π system was subsequently studied by several track chamber experiments [Bingham et al., 1972; Davier et al., 1973] and found to exhibit a clear enhancement around 1600 MeV, as shown in fig. 48. The cross section for production of this peak was estimated to be between 1 and 1.6 μb and is independent of energy between 9 and 18 GeV. The differential cross section is shown in fig. 49 for the streamer chamber experiment, and is well fit by

$$\frac{d\sigma}{dt} = \left.\frac{d\sigma}{dt}\right)_0 \exp At$$

with a slope, A, of (5.7 ± 0.3) GeV^{-2}.

The 4π bump is identified to be mainly a $\rho^o\pi^+\pi^-$ final state. From a study of other final states the isospin of the non-rho pion pair may be determined. The fact that $\rho^o\rho^o$ is not observed excludes $I_{2\pi} = 1$, while the ratio $(\rho^o\pi^o\pi^o : \rho^o\pi^+\pi^-) \approx 0.5$, favors $I_{2\pi} = 0$ rather than $I_{2\pi} = 2$. This gives an assignment I=1 for the total bump, and since the G-parity of a 4π system is +1, the change conjugation, C must be -1 (since $G = C(-1)^I$). We then have $I^{CG} = 1^{-+}$ for the 4π state.

A study of the decay angular distribution from the linearly polarized photon experiment yields the familiar $\sin^2\theta \cos^2\Psi$ correlations we have seen in ρ^o, ω, and ϕ production, where the vector sum of the two π^+ momenta is used as the analyzer for the 4π system decay [Bingham et al., 1972]. Examples of the decay correlations are shown in fig. 50. They imply mainly natural parity exchanges in the t-channel and mainly SCHC for the production of the 4π state. In addition, they indicate that the spin-parity of the 1600 MeV bump is $J^P = 1^-$. The I=0 exchange character of the production process is further emphasized by the observation of coherent production of ρ'' (1600) on deuterium [Eisenberg et al., 1976].

Thus, the experimental information from photoproduction reactions indicate that a $(\rho^o \pi^+ \pi^-)$ enhancement with quantum numbers, I^{CG} $J^P = 1^-$, is diffractively produced at energies around 10 GeV. Such a state should be seen in e^+e^- annihilations through the one-photon-exchange process. The cross section for $e^+e^- \to \pi^+\pi^-\pi^+\pi^-$ is shown in fig. 51, where it may be observed to rise rapidly from threshold, peak around 1600 MeV and then fall rapidly as the energy further increases [Bartoli et al., 1970; Barbarino et al., 1972; Ceradini et al., 1973]. This bump may be interpreted as confirmation of the production of a vector state in e^+e^- collisions. The ratio of the $(\pi^+\pi^-\pi^o\pi^o : \pi^+\pi^+\pi^-\pi^-)$ cross sections is consistent with that expected for the decay of an I=1 $\rho^o\pi^+\pi^-$ system. It appears that the e^+e^- and γp experiments are producing the same heavy vector meson, which we call the ρ'' (1600).

Indeed, one finds good agreement between the measured peak cross section in e^+e^- annihilations and that calculated from the photoproduction data using the vector dominance model. We may write

$$\frac{\sigma(\gamma p \to \rho^o p)}{\sigma(\gamma p \to \rho'' p)_{\hookrightarrow 4\pi}} = \left(\frac{\gamma^2_{\rho''}}{\gamma^2_{\rho}}\right) \frac{\Gamma_{\rho''}}{\Gamma_{\rho'' \to 4\pi}} \tag{4.1}$$

assuming that the elastic $\rho^o p$ and $\rho'' p$ cross sections are comparable and that the process $\rho^o p \to \rho'' p$ is weak. Similarly we may relate the peak cross sections for $e^+e^- \to \rho^o$ and ρ'' through

$$\frac{\sigma(e^+e^- \to \rho^o)_{peak}}{\sigma(e^+e^- \to \rho'' \to 4\pi)_{peak}} = \left(\frac{\gamma^2_{\rho''}}{\gamma^2_{\rho}}\right) \frac{\Gamma^2_{\rho}}{\Gamma_{\rho} \cdot \Gamma_{\rho'' \to 4\pi}} \frac{M_{\rho''}}{M_{\rho}} \tag{4.2}$$

From eqns. (4.1) and (4.2), we find

$$\sigma(e^+e^- \to \rho'' \to 4\pi)_{peak} = \sigma(e^+e^- \to \rho)_{peak} \cdot \frac{M_{\rho}}{M_{\rho''}} \cdot \frac{\Gamma_{\rho}}{\Gamma_{\rho''}} \frac{\sigma(\gamma p \to \rho^o p)}{\sigma(\gamma p \to \rho'' p)_{\hookrightarrow 4\pi}} \tag{4.3}$$

Substituting the measured quantities on the right hand side of eqn. (4.3), we find

$$\sigma(e^+e^- \to \rho'' \to 4\pi) = (12 - 25) \text{ nb},$$

consistent with the measured cross section of (16 ± 5) nb from the storage ring experiments [Ceradini et al., 1973].

No other strong decay modes of the ρ'' have been observed. The 2π mode is not observed in e^+e^- reactions, while limits of $< 20\%$ and $< 14\%$ for the ratio of 2π to 4π decay have been set by the photoproduction studies in hydrogen and complex nuclear targets, respectively. However, preliminary results from a high energy experiment at FNAL [Lee, 1975], have shown a signal in both 2π and 4π in the reactions

$$\gamma Be \rightarrow \pi^+\pi^- X$$
$$\rightarrow \pi^+\pi^+\pi^-\pi^- X$$

at energies of around 80 GeV. The mass distributions, uncorrected for the apparatus detection efficiency, are shown in fig. 52. A very rough estimate of the $(2\pi/4\pi)$ branching ratio from these measurements would indicate $R > 0.05$.

A state with the same quantum numbers has been identified in a π-π scattering phase shift analysis [Hyams et al., 1975]. The data comes from a high statistics measurement [Grayer et al., 1974] of the reaction

$$\pi^- p \rightarrow \pi^+\pi^- n$$

at 17 GeV. The analysis of the (π-π) angular distribution finds evidence of a p-wave (π-π) state lying below the spin 3 state called the g-meson. The resonance has a mass $M = (1590 \pm 20)$ MeV, and width, $\Gamma = (180 \pm 50)$ MeV. The properties of this state, in terms of mass and spin-parity quantum numbers, agree well with those found in photoproduction and e^+e^- experiments, but it is much narrower, and couples more strongly to 2π. However these differences are probably the result of difficulties in interpretation of the experiments; the photoproduction (4π) bump may not be all resonant [Slattery and Ferbel, 1974], while the ρ'' (1600), found in the π-π scattering studies, is a rather small contribution to the total π-π cross section (see fig. 53).

A summary of the properties of the ρ'' (1600) are given in table 8.

4.4 New Particle Production

Near the end of 1974 there was great excitement at the discovery of a very narrow peak in the e^+e^- system at a mass of 3100 MeV from experiments at Stanford [Augustin et al., 1974] and at Brookhaven [Aubert et al., 1974]. The cross section as measured in e^+e^- collisions at SPEAR is shown in fig. 54. The width of the new particle was found to be (69 ± 15) keV. Shortly afterwards another peak was found at 3700 MeV, with a width of (225 ± 56) keV [Abrams et al., 1975]. Such narrow widths at such high mass imply some new selection rule is at work in the decay of these particles—the $\Psi(3100)$ and $\Psi'(3700)$. The most popular, and currently the most successful, model explaining the existence of these new particles invokes a new quantum number, called charm, and an additional quark—the charmed quark (c)—[DeRujula and Glashow, 1975]. The Ψ states are then described as being $(c\bar{c})$ states, very much like the ϕ meson is thought of as a system of strange quarks $(\lambda\bar{\lambda})$. Systematic studies of the decay modes of the Ψ and Ψ' have shown that they are heavy vector mesons formed via the one-photon-exchange in the e^+e^- annihilation, and that they both have $I^{CG}\, J^P = 0^{--}1^-$. One would expect these states to be produced diffractively in the photoproduction reaction.

Three experimental groups at Cornell [Gittelman et al., 1975], SLAC [Camerini et al., 1975] and FNAL [Knapp et al., 1975], have observed the photoproduction of these heavy vector mesons, over the energy range (10 - 100) GeV. In fig. 55 the effective mass of the detected $(\mu^+\mu^-)$ pair is shown for the SLAC and FNAL experiments, and the $\Psi(3100)$ signal is clearly observed.

The forward cross section for the reaction

$$\gamma N \rightarrow \Psi N \tag{4.4}$$

exhibits a very interesting energy dependence, as shown in fig. 56. The cross section rises very steeply for energies above ~11 GeV, increasing by almost two orders of magnitude ~ 18 GeV. Beyond 20 GeV the growth is quite gradual, increasing by at most a factor of two in the interval up to 100 GeV.

The differential cross section is observed to change dramatically through this region of rapid rise in the forward cross section. The measured distributions at 11 GeV [Gittelman et al., 1975] and 19 GeV [Camerini et al., 1975] are shown in fig. 57. The differential cross sections are well fit by an exponential form

$$\frac{d\sigma}{dt} = \left.\frac{d\sigma}{dt}\right|_0 \exp\,(At)$$

with the slope, A, equal to 1.25 GeV^{-2} at 11 GeV, and $\sim 3\ \mathrm{GeV}^{-2}$ at 19 GeV. The highest energy data are compatible with a slope $\sim 4\ \mathrm{GeV}^{-2}$ [Knapp et al., 1975]. This indicates that the production angular distribution is almost isotropic at energies near to the kinematic threshold, and that in the region of the rapid rise of the cross section, the distribution becomes quite sharply peaked, but does not change much as the energy is further increased.

The SLAC experiment found that inelastic photoproduction of Ψ-mesons,

$$\gamma N \rightarrow \Psi N'$$

was small, being only $\sim$20-30% of the elastic production.

The photoproduction of the other high mass particle, the $\Psi'(3700)$, is observed in both the SLAC and FNAL experiments, and the ratio of Ψ to Ψ' production at 19 GeV photon energy is measured to be

$$R = \frac{\sigma(\gamma \rightarrow \Psi)}{\sigma(\gamma \rightarrow \Psi')} = 6.8 \pm 2.4 \quad .$$

Several interesting observations may be made in applying the vector dominance model (section 5) to the above data. Taking the measured forward cross section, $\left.\frac{d\sigma}{dt}\right)_0$, and assuming that the ΨN scattering amplitude is purely imaginary we may use eqn. (5.4) to determine $\sigma^T(\Psi N)$, the total ΨN cross section, in the same way we find $\sigma^T(\rho N)$ in section 5 below. We take the photon-vector meson coupling strength from the e^+e^- experiments ($\gamma_\Psi^2/4\pi = 2.6$) and find $\sigma^T(\Psi N) \sim 1$ mb. This implies that the ΨN interaction is typically hadronic, but with a much smaller strength than the πN and ρN interaction. Recent measurements comparing the relative A-dependence of Ψ photoproduction on complex nuclei, and applying an analysis similar to that discussed in section 5.2 below, yield an estimate of $\sigma^T(\Psi N) = (3 \pm 1)$ mb, independent of the vector dominance model assumptions [Prepost, 1976; Ritson, 1976].

We may now use this value of $\sigma^T(\Psi N)$, and the measured slope of the production distribution to learn of the ratio σ_{el}/σ_T. From the optical theorem, we have a relationship between the forward elastic cross section and the total cross section

$$\left.\frac{d\sigma}{dt}\right)_0 = \frac{1}{16\pi}\,\sigma^{T^2} \tag{4.5}$$

If $\frac{d\sigma}{dt} = \left.\frac{d\sigma}{dt}\right)_0$ exp At, them we may integrate to find the elastic cross section, σ_{el}, and rewrite eqn. (4.5) as

$$\sigma_{el} = \frac{1}{16\pi A} \cdot \sigma_T^2 \tag{4.6}$$

or

$$\frac{\sigma_{el}}{\sigma_T} = \frac{1}{16\pi A} \cdot \sigma_T \tag{4.7}$$

This relation (4.6) applies both to ΨN scattering, and, through VDM, to Ψ photoproduction, and for either process we have

$$\frac{\sigma_{el}}{\sigma_T} \sim 10^{-2} .$$

This means that most of the ΨN scattering cross section is inelastic. Furthermore, for a 5 nb cross section for reaction (4.4), the total cross section for the 'Ψ-like' part of the photon must be of order 0.5 μb, or about half a percent of the total γp cross section. However, we know from the measurements discussed above that inelastic processes involving the Ψ-meson itself are only $\sim$(20 - 30)% of the elastic cross section and so negligible in this context. What then, are these inelastic 'Ψ-like' photoprocesses which must account for 1/2% of all the γp interactions? Within the context of the charmed quark model, this inelastic cross section represents the production of charmed mesons, and one may look at the steep rise of the Ψ-production cross section seen in fig. 56, as an indication of the threshold of such a process.

These are intriguing thoughts, and it will be very interesting to watch the results of the photoproduction experiments over the next few years for further insight into the nature of the Ψ and Ψ' mesons and the possibility of a charmed world.

5 VECTOR DOMINANCE AND THE PHOTON COUPLINGS

5.1 V.D.M.

The origin of the vector dominance model dates back to the early 1960's when the isovector nucleon form factor was described in terms of a strong $\pi\pi$ resonance (later identified as the ρ meson) [Frazer and Fulco, 1960; Nambu, 1957] and when Sakurai suggested that just as the electromagnetic current had a photon associated, so the isospin current and baryon current and hypercharge current had associated vector mesons, and that there would be strong coupling between the "current-associated" particles [Sakurai, 1960].

Basically, the electromagnetic interaction of hadrons is described by the coupling of the electromagnetic field to the hadronic electromagnetic current

$$j_\mu^{em}(x) = j_\mu^I(x) + \frac{1}{2}\, j_\mu^Y(x) \tag{5.1}$$

where $j_\mu^I(x)$ and $j_\mu^Y(x)$ are the zero component of the isospin and the hypercharge currents respectively. The smallness of the coupling constant, $\alpha = e^2/4\pi$, allows the photoproduction process to be treated in lowest order of the electromagnetic interaction.

The vector dominance model then connects the hadronic electromagnetic current with the fields of the vector mesons ρ^o, ω, ϕ which have the same quantum numbers as the electromagnetic current, namely J=1, P=-1, C=-1, Y=0. This connection can be made via the current field identity [Joos, 1967],

$$j_\mu^{em}(x) \equiv -\sum_V \frac{m_V^2}{2\gamma_V} V_\mu(x) = -\left[\frac{m_\rho^2}{2\gamma_\rho}\rho_\mu^o(x) + \frac{m_\omega^2}{2\gamma_\omega}\omega_\mu(x) + \frac{m_\phi^2}{2\gamma_\phi}\phi_\mu(x) + \dots\right] \tag{5.2}$$

where $\gamma_\rho, \gamma_\omega, \gamma_\phi$ are the coupling constants of the electromagnetic current to the vector meson fields $\rho_\mu(x), \omega_\mu(x), \phi_\mu(x)$ respectively and m_ρ, m_ω, m_ϕ are the masses of the vector mesons.

Initially, the model implied that the three vector mesons ρ, ω, ϕ completely saturated the above identity. The model has since been generalized to include contributions from other higher mass vector mesons in the summation of eqn. (5.2) and also to reflect the coupling of the photon to the continuum "background" seen in e^+e^- annihilations [Sakurai and Schildknecht, 1972].

The above relationship between the electromagnetic current and the vector meson fields implies that any amplitude involving real or virtual photons may be expressed as a linear combination of vector meson amplitudes each multiplied by a vector meson propagator. The assumption is usually made that the invariant vector meson amplitudes are slowly varying functions of the vector mass, m_V, and that the energy dependence comes from the propagator, not the coupling constants.

More specifically, these arguments allow one to relate vector meson photoproduction to the elastic scattering of transversely polarized vector mesons on nucleons. The relationship is written

$$\frac{d\sigma}{dt}(\gamma N \rightarrow VN) = \frac{\alpha}{4} \cdot \frac{4\pi}{\gamma_V^2} \frac{d\sigma}{dt}(VN \rightarrow VN) \tag{5.3}$$

where $\gamma_V^2/4\pi$ represents the strength of the photon-vector meson, V, coupling. This is represented diagrammatically in fig. 58a. Such a description assumes that off-diagonal terms like $V' \rightarrow V$, where V, V' are different vector mesons, do not exist (i.e., one may neglect processes like those in fig. 58b).

We may extend eqn. (5.3) by using the optical theorem to relate the forward elastic vector meson nucleon scattering to the total cross section, $\sigma^{T}(VN)$, and write:

$$\left.\frac{d\sigma}{dt}\right|_0 (\gamma N \rightarrow VN) = \frac{\alpha}{64\pi} \cdot \frac{4\pi}{\gamma_V^2} \cdot (1+\eta_V^2) \cdot \sigma_T^2(VN) \qquad (5.4)$$

where η_V is the ratio of the real to imaginary forward scattering amplitude, and $\sigma_T(VN)$, the total cross section, for the vector meson-nucleon interaction.

The photon-vector meson coupling can be measured directly in e^+e^- annihilations, where the vector meson is formed via one-photon-exchange (see fig. 58c). From a measurement of the excitation spectrum in the storage ring experiments one may determine γ_V^2 through the relation;

$$\frac{\gamma_V^2}{4\pi} = \frac{\pi\alpha^2}{12\, m_V \cdot \Gamma_{V \rightarrow e^+e^-}} \qquad (5.5)$$

where m_V is the mass of the vector meson, V, and $\Gamma\, e^+e^-$ is the partial width for its decay into lepton pairs.

Clearly the photoproduction experiments determine γ_V^2 with the photon on the mass shell (q^2=0), while the e^+e^- experiments measure the coupling strength with the vector meson on the mass shell ($q^2=m_V^2$). It is the assumption of the VDM that these couplings strengths should be the same. As we shall see below, in section 5.3, the experiments indicate reasonable agreement with this hypothesis for the ρ^o, ω, and ϕ, but are unable to exclude the possibility of some q^2 dependence. We will discuss this further later.

We may directly test the vector dominance model through a comparison of the Compton scattering process, $\gamma N \rightarrow \gamma N$ and vector meson photoproduction. The relationship may be written as

$$\frac{d\sigma}{dt}(\gamma N \rightarrow \gamma N) = \frac{\alpha}{4}\left|\sum_{V}\sqrt{\frac{d\sigma}{dt}(\gamma N \rightarrow VN)\cdot\left(\frac{4\pi}{\gamma_V^2}\right)}\, e^{i\delta_V}\right|^2 \qquad (5.6)$$

where δ_V relates the phases of the various vector meson amplitudes. Again, using the optical theorem, we can rewrite eqn. (5.6) as

$$\sigma^T(\gamma N) = \sum_{V}\sqrt{\frac{16\pi^2\alpha}{\gamma_V^2}\cdot\frac{1}{\left(1+\eta_V^2\right)}\cdot\left.\frac{d\sigma}{dt}\right|_0(\gamma N \rightarrow VN)} \qquad (5.7)$$

The equalities indicated in eqns. (5.6) and (5.7) should be attained when all of the vector couplings of the photon are identified and included in the summations. Such tests are described in section 5.4 below.

Finally, we have various predictions for the ratios of the coupling strengths at the $\gamma \rightarrow V$ vertex. Application of SU(6) predicts that

$$\frac{1}{\gamma_\rho} : \frac{1}{\gamma_\omega} : \frac{1}{\gamma_\phi} = 3 : 1 : -\sqrt{2}$$

which implies that the coupling strengths for $\gamma \rightarrow \rho, \omega, \phi$ are in the ratio

$$9 : 1 : 2 \qquad (5.8)$$

There are several calculations of symmetry breaking schemes [Oakes and Sakurai, 1967; Das, Mathur and Okubo, 1967] which alter these predicted ratios to

$$9 : 0.65 : 1.33$$

and

$$9 : 1.2 : 1$$

Further, if one includes the possibility of additional quarks as in the charm scheme, then it has been shown that for charmed quarks with charge 2/3, the predicted ratio of the couplings, including the ($c\bar{c}$) state, Ψ [Gaillard, Lee and Rosner, 1974], would be

$$\rho : \omega : \phi : \Psi = 9:1:2:8 \tag{5.9}$$

In the following sections we will consider these various relationships in the light of the available experimental data, extract the photon-vector meson coupling strength and see how well the vector dominance model holds up.

5.2 Experiments on Complex Nucleii

We have discussed the $\gamma N \rightarrow VN$ reaction in sections 3 and 4 above and have shown that it has the characteristics of a diffractive process. In this section we review experiments studying the coherent photoproduction of vector mesons on complex nuclear targets. These experiments are of interest since they provide information on the vector meson-nucleon interaction from studies of the absorption in nuclear matter and they also allow an independent measurement of the photon-vector meson coupling strength. We first discuss the analysis of the experiments and then review the data.

Since for energies above a few GeV almost all the photoproduced vector mesons live long enough to traverse the nucleus and decay in vacuum, it was suggested that by observing the relative yield of vector mesons transmitted through varying path lengths of nuclear matter, the total interaction cross section for the vector mesons on nucleons could be determined [Drell and Trefil, 1966; Ross and Stodolsky, 1966]. Such a scheme is shown schematically in fig. 59, where the variation in nuclear path length is achieved by studying the A-dependence of the forward cross section for the reaction:

$$\gamma A \rightarrow VA$$

More quantitatively, we may write, after applying Glauber multiple scattering theory [Franco and Glauber, 1966];

$$f_0(\gamma A \rightarrow VA) = f_0(\gamma N \rightarrow VN) \int d^2b \int dz\ \rho(\bar{b}, z) \exp(iq_{\parallel} z + iq_{\perp} \bar{b})$$
$$\times \exp\left(-\frac{1}{2}\sigma_{VN}(1 - i\eta_V)\ T\right) \qquad (5.10)$$

where $\rho(\bar{b}, z)$ is the nuclear density distribution, $q_{\parallel}$ is the longitudinal momentum transfer necessary to put the vector meson, V, on its mass shell, $\bar{q}_{\perp}$ is the transverse momentum transfer, with $t = -\left(q_{\perp}^2 + q_{\parallel}^2\right)$, and

$$T = \int_z^{\infty} dz' \cdot \rho(\bar{b}, z')$$

This describes the process in which a photon converts into a vector meson at $(\bar{b}, z)$ where $\bar{b}$ is the impact parameter and z is the distance along the incident photon direction. The probability of the conversion is given in terms of the average of the forward photoproduction amplitude for protons and neutrons, $\left.\frac{d\sigma}{dt}\right|_0 (\gamma N \rightarrow VN) = |f_0|^2$. The vector meson amplitude is then subject to absorption and refraction in passing through the remaining nuclear matter.

Assuming $\rho(\bar{b}, z)$ is known, the relative A-dependence allows a determination of the total vector meson-nucleon cross section, σ_{VN}, and therefore the forward scattering amplitude through the relation

$$f_0(VN \rightarrow VN) = \frac{ik}{4\pi}\sigma^T(VN)(1 - i\eta_V) \qquad (5.11)$$

where η_V is the ratio of real to imaginary forward scattering amplitudes. This determination of $f_0(VN \rightarrow VN)$ is obtained from the measured A dependence only, and is independent of the vector dominance model. The absolute nomalization of the cross section for the reaction determines $f_0(\gamma N \rightarrow VN)$ through vector dominance, and allows a determination of the photon-vector meson coupling strength, $(\gamma_V^2/4\pi)$.

It is interesting to note that the amplitude in eqn. (5.10) differs from an elastic scattering amplitude by the phase factor involving the interference between the longitudinal momentum transfer and the real part of the scattering amplitude. This is an important factor in determining the forward cross section, especially at low photon energies [Swartz and Talman, 1969].

The nuclear density distributions most commonly used in the analysis of these experiments are:

a) the harmonic oscillator, for low A nuclei

$$\rho(r) = \rho_0 \left(1 + \alpha \frac{r^2}{a_0^2}\right) \exp\left(-\frac{r^2}{a_0^2}\right) \tag{5.12}$$

where α=4/3 for carbon, and 5/6 for beryllium and a_0 is a parameter of the fit; and

b) the Wood-Saxon distribution, for heavy nuclei

$$\rho(r) = \rho_0 \left[1 + \exp\left\{(r-R)/\epsilon\right\}\right]^{-1} \tag{5.13}$$

where R is the nuclear radius and $\epsilon = 0.545$ fermi.

Modifications to these distributions to make allowance for two-body correlations have generally been applied in the data analysis [von Bockman, 1969; Bauer, 1971].

There remains the question of what nuclear radius to use in a particular density distribution. The DESY-MIT group [Alvensleben et al., 1970] determined the nuclear radius as a function of A from their measurements of the t-distribution in the reaction $\gamma A \rightarrow \rho^o A$. They found $R(A) = (1.12 \pm 0.02)\, A^{1/3}$ fermi. Other choices of radius are derived from electron scattering data or from fits to neutron-nucleus, and proton-nucleus total cross section data. The results of the analyses do not strongly depend on which nuclear radii are used.

A summary of the experiments studying the coherent vector meson production on complex nuclei is given in table 9. The most extensive measurements are those of the DESY-MIT and CORNELL groups for ρ^o photoproduction, and CORNELL on ϕ production, while the Rochester-Cornell and DESY groups provide the only heavy nuclei data on ω production. An example of the DESY-MIT measurements on

$$\gamma A \rightarrow \pi^+ \pi^- A$$

at 6 GeV, is given in fig. 60 where the $\pi^+\pi^-$ mass spectrum is shown as a function of momentum transfer for thirteen different targets. The CORNELL measurement of the differential cross section for ϕ photoproduction in the reaction

$$\gamma A \rightarrow K^+ K^- A$$

at 6 GeV, is shown in fig. 61. The sharp forward peak characteristic of a coherent process is clearly observed. Finally fig. 62 shows the differential cross section for ω photoproduction from beryllium and copper targets from the Rochester-Cornell experiment.

The analysis of these experiments has proven to be nonunique, in that due to the very strong correlation between the size of the total vector meson-nucleon cross section and the ratio of the real to imaginary parts of the forward scattering amplitude, they have been unable to separately determine all three unknowns $\sigma(VN)$, η_V, $(\gamma_V^2/4\pi)$. In general, if one is known, then the other two quantities are well determined.

The analyses of the heavy nuclei experiments are usually expressed as the correlated determination of η_V and $\sigma(VN)$, and subsequently a choice of $\sigma(VN)$ fixes the value of the coupling strength, $(\gamma_V^2/4\pi)$. An example of such an analysis for the ρ^o data is shown in fig. 63. The χ^2 contours indicate the strong correlation between η_ρ and $\sigma(\rho N)$ by the narrow valley running across the plot. Roughly speaking it indicates that $\sigma(\rho N) = (32 + \eta_\rho/.05)$ mb. Also indicated on fig. 63 are the limits on η_ρ from the interference experiments $(\eta_\rho = -.2 \pm .1)$ [Alvensleben et al., 1970], and from the Compton scattering analysis $(\eta_\rho = -0.24 \pm 0.03)$ (see section 2.2).

The ρ^o data has been analyzed by the DESY-MIT [Alvensleben et al., 1970a] and CORNELL [McClellan et al., 1971a] groups, and recently both experiments and analyses were very beautiful reviewed and independently evaluated [Spittal and Yennie, 1975]. Good agreement is obtained among the different analyses and if η_ρ is taken to be -0.2 for energies around 7 GeV, then

$$\sigma^T(\rho N) = 28 \pm 1.5 \text{ mb}$$

and

$$\gamma_\rho^2/4\pi = 0.61 \pm .03 \qquad . \tag{5.14}$$

Fortunately, in the case of the ρ^o data another experiment allows the determination of $\sigma^T(\rho N)$ independent of the question on the size of the real part, η_ρ. These measurements comes from a study of coherent

ρ^o production from deuterium at 6, 12 and 18 GeV, and for large momentum transfers ($t > .6$ GeV^2) [Anderson et al., 1971]. The requirement that the deuteron remain bound causes the reaction to be dominated by a two-step process in which the ρ^o is produced on one nucleon and scatters on the other, giving approximately equal recoils to both nucleons. Therefore, at large t values this double scattering amplitude is roughly given by the product of the rho production and scattering amplitudes ($f_{\gamma \to \rho} \cdot f_{\rho \to \rho}$), and is proportional to $\sigma^2(\rho N)/\gamma_\rho$ and independent of η_ρ, while at small t it is proportional to $\sigma(\rho N)/\gamma_\rho$. They find that their data is well described at all t-values, and at all three energies with $\sigma^T(\rho N) = (28.6 \pm .5)$ mb, and $\gamma_\rho^2/4\pi = (0.69 \pm .04)$.

The Rochester-Cornell experiments [Behrend et al., 1970 ; Abramson et al., 1975] provide the best data on ω photoproduction in heavy nuclei. The analysis leans heavily on the knowledge of ρN scattering, and on the one-pion-exchange model description of the nondiffractive contribution to the ω production process. They obtain

$$\sigma(\omega N) = 25.4 \pm 2.7 \text{ mb}$$

and

$$\frac{\gamma_\omega^2}{4\pi} = 7.5 \pm 1.3 \tag{5.15}$$

The analysis of the ϕ data exhibits the same strong correlation between $\sigma(\phi N)$, $(\gamma_\phi^2/4\pi)$ and η_ϕ, discussed above for the ρ^o, only in this case we have no good independent information on either η_ϕ or $\sigma(\phi N)$. A measurement of the ratio of real to imaginary forward ϕ-N amplitudes, η_ϕ, was obtained by observing the interference between $\phi \to e^+e^-$ decays and the Bethe-Heitler pair production process [Alvensleben et al., 1971].

Unfortunately this is a very difficult experiment and the result— $\eta_\phi = 0.48^{+.33}_{-.45}$ —does not allow a strong constraint on these analyses. The results of the CORNELL analysis [McClellan et al., 1971] are shown in fig. 64, where both $(\gamma_\phi^2/4\pi)$ and $\sigma(\phi N)$ are plotted against possible values of η_ϕ. If one assumes that the total cross section is equal to the quark model value of 13 mb, then $\eta_\phi \sim -0.22$ and $\gamma_\phi^2/4\pi \sim 6.5$, twice the value found in e^+e^- annihilation experiments. If, on the other hand, $\gamma_\phi^2/4\pi$ is taken consistent with the storage ring value then $\eta_\phi \sim -0.5$ and $\sigma(\phi N) \sim 8$ mb.

The results from these experiments on coherent photoproduction of ρ^o, ω, and ϕ-mesons are discussed with the other determinations of the photon coupling strength in section 5.3 below.

5.3 Photon-Vector Meson Coupling Strength $(\gamma_V^2/4\pi)$

5.3.1 General

In this section we summarize the various measurements of the photon-vector meson couplings and evaluate how well the vector dominance model works.

5.3.2 Storage ring experiments

The vector mesons are strongly produced e^+e^- annihilations via the one-photon-exchange process. In fig. 65 the ratio of the total hadronic cross section to the point cross section for the production of muon pairs is shown for data from Orsay [Benaksas et al., 1972], Frascati [Salvini, 1974] and SLAC [Augustin et al., 1975]. The ρ, ω, ϕ mesons are clearly seen, as are the new narrow states, the Ψ and Ψ' mesons. In table 10 the leptonic widths obtained from this data, are given together with the coupling strength, as calculated via eqn. (5.5).

The couplings of the first four entries in table 10 are expected to be in the ratio 9:1:2:8, as discussed in relation (5.9) above. The experimental results indicate

$$9:(1.25\pm 0.1) : (2.04\pm 0.2) : (2.22\pm 1.1) \quad . \qquad (5.16)$$

The "old" mesons seem to work fairly well, but the Ψ meson misses by about a factor of four. This may be an indication of some problems with VDM, or that the charmed quark does not have charge 2/3, or perhaps, there is after all, some q^2 dependence of the coupling constant, and the values at $q^2=0$, and for $q^2=m_\Psi^2$ are indeed different. For the case of the Ψ meson, q^2 is large and of order 10 GeV^2 and so would be sensitive to such a variation. Another possibility is that there are other contributions to the $\gamma N \rightarrow \Psi N$ process, such as the off-diagonal terms ($V' \rightarrow V$, $V' \neq V$), which have been neglected in the vector dominance model calculations. See, for example fig. 66. (This possibility will be further discussed below in connection with ϕ photoproduction in section 5.3.3.)

An interesting observation on the relative vector meson coupling [Yennie, 1975] points out that the predicted SU(6) relationship for the $\rho:\omega:\phi:\Psi$ couplings (eqn. (5.9)) is rather well obeyed by the leptonic widths if not by the coupling strengths themselves. He showed that

$$\frac{\Gamma_{\rho\rightarrow e^+e^-}}{9} : \frac{\Gamma_{\omega\rightarrow e^+e^-}}{1} : \frac{\Gamma_{\phi\rightarrow e^+e^-}}{2} : \frac{\Gamma_{\Psi\rightarrow e^+e^-}}{8}$$

$$= (0.72\pm .1) : (0.76\pm .08) : (0.67\pm .07) : (0.6\pm .09) \qquad (5.17)$$

since

$$\Gamma_{e^+e^-} \propto \frac{m_v}{\gamma_v^2} \quad ,$$

an indication of some q^2 dependence in the coupling strength, and would indicate corrections to our treatment of the ρ, ω and ϕ mesons.

The values of $(\gamma_V^2/4\pi)$ obtained from the storage ring measurements are listed on the first line of table 11.

5.3.3 Photoproduction experiments

The experiments on coherent production, discussed above in section 5.2 provide a measurement of the total cross section, $\sigma(VN)$, from the observed A-dependence (given additional information of η_V) while the absolute normalization of the cross sections allows the extraction of the photon coupling strengths $(\gamma_V^2/4\pi)$.

In table 12, a summary of the various attempts to extract $\sigma(VN)$ are presented. The quark model relates the vector meson cross section to the measured $\pi^{\pm}p$ data through

$$\begin{aligned} \sigma(\rho^o p) = \sigma(\omega p) &= \frac{1}{2}\left[\sigma(\pi^+ p) + \sigma(\pi^- p)\right] \\ &= 27 \text{ mb.} \end{aligned} \tag{5.18}$$

$$\begin{aligned} \sigma(\phi p) &= \sigma(K^+ p) + \sigma(K^- n) - \sigma(\pi^+ p) \\ &= 13 \text{ mb.} \end{aligned}$$

The double scattering experiment on deuterium [Anderson et al., 1971], discussed above, provides a good measurement of $\sigma(\rho^o p)$, independent of assumptions on η_ρ. The analysis of the A-dependence of the ρ^o and ω data, together with an assumed $\eta_\rho = \eta_\omega \sim -0.2$ yields values of $\sigma(VN)$ in good agreement with the quark model cross sections. The ϕ cross section is given for two values of the ratio of real to imaginary amplitudes, $\eta_\phi = -.25$ and $-.5$. Also shown are estimates of the total cross section obtained using the VDM relation (5.4) and the storage ring value of $(\gamma_V^2/4\pi)$ together with the measured forward cross section on protons, $\frac{d\sigma}{dt}_0(\gamma p \rightarrow Vp)$. The data for ρ^0 and ω are in good agreement with each other and with the quark model, while for the ϕ the cross section is (8-9) mb and substantially smaller than the quark model value.

Having determined $\sigma(VN)$, the experiments on coherent production then provide measurement of the couplings $(\gamma_V^2/4\pi)$. These are listed on lines two and three in table 11. The other entries in table 11 are obtained from photoproduction experiments on hydrogen and deuterium targets. In line 4 the measured forward cross section for vector meson production is used together with the VDM relation (5.4), the quark model values of the vector meson-nucleon total cross sections and an estimate of $\eta_\rho = \eta_\omega = -0.2$ to yield a value of $(\gamma_V^2/4\pi)$. In line 5 these calculations are repeated for the ϕ data, but using $\sigma^T(\phi N) = 9$ mb, rather than the quark model value of 13 mb. Finally, since $\sigma(VN)$ and η_V are the same for the rho and omega mesons, the ratio of the forward ρ^0 and ω production cross section directly measures $(\gamma_\omega^2/4\pi)$ given that $(\gamma_\rho^2/4\pi)$ is known. In line 6 the values for $(\gamma_\omega^2/4\pi)$ obtained from studies of ρ^0 and ω production in hydrogen and deuterium are listed.

Table 11 also includes a column for the coupling of the $\rho''(1600)$. The photoproduction value is obtained from the ratio of the coherent ρ^0 and ρ'' production in the 7.5 GeV bubble chamber experiment [Alexander et al., 1975], in which they find

$$R = \frac{\frac{d\sigma}{dt}(\gamma D \rightarrow \rho D)}{\frac{d\sigma}{dt}(\gamma D \rightarrow \rho'' D)} = 6.0 \pm 1.2 \qquad (5.19)$$

If one assumes that the ρ''N scattering has the same phase and total cross section as ρN scattering, and $\gamma_\rho^2/4\pi = 0.64$ then one obtains $\gamma_{\rho''}^2/4\pi = 3.8 \pm 0.8$. This has to be compared with the value from the storage rings of (2.8 ± 0.5) [Grilli et al., 1973].

The agreement among the different methods on the value of $(\gamma_\rho^2/4\pi)$ ($\sim$0.65) is very good—perhaps surprisingly good when one considers the number of steps and approximations that go into the evaluation. For $\gamma_\omega^2/4\pi$ ($\sim$5.0), there is also good agreement (at the 15% level), between the various estimates if one excludes those derived from the Rochester-Cornell experiment.† The values of the coupling constants derived from the forward cross section in hydrogen and deuterium using all other experiments, agree well with the storage ring values.

For the ϕ meson the uncertainty in the value of η_ϕ makes it difficult to draw a conclusion. Two clear possibilities emerge:

a) from the A-dependence studies summarized in fig. 64, we see that the coupling constant would be consistent with the storage ring determination if η_ϕ were ~ -0.5. This implies that $\sigma(\phi N) \sim 9$ mb (line 2, table 11 and line 5, table 12). The data on hydrogen and deuterium, using eqn. (5.4), are also consistent with the storage ring $(\gamma_\phi^2/4\pi)$, if $\sigma(\phi N) \sim 9$ mb (line 5, table 11).

---

†The values of $\gamma_\omega^2/4\pi$ on line 4 based on that experiment were not averaged with all of the other ω data since their measured cross section were so much lower than the other experiments. (See back to section 3.3.3 and table 7.) The values of $\gamma_\omega^2/4\pi$ from this experiment are consequently much higher than the others; they are shown in parenthesis in line 4 of table 11.

b) if one assumes that the quark model cross section $\sigma(\phi N) = 13$ mb is correct, then the heavy nuclei experiments imply that η_ϕ must be $\sim -.2$ and $\gamma_\phi^2/4\pi \sim 6$, i.e., about twice the value from the e^+e^- experiments (line 2, table 11). In this case the forward cross sections from hydrogen and deuterium, also yield $\gamma_\phi^2/4\pi \sim 6$ (line 4, table 11).

Thus a consistent picture is possible and good agreement with the vector dominance model, if $\sigma(\phi N) \sim 9$ mb. This solution implies a large real part for forward (ϕN) scattering, consistent with the measurements on η_ϕ discussed above. Otherwise, a more conventional picture of nearly imaginary (ϕN) scattering and the canonical quark model cross section, implies that $(\gamma_\phi^2/4\pi)$ is about twice the expected VDM value of $2.83 \pm .2$.

There are other possible explanations of the ϕ problems. It has been suggested [Bauer and Yennie, 1975] that off-diagonal terms have been neglected in the vector dominance relation discussed in eqn. (5.3) and eqn. (5.4) above, and that processes like that shown in fig. 58b with $V' = \phi$, and $V = \omega$, may contribute. Such processes would mean that the ϕ meson is not a pure strange quark state, but involves a small admixture of the nonstrange quark state. The physical ϕ, ω states were allowed to mix through the relations:

$$\begin{aligned} |\phi\rangle &= \cos\beta\,|s\rangle + \sin\beta\,|ns\rangle \\ -|\omega\rangle &= -\sin\beta\,|s\rangle + \cos\beta\,|ns\rangle \end{aligned} \tag{5.20}$$

where $|s\rangle$ denotes a state of strange quarks and $|ns\rangle$ a state of non-strange quarks. If θ is the mixing angle from the pure SU(3) octet and singlet states $(|\phi^o\rangle, |\omega^o\rangle)$, and θ_q is the magic mixing angle (tan $\theta_q = 1/\sqrt{2}$ or $\theta_q = 35.26^o$) whereby the physical $|\phi\rangle$, $|\omega\rangle$ states consist of only strange and nonstrange quarks, respectively, then $\beta = (\theta - \theta_q)$. Silverman extending Bauer and Yennie's original calculation, claims that good agreement can be obtained for a value of $\beta \sim 8^o$. [Silverman, 1975]. However, it is important to remember that β is not a free parameter in such a model, but that there are strong constraints on the value of θ ($= \beta + \theta_q$) from conventional meson spectroscopy [Barash-Schmidt et al., 1974; Samios et al., 1974]. From these considerations, it would seem unlikely that θ could be more than a few degrees different from θ_q, and therefore one would expect $\beta \lesssim 5^o$.

Yet another possibility is that the basic vector dominance assumption of q^2 independence of the couplings may not be valid, i.e.,

$$\gamma_V^2(q^2 = 0) \neq \gamma_V^2\left(q^2 = m_V^2\right) \quad .$$

The discussion on the Ψ meson couplings in section 5.3.2 above, may be an indication that such a q^2 dependence of the vector meson-photon couplings has to be taken into account. For the purpose of this review, we merely leave this as an interesting remark.

5.4 <u>Compton Sum Rule Test</u>

In this section we consider yet another check of the vector dominance model introduced above in section 5.1, namely testing the Compton sum rule through eqns. (5.6) and (5.7).

First we consider the ratio, R, developed from the eqn. (5.7)

$$R = \sqrt{\left.\frac{d\sigma}{dt}\right|_0 (\gamma N \rightarrow \gamma N)} \Bigg/ \sqrt{\frac{\alpha}{4} \cdot \sum_V \left(\frac{4\pi}{\gamma_V^2}\right) \cdot \left.\frac{d\sigma}{dt}\right|_0 (\gamma N \rightarrow VN)} \qquad (5.21)$$

where N refers to production from a proton, or coherent production from a deuteron. The forward cross section measurements used to calculate R are listed in table 13. For the 9.3 GeV hydrogen data the ρ^o accounts for 71% of the summation in the denominator, the ω for 9%, the ϕ for 6% and the $\rho''(1600)$ for 14%. The value of the ratio R, for the three energies was found to be

$$\begin{aligned} &\text{at 4.3 GeV, on deuterium, } R = 1.20 \pm 0.09 \\ &\text{at 7.5 GeV, on deuterium, } R = 1.26 \pm 0.09 \\ &\text{at 9.3 GeV, on hydrogen, } R = 1.19 \pm 0.07 \end{aligned} \tag{5.22}$$

These values of R imply that ~20% of the vector meson contribution to the Compton amplitude are still missing.

A similar story emerges in considering the test as a function of momentum transfer, as indicated in eqn. (5.6). In fig. 67, the ratio of the predicted Compton cross section from the right hand side of eqn. (5.6) is divided by the actual measured cross section as a function of t for energies of 3.5 and 16 GeV. The assumption is made that the ratios of real to imaginary parts of the forward vector meson scattering amplitudes are the same, which should be a good assumption for the ρ^o and ω, and the error introduced in the case of the ϕ is negligible. The storage ring values for $(\gamma_V^2/4\pi)$ are used. The t-dependence of both the Compton scattering and the vector meson production are similar, but there must be missing contributions from other vector mesons if the sum rule is to be satisfied. (Note this t-dependent comparison did not include the contributions from the $\rho''(1600)$.)

Both tests imply that ~20% additional contribution is required beyond ρ^o, ω, ϕ and ρ'' to satisfy the sum rule, and verify the VDM relation. (The contributions of Ψ and Ψ' are negligible.)

There are many claims on this missing 20%. Yennie estimates that there should be a contribution from nonresonant 2π final states included in the summation on the denominator of eqn. (5.21) which would add another 10% [Yennie, 1975a]. There are also the contributions from the higher mass vector continuum, which have been estimated at ~20% [Sakurai and Schildknecht, 1972]. So the naive vector dominance picture in which the ρ^o, ω, ϕ mesons completely saturate the photon's vector field couplings is clearly wrong, but the generalized picture which includes the higher mass states, may work reasonably well.

5.5 Summary

Vector dominance has worked well as a guide to the qualitative features of vector meson photoprocesses, and has been especially useful in its naive form of ρ^o dominance. More quantitatively, we have seen that it works well for the ρ^o meson, and perhaps the ω meson, but that signs of trouble emerge with the ϕ and the Ψ mesons. It appears that to obtain a good quantitative description of photoreactions the vector dominance model will have to take into account the possibility of the mixing of the vector meson states and of off-diagonal contributions to the scattering process ($V' \rightarrow V$, where $V' \neq V$). It is also likely that the VDM will have to incorporate some q^2 dependence of the couplings.

6 CONCLUSION

We have reviewed the exclusive diffractive reactions of the photon, and found that they behave very much like other hadronic processes:

- the total cross section shows the same behavior with energy as other meson-nucleon interactions, namely, a rapid fall-off with energy as meson exchange processes die out, a flattening out as the diffractive amplitude dominates and finally we expect to see the total photon-nucleon cross section rising around energies of (200 - 300) GeV.
- the elastic scattering, and the quasi-elastic reaction (vector meson photoproduction), behave very much like other meson-nucleon scattering reactions;
    - little energy dependence in the cross section,
    - sharply peaked scattering distribution, with an indication of steepening in the very forward direction,
    - mainly imaginary forward scattering amplitude,
    - mainly natural parity exchange,
    - mainly I=0 exchange,
    - mainly s-channel helicity conservation.

The vector dominance model gives a good guide to the systematics of the photon-nucleon interaction and for the lower mass states, allows calculations to 10 - 20% precision. However, it appears that additional effects such as mixing of states and/or a q^2 dependence of the coupling will have to be included to allow a good description of the high mass vector meson processes.

ACKNOWLEDGEMENTS

I would like to thank Dr. E. Kogan for many invaluable discussions during the preparation of this review, and Drs. M. Ferro-Luzzi, E. Kogan and Prof. F. Gilman for reading the manuscript.

REFERENCES

Abrams, G.S., Briggs, D., Chinowsky, W., Friedberg, C.E., Goldhaber, G., Hollebeek, R.J., Kadyk, J.A., Litke, A., Lulu, B., Pierre, F., Sadoulet, B., Trilling, G.H., Whitaker, J.S., Wiss, J., Zipse, J.E., Augustin, J.-E., Boyarski, A.M., Breidenbach, M., Bulos, F., Feldman, G.J., Fischer, G.E., Fryberger, D., Hanson, G., Jean-Marie, B., Larsen, R.R., Lüth, V., Lynch, H.L., Lyon, D., Morehouse, C.C., Paterson, J.M., Perl, M.L., Richter, B., Rapidis, P., Schwitters, R.F., Tanenbaum, W., and Vannucci, F. (1975), Phys. Rev. Lett. 33, 1453.

Abramson, J., Andrews, D.E., Harvey, J., Lobkowicz, F., May, E.N., Nelson, C.A., Singer, M., Thorndike, E.M. (1976), Rochester University report UR-566 (submitted for publication).

Alexander, G., Bar-Nir, I., Brandstetter, A., Benary, O., Gandsman, J., Levy, A., Oren, Y., Ballam, J., Chadwick, G.B., Menke, M.M., Eisenberg, Y., Haber, B., Kogan, E., Ronat, E.E., Shapira, A., Yekutieli, G. (1972), Phys. Rev. D 5, 15; ibid. D 8, 1965; ibid. D 9, 644.

Alexander, G., Gandsman, J., Jacobs, L.D., Levy, A., Lissauer, D., Rosenstein, L.M. (1973), Nucl. Phys. B 61, 32; ibid. B 68, 1; ibid. B 69, 445.

Alexander, G., Benary, O., Gandsman, J., Levy, A., Lissauer, D., Oren, Y. (1975), Tel Aviv University preprint TAUP-481-75 (unpublished).

Alvensleben, H., Becker, U., Chen, M., Cohen, K.J., Edwards, R.T., Knasel, T.M., Marshall, R., Quinn, D.J., Rohde, M., Sanders, G.H., Schubel, H., Ting, Samuel C.C. (1970), Phys. Rev. Lett. 25, 1377. See also (1971), Nucl. Phys. B 25, 342.

Alvensleben, H., Becker, U., Bertram, William K., Chen, M., Cohen, K.J., Knasel, T.M., Marshall, R., Quinn, D.J., Rohde, M., Sanders, G.H., Schubel, H., Ting, Samuel C.C. (1970a), Nucl. Phys. B 18, 333.

Alvensleben, H., Becker, U., Busza, W., Chen, M., Cohen, K.J., Edwards, R.T., Mantsch, P.M., Marshall, R., Nash, T., Rohde, M., Sadrozinski, H.F.W., Sanders, G.H., Schubel, H., Ting, Samuel C.C., Wu, Sau-Lan (1971), Phys. Rev. Lett. 27, 444.

Alvensleben, H., Becker, U.J., Bertram, William K., Chen, M., Cohen, K.J., Edwards, R.T., Knasel, T.M., Marshall, R., Quinn, D.J., Rohde, M., Sanders, G.H., Schubel, H., Ting, Samuel C.C. (1971a), Phys. Rev. Lett. 26, 273.

Alvensleben, H., Becker, U., Biggs, P., Binkley, M., Busza, W., Chen, M., Cohen, K.J., Coleman, E., Edwards, R.T., Mantsch, P.M., Marshall, R., Nash, T., Quinn, D.J., Rohde, M., Sadrozinski, H.F.W., Sanders, G.H., Schubel, H., Ting, Samuel C.C., Wu, Sau Lan (1972), Phys. Rev. Lett. 28, 66.

Anderson, R.L., Gustavson, D., Johnson, J., Overman, I., Ritson, D., Wiik, B.H., Talman, R., Walker, J.K., Worcester, D. (1970), Phys. Rev. Lett. 25, 1218.

Anderson, R., Gustavson, D., Johnson, J., Ritson, D., Wiik, B.H., Jones, W.G., Kreinick, D., Murphy, F., Weinstein, R. (1970a), Phys. Rev. D 1, 27.

Anderson, R.L., Gustavson, D., Johnson, J., Overman, I., Ritson, D.M., Wiik, B.H., Talman, R., Worcester, D. (1971), Phys. Rev. D 4, 3245.

Anderson, R.L., Gottschalk, B., Gustavson, D.B., Ritson, D.M., Weitsch, G.A., Wiik, B.H., Halpern, H.J., Prepost, R., Tompkins, D.H. (1973), Phys. Rev. Lett. 30, 149.

Armstrong, T.A., Hogg, W.R., Lewis, G.M., Robertson, A.W., Brookes, G.R., Clough, A.S., Freeland, J.H., Galbraith, W., King, A.F., Rawlinson, W.R., Tait, N.R.S., Thompson, J.C., Tolfree, D.W.L. (1972), Phys. Rev. D 5, 1640; Nucl. Phys. B 41, 445.

Aubert, J.J., Becker, U., Biggs, P.J., Burger, J., Chen, M., Everhart, G., Goldhagen, P., Leong, J., McCorriston, T., Rhoades, T.G., Rohde, M., Ting, Samuel C.C., Wu, Sau Lan, Lee, Y.Y. (1974), Phys. Rev. Lett. 33, 1404.

Augustin, J.-E., Boyarski, A.M., Breidenbach, M., Bulos, F., Dakin, J.T., Feldman, G.J., Fischer, G.E., Fryberger, D., Hanson, G., Jean-Marie, B., Larsen, R.R., Lüth, V., Lynch, H.L., Lyon, D., Morehouse, C.C., Paterson, J.M., Perl, M.L., Richter, B., Rapidis, P., Schwitters, R.F., Tanenbaum, W.M., Vannucci, F., Abrams, G.S., Briggs, D., Chinowsky, Friedberg, C.E., Goldhaber, G., Hollebeek, R.J., Kadyk, J.A., Lulu, B., Pierre, F., Trilling, G.H., Whitaker, J.S., Wiss, J., Zipse, J.E. (1974), Phys. Rev. Lett. 33, 1406.

Augustin, J.-E., Boyarski, A.M., Breidenbach, M., Bulos, F., Dakin, J.T., Feldman, G.J., Fischer, G.E., Fryberger, D., Hanson, G., Jean-Marie, B., Larsen, R.R., Lüth, V., Lynch, H.L., Lyon, D., Morehouse, C.C., Paterson, J.M., Perl, M.L., Richter, B., Schwitters, R.F., Vannucci, F., Abrams, G.S., Briggs, D., Chinowsky, W., Friedberg, C.E., Goldhaber, G., Hollebeek, R.J., Kadyk, J.A., Trilling, G.H., Whitaker, J.S., Zipse, J.E. (1975), Stanford Linear Accelerator Center preprint SLAC-PUB-1520 (unpublished).

Ballam, J., Chadwick, G.B., Gearhart, R., Guiragossián, Z.G.T., Murray, J.J., Seyboth, P., Sinclair, C.K., Skillicorn, I.O., Spitzer, H., Wolf, G., Bingham, H.H., Fretter, W.B., Moffeit, K.C., Podolsky, W.J., Rabin, M.S., Rosenfeld, A.H., Windmolders, R., Milburn, R.H. (1972), Phys. Rev. D 5, 545; and also Bingham, H.H., Fretter, W.B., Podolsky, W.J., Rabin, M.S., Rosenfeld, A.H., Smadja, G., Ballam, J., Chadwick, G.B., Eisenberg, Y., Gearhart, R., Kogan, E., Moffeit, K.C., Murray, J.J., Seyboth, P., Sinclair, C.K., Skillicorn, I.O., Spitzer, H., Wolf, G. (1973), Phys. Rev. D 8, 1277.

Ballam, J., Chadwick, G.B., Eisenberg, Y., Kogan, E., Moffeit, K.C., Seyboth, P., Skillicorn, I.O., Spitzer, H., Wolf, G., Bingham, H.H., Fretter, W.B., Podolsky, W.J., Rabin, M.S., Rosenfeld, A.H., Smadja, G. (1973), Phys. Rev. D 7, 3150.

Ballam, J., Chadwick, G.B., Eisenberg, Y., Kogan, E., Moffeit, K.C., Skillicorn, I.O., Spitzer, H., Wolf, G., Bingham, H.H., Fretter, W.B., Podolsky, W.J., Rabin, M.S., Rosenfeld, A.H., Smadja, G., Seyboth, P. (1974), Nucl. Phys. B 76, 375; see also Bingham, H.H., Fretter, W.B., Podolsky, W.J., Rabin, M.S., Rosenfeld, A.H., Smadja, G., Yost, G.P., Ballam, J., Chadwick, G.B., Eisenberg, Y., Kogan, E., Moffeit, K.C., Seyboth, P., Skillicorn, I.O., Spitzer, H., Wolf, G. (1972), Phys. Lett. B 41, 635.

Barash-Schmidt, N., Barbaro-Galtieri, A., Bricman, C., Chaloupka, V., Chew, D.M., Kelly, R.L., Lasinski, T.A., Rittenberg, A., Roos, M., Rosenfeld, A.H., Söding, P., Trippe, T.G., Uchiyama, F. (1974), Particle Property Tables, Lawrence Berkeley Laboratory report (unpublished).

Barbiellini, G., Bozzo, M., Darriulat, P., Diambrini-Palazzi, G., De Zorzi, G., Fainberg, A., Ferrero, M.I., Holder, M., McFarland, A., Maderni, G., Orito, S., Pilcher, J., Rubbia, C., Santroni, A., Sette, G., Staude, A., Strolin, P., Tittel, K. (1972), Phys. Lett. B 39, 663.

Barbarino, G., Grilli, M., Iarocci, E., Spillantini, P., Valente, V., Visentin, R., Ceradini, F., Conversi, M., Paoluzi, L., Santonico, R., Nigro, M., Trasatti, L., Zorn, G.T. (1972), Nuo. Cim. Lett. 3, 689.

Bartoli, B., Coluzzi, B., Felicetti, Silvestrini, V., Goggi, G., Scannicchio, D., Marini, G., Massa, F., Vanoli, F. (1970), Nuo. Cim. 70, 615; see also (1972), Phys. Rev. D 6, 2374.

Barger, V., Philips, R. (1971), Nucl. Phys. B 32, 93.

Barish, B., Gomez, R., Kreinick, D., Peck, C., Pine, J., Sciulli, F., Sherwood, B., Tollestrup, A., Young, K. (1972), Phys. Rev. D 9, 566.

Bauer, T., Yennie, D.R. (1970), Phys. Rev. Lett. 25, 485.

Bauer, T. (1971), Phys. Rev. D 3, 2671.

Bauer, T., Yennie, D. (1975), Cornell preprint (unpublished).

Behrend, H.-J., Lobkowicz, F., Thorndike, E.H., Wehmann, A.A., Nordberg, Jr., M.E. (1970), Phys. Rev. Lett. 24, 1246.

Behrend, H.-J., Lee, C.K., Lobkowicz, F., Thorndike, E.H., Wehmann, A.A., Nordberg, Jr., M.E. (1971), Phys. Rev. Lett. 26, 151.

Behrend, H.-J., Lee, C.K., Lobkowicz, F., Thorndike, E.H., Nordberg, Jr., M.E., Wehmann, A.A. (1971), Phys. Rev. Lett. 27, 65.

Behrend, J.-J., Bodenkamp, J., Hesse, W.P., Fries, D.C., Heine, P., Hirschmann, H., McNeely, Jr., W.A., Markou, A., Seitz, E. (1975), Phys. Lett. B 56, 408.

Belousov, A.S., Budanov, N.P., Govorkov, B.B., Lebedev, A.I., Malinovsky, E.I., Minarik, E.V., Michaclov, I.V., Plaksin, V.P., Rusakov, S. V., Sergienkov, V.I., Tamm, E.I., Chevenkov, P.A., Shaveiko, P.N., Alikanian, A.I., Baiatian, G.L., Markarvian, A.T., Vartanian, G.S., Frolov, A.M., Samoylov, A.V. (1972), Lebedev preprint.

Benaksas, D., Cosme, G., Jean-Marie, B., Jullian, S., Laplanche, F., LeFrançois, J., Liberman, A.D., Parrour, G., Repellin, J.P., Sauvage, G. (1972), Phys. Lett. B 39, 289; see also ibid. B 42, 507; ibid. B 48, 155; ibid. B 48, 159; ibid. B 40, 685.

Benecke, J., Durr, H.P. (1968), Nuo. Cim. 56, 269.

Benz, P., Braun, O., Butenschön, H., Finger, H., Gall, D., Idschok, U., Kiesling, C., Knies, G., Kowalski, H., Müller, K., Nellen, B., Schiffer, R., Schlamp, P., Schnackers, H.J., Schulz, V., Söding, P., Spitzer, H., Stiewe, J., Storim, F., Weigl, J. (1973), Nucl. Phys. B 65, 158.

Benz, P., Braun, O., Butenschön, H., Gall, D., Idschok, U., Kiesling, C., Knies, G., Müller, K., Nellen, B., Schiffer, R., Schlamp, P., Schnackers, H.J., Söding, P., Stiewe, J., Storim, F. (1974), Nucl. Phys. B 79, 10.

Berger, C., Mistry, N., Roberts, L., Talman, R., Walstrom, P. (1972), Phys. Lett. B 39, 659.

Biggs, P.J., Braben, D.W., Clifft, R.W., Gabathuler, E., Rand, R.E. (1971), Phys. Rev. Lett. 27, 1157.

Blechschmidt, H., Dowd, J.P., Elsner, B., Heinloth, K., Höhne, K.H., Raither, S., Rathje, J., Schmidt, D., Smith, J.H., Weber, J.H. (1967), Nuo. Cim. A 52, 1348.

Bloom, E.D., Cottrell, R.L., Coward, D.H., DeStaebler, Jr., H., Drees, J., Miller, G., Mo, L.W., Taylor, R.E., Friedman, J.I., Hartmann, G.C., Kendall, H.W. (1969), Stanford Linear Accelerator Center preprint SLAC-PUB-653.

Braccini, P.L., Bradaschia, C., Castaldi, R., Foa, L., Lubelsmeyer, K., Schmitz, D. (1970), Nucl. Phys. B 24, 173.

Boyarski, A.M., Coward, D.H., Ecklund, S., Richter, B., Sherden, D., Siemann, R., Sinclair, C. (1971), Phys. Rev. Lett. 26, 1600; and (1973), Phys. Rev. Lett. 30, 1098.

Buschhorn, G., Griegee, L., Dubal, L., Franke, G., Geweniger, C., Heide, P., Kotthaus, R., Poelz, G., Timm, U., Wegener, K., Werner, H., Wong, M., Zimmerman, W. (1970), Phys. Lett. B 33, 241.

Bulos, F., Busza, W., Giese, R., Larsen, R.R., Leith, D.W.G.S., Richter, B., Perez-Mendez, V., Stetz, A., Williams, S.H., Beniston, M., Rettberg, J. (1969), Phys. Rev. Lett. 22, 490.

Bulos, F., Busza, W., Giese, R., Larsen, R.R., Leith, D.W.G.S., Richter, B., Williams, S. (1970), reported by D.W.G.S. Leith in Lectures on Photoproduction in Scottish Universities Summer School Proceedings, Eds. Cummings and Osborn.

Bulos, F., Busza, W., Giese, R., Kluge, E.E., Larsen, R.R., Leith, D.W.G.S., Richter, B., Williams, S.H., Kehoe, B., Beniston, M., Stetz, A. (1971), Phys. Rev. Lett. 26, 149.

Caldwell, D.O., Elings, V.B., Hesse, W. P., Morrison, R.J., Murphy, F.V., Yount, D.E. (1973), Phys. Rev. D 7, 1362.

Camerini, U., Learned, J.G., Prepost, R., Spencer, C.M., Wiser, D.E., Ash, W.W., Anderson, R.L., Ritson, D.M., Sherden, D.J., Sinclair, C.K. (1975), Phys. Rev. Lett. 35, 483.

Carnegie, R.K., Cashmore, R.J., Davier, M., Leith, D.W.G.S., Walden, P., Williams, S.H. (1975), Phys. Lett. B 59, 313.

CEA Bubble Chamber Collaboration (1966), Phys. Rev. 146, 994; ibid. 155, 1468; ibid. 156, 1426; ibid. 169, 1081.

Ceradini, F., Conversi, M., D'Angelo, S., Paoluzi, L., Santonico, R., Ekstrand, K., Grilli, M., Iarocci, E., Spillantini, P., Valente, V., Visentin, R., Nigro, M. (1973), Phys. Lett. B 43, 341.

Chadwick, G., Eisenberg, Y., Kogan, E. (1973), Phys. Rev. D 8, 1607.

Criegee, L., Franke, G., Löffler, G., Schüler, K. P., Timm, U., Zimmermann, W., Werner, H., Dougan, P.W. (1970), Phys. Rev. Lett. 25, 1306.

Conversi, M., Paoluzi, L., Ceradini, F., d'Angelo, S., Ferrer, M.L., Santonico, R., Grilli, M., Spillantini, P., Valente, V. (1974), paper 137 submitted to the IVth International Conference on Experimental Meson Spectroscopy, Boston.

Cozzika, G., Ducros, Y., Gaidot, A., De Lesquen, A., Merlo, J.P., Van Rossum, L. (1972), Phys. Lett. B 40, 281; see also De Lesquen, A., Amblard, B., Beurtey, R., Cozzika, G., Bystricky, J., Deregel, J., Ducros, Y., Fontaine, J.M., Gaidot, A., Hansroul, M., Lehar, F., Merlo, J.P., Miyashita, S., Movchet, J., Van Rossum, L. (1972), Phys. Lett. B 40, 277.

Das, T., Mathur, V.S., Okubo, S. (1967), Phys. Rev. Lett. 19, 470.

Damashek, M., Gilman, F.J. (1970), Phys. Rev. D 1, 1319.

Davier, M., Derado, I., Drickey, D., Fries, D., Mozley, R.,
Odian, A., Villa, F., Yount, D. (1970), Phys. Rev. D 1, 790;
and (1972), Nucl. Phys. B 36, 404.

Davier, M. (1972), Phys. Lett. B 40, 369.

Davier, M., Derado, I., Fries, D., Liu, F., Mozley, R. F., Odian, A.,
Park, J., Swanson, W.P., Villa, F., Yount, D. (1973), Stanford
Linear Accelerator Center preprint SLAC-PUB-1205.

De Rujula, A., Glashow, S.L. (1975), Phys. Rev. Lett. 34, 46.

DESY/ABBHHM Collaboration (1968), Phys. Rev. 175, 1669; ibid. 188,
2060.

DESY/AHHM Collaboration (1971); see Wolf, 1971 and Moffeit, 1973.

Diambrini-Palazzi, G., McClellan, G., Mistry, N., Mostek, P.,
Ogren, H., Swartz, J., Talman, R. (1970), Phys. Rev. Lett.
25, 478.

Drell, S.D. (1961), Rev. Mod. Phys. 33, 458.

Drell, S.D., Trefil, J.S. (1966), Phys. Rev. Lett. **16**, 552; Phys. Rev. Lett. **16**, 832.

Dominguez, C.A., Gunion, J.F., Suaya, R. (1972), Phys. Rev. D **6**, 1404.

Eisenberg, Y., Haber, B., Ronat, E.E., Shapira, A., Stahl, Y., Yekutieli, G., Ballam, J., Chadwick, G.B., Menke, M.M., Seyboth, P., Dagan, S., Levy, A. (1972), Phys. Rev. D **5**, 15.

Eisenberg, Y., Haber, B., Kogan, E., Ronat, E.E., Shapira, A., Yekutieli, G. (1972a), Nucl. Phys. B **25**, 499; ibid. B **42**, 349.

Eisenberg, Y., Haber, B., Kogan, E., Karshon, U., Ronat, E.E., Shapira, A., Yekutieli, G. (1976), Nucl. Phys. B **104**, 61.

Franco, V., Glauber, R.J. (1966), Phys. Rev. 142, 1195.

Franco, V., Varma, G.K. (1974), Phys. Rev. Lett. 33, 44.

Frazer, W.R., Fulco, J.R. (1960), Phys. Rev. 117, 1603.

Freund, P. (1967), Nuo. Cim. 48, 541.

Gaillard, M.K., Lee, B.W., Rosner, J.L. (1974), Fermi-Lab report 74/86 (unpublished).

Gell-Mann, M., Goldberger, M.L., Thirring, W.E. (1954), Phys. Rev. 95, 1612.

Giacomelli, G. (1969), CERN report CERN-HERA-69-30.

Giese, R. (1974), Stanford University Thesis (unpublished).

Gilman, F., Pumplin, J., Schwimmer, A., Stodolsky, L. (1970), Phys. Lett. B 31, 387.

Gittelman, B., Hanson, K.M., Larson, D., Loh, E., Silverman, A., Theodosiou, G. (1975), Phys. Rev. Lett. 35, 1616.

Gladding, Gary E., Russell, John J., Tannenbaum, Michael J., Weiss, Jeffrey M., Thomson, Gordon B. (1973), Phys. Rev. D 8, 3721.

Grayer, G., Hyams, B., Jones, C., Schlein, P., Weilhammer, P., Blum, W., Dietl, H., Koch, W., Lorenz, E., Lütjens, G., Männer, W., Meissburger, J., Ochs, W., Stierlin, U. (1974), Nucl. Phys. B 75, 189.

Grilli, M., Iarocci, E., Spillantini, P., Valente, V., Visentin, R., Borgia, B., Ceradini, F., Conversi, M., Paoluzi, L., Santonico, R., Nigro, M., Trasatti, L., Zorn, G.T. (1973), Nuo. Cim. A 13, 593.

Halpern, H. J., Prepost, R., Tompkins, D. H., Anderson, R. L., Gottschalk, B., Gustayson, D. B., Ritson, D. M., Weitsch, G. A., Wiik, B. H. (1972), Phys. Rev. Lett. 29, 1425.

Harari, H. (1969), Proceedings of IV International Symposium of Electron and Photon Physics, Liverpool.

Harari, H. (1971), Ann. Phys. 63, 432.

Hicks, N., Eisner, A., Feldman, G., Litt, L., Lockeretz, W., Pipkin, F. M., Randolph, J. K., Stanfield, K. C. (1969), Phys. Lett. B 29, 602.

Hyams, B., Jones, C., Weilhammer, P., Blum, W., Dietl, H., Grayer, G., Koch, W., Lorenz, E., Lütjens, G., Männer, W., Meissburger, J., Ochs, W., Stierlin, U. (1975), Nucl. Phys. B 100, 205; see also Estabrooks, P., Martin, A. (1975), Nucl. Phys. B 95, 322.

Joos, H. (1967), Acta Physica Austriaca Suppl. IV.

Knapp, B., Lee, W., Leung, P., Smith, S.D., Wijangco, A., Knauer, J., Yount, D., Nease, D., Bronstein, J., Coleman, R., Cormell, L., Gladding, G., Gormley, M., Messner, R., O'Halloran, T., Sarracino, J., Wattenberg, A., Wheeler, D., Binkley, M., Orr, R., Peoples, J., Read, L. (1975), Phys. Rev. Lett. 34, 1040.

Kogan, E. (1975), Weizman Institute Thesis (unpublished).

Lakin, W.L., Braunstein, T.J., Cox, J., Dieterle, B.D., Perl, M.L., Toner, W.T., Zipf, T.F., Bryant, H. (1971), Phys. Rev. Lett. 26, 34.

Lanzerotti, L.J., Blumenthal, R.B., Ehn, D.C., Faissler, W.L., Joseph, P.M., Pipkin, F.M., Randolph, J.K., Russell, J.J., Stairs, D.G., Tenenbaum, J. (1968), Phys. Rev. 166, 1365.

Lee, W.Y. (1975), Invited talk at International Symposium on Electron and Photon Interactions, Stanford.

Leith, D.W.G.S. (1975), Proceedings of 1974 SLAC Summer Institute, Stanford Linear Accelerator Center report SLAC-179.

Leith, D.W.G.S. (1975a), Lectures presented at the Canadian IPP International School, McGill University, Montreal and Stanford Linear Accelerator Center preprint SLAC-PUB-1646.

Meyer, H., Naroska, B., Weber, J.H., Wong, M., Heynen, V., Mandelkow, E., Notz, D. (1970), Phys. Lett. B 33, 189.

McClellan, G., Mistry, N., Mostek, P., Ogren, H., Osborne, A., Silverman, A., Swartz, J., Talman, R., Diambrini-Palazzi, G. (1969), Phys. Rev. Lett. 23, 718.

McClellan, G., Mistry, N., Mostek, P., Ogren, H., Osborne, A., Swartz, J., Talman, R., Diambrini-Palazzi, G. (1971), Phys. Rev. Lett. 26, 1593.

McClellan, G., Mistry, N., Mostek, P., Ogren, H., Silverman, A., Swartz, J., Talman, R. (1971a), Phys. Rev. D 4, 2683; see also (1969), Phys. Rev. Lett. 22, 374.

Moffeit, K. (1973), Review talk in the International Lepton-Photon Symposium, Bonn.

Nambu, Y. (1957), Phys. Rev. 106, 1366.

Oakes, R.J., Sakurai, J.J. (1967), Phys. Rev. Lett. 19, 1266.

Ogren, H.O. (1970), Cornell University Thesis (unpublished).

Park, J., Davier, M., Derado, I., Fries, D.C., Liu, F.F., Mozley, R.F., Odian, A.C., Swanson, W.P., Villa, F., Yount, D. (1972), Nucl. Phys. B 36, 404.

Prepost, R. (1976), private communication.

Pumplin, J. (1970), Phys. Rev. D 2, 1859.

Ritson, D. (1976), Talk presented at 2nd International Conference on New Results in High Energy Physics, Vanderbilt, Stanford Linear Accelerator Center preprint SLAC-PUB-1728.

Roos, M., Stodolsky, L. (1966), Phys. Rev. 149, 1172.

Sakurai, J.J. (1960), Ann. Phys. 11, 1.

Sakurai, J.J., Schildknecht, D. (1972), Phys. Lett. B 40, 121.

Salvini, D. (1974), Talk presented to the Italian Physical Society summarizing best Frascati results (unpublished).

Samios, N.P., Goldberg, M., Meadows, B.T. (1974), Rev. Mod. Phys. 46, 49.

Schilling, K., Seyboth, P., Wolf, G. (1971), Nucl. Phys. B 15, 397.

Shapiro, J.A. (1969), Phys. Rev. 179, 1345.

Schumacher, G., Eugle, I. (1971), Argonne National Laboratory report ANL/HEP-7032 (unpublished).

Silverman, A. (1975), Review talk in the International Lepton-Photon Symposium, Stanford.

Slattery, P., Ferbel, T. (1974), Phys. Rev. D 9, 824.

Söding, P. (1966), Phys. Lett. 19, 702; see also Krass, A. (1967), Phys. Rev. 159, 1496.

Spital, Robin, Yennie, Donald R. (1975), Phys. Rev. D 9, 138.

Swartz, J., Talman, R. (1969), Phys. Rev. Lett. 23, 1078.

Veneziano, G. (1968), Nuo. Cim. A 57, 190.

Von Bockman, G., Margolis, B., Tang, C.L. (1969), Phys. Lett. B 30, 254.

West, G.B. (1971), Phys. Lett. B 37, 509.

Williams, S. (1973), University of California, Berkeley, Thesis (unpublished).

Wolf, G. (1969), Phys. Rev. 182, 1538.

Wolf, G. (1971), Review talk in the International Lepton-Photon Conference, Liverpool.

Wolf, G. (1972), DESY report 72/61 (unpublished).

Yennie, D. (1975), Phys. Rev. Lett. 34, 239.

Yennie, D. (1975a), Rev. Mod. Phys. 47, 311.

Table 1

Summary of Compton Scattering Cross Sections

$$\left(\frac{d\sigma}{dt} = \frac{d\sigma}{dt}\bigg|_0 \exp(At + Bt^2)\right)$$

Experiment	E (GeV)	t Range (GeV^2)	$(d\sigma/dt)_0$ ($\mu b/GeV^2$)	A (GeV^{-2})	B (GeV^{-4})
	2.2 - 2.7	0.1 - 0.4	1.26 ± 0.13	5.2 ± 0.5	-
	2.7 - 3.2	-	1.14 ± 0.11	5.7 ± 0.4	-
	3.2 - 3.7	-	1.24 ± 0.11	6.2 ± 0.4	-
[Buschhorn et al., 1970]	3.7 - 4.2	-	1.02 ± 0.14	5.3 ± 0.5	-
	4.0 - 5.2	0.06 - 0.4	0.92 ± 0.09	6.0 ± 0.4	-
	5.0 - 6.2	-	0.76 ± 0.06	5.5 ± 0.3	-
	6.0 - 7.0	-	0.76 ± 0.07	5.9 ± 0.4	-
[Boyarski et al., 1971]	8	0.014 - 0.17	0.82 ± 0.04	7.7 ± 0.5	-
		0.014 - 0.8	0.79 ± 0.03	7.6 ± 0.4	2.3 ± 0.5
[Anderson et al., 1970]	16	0.014 - 0.17	0.69 ± 0.03	7.9 ± 0.5	-
		0.014 - 1.1	0.64 ± 0.02	7.3 ± 0.3	1.7 ± 0.3

Table 2

Summary of Vector Meson Photoproduction Experiments

Experiment	Vector Mesons Studied	Technique	Beam	Photon Energy (GeV)
		$\gamma p \to Vp$		
[CEA Collab., 1966]	ρ, ω, ϕ	bubble chamber	bremsstrahlung	6
[DESY Collab., 1968]	ρ, ω, ϕ	bubble chamber	bremsstrahlung	6
[Alexander et al., 1972]	ρ, ω, ϕ	bubble chamber	annihilation (quasi-monochromatic)	4.3, 5.3, 7.5
[Ballam et al., 1973]	ρ, ω, ϕ	bubble chamber	backscattered laser (monochromatic)	2.8, 4.7, 9.3
[Davier et al., 1970]	ρ, ω, ϕ	streamer chamber	bremsstrahlung	16
[DESY/AHHM Collab., 1971]	ρ, ω, ϕ	streamer chamber	tagged beam	3 - 6
[Blechschmidt et al., 1967]	ρ	counter setup	tagged beam	3 - 5
[McClellan et al., 1971; 1971a]	ρ, ϕ	counter setup	bremsstrahlung	8.5
[Alvensleben et al., 1970a; 1972]	ρ, ϕ	counter setup	bremsstrahlung	7
[Bulos et al., 1970]	ρ	counter setup	annihilation (quasi-monochromatic)	9
[Giese, 1974]	ρ	counter setup	bremsstrahlung	16
[Anderson et al., 1970]	ρ	counter setup	bremsstrahlung	18
[Barish et al., 1974]	ρ	counter setup	bremsstrahlung	12
[Gladding et al., 1973]	ρ, ω	counter setup	tagged beam	3, 4.2
[Behrend et al., 1971]	ω	counter setup	bremsstrahlung	9
[Behrend et al., 1975]	ϕ	counter setup	tagged beam	3 - 7
[Berger et al., 1972]	ρ, ϕ	counter setup	bremsstrahlung	8.5
		$\gamma n \to Vn$		
[DESY/ABHHM Collab., 1971]	ρ, ω, ϕ	bubble chamber	bremsstrahlung	6
[Eisenberg et al., 1972; 1975]	ρ, ω	bubble chamber	backscattered laser (monochromatic)	4.3
[Alexander et al., 1973; 1975]	ρ, ω	bubble chamber	backscattered laser (monochromatic)	7.5
[McClellan et al., 1971a]	ρ, ϕ	counter setup	bremsstrahlung	8
[Bulos et al., 1970]	ρ	counter setup	annihilation (quasi-monochromatic)	9
[Giese, 1974]	ρ	counter setup	bremsstrahlung	16
[Abramson et al., 1976]	ω	counter setup	tagged beam	8
[Behrend et al., 1971]	ω	counter setup	bremsstrahlung	9

Table 3

Summary of Forward Cross Section Analysis for $\gamma p \rightarrow \rho^o p$

Experiment	Photon Energy (GeV)	Momentum Transfer Range (GeV^{-2})	Forward Cross Section, $\left.\frac{d\sigma}{dt}\right)_0$ ($\mu b/GeV^2$)	Forward Slope, A (GeV^{-2})
[Ballam et al., 1973]	2.8	(.02 - .4)	104 ± 6	5.4 ± .3
	4.7	(.02 - .4)	94 ± 6	5.9 ± .3
	9.3	(.02 - .5)	86 ± 4	6.6 ± .3
[Alexander et al., 1972]	2.2	(.06 - .4)	134 ± 20	6.4 ± .8
	2.7	(.06 - .4)	177 ± 26	8.8 ± 1.1
	3.4	(.06 - .4)	124 ± 20	7.5 ± 1.2
	4.2	(.06 - .4)	101 ± 12	6.5 ± .5
	5.2	(.06 - .4)	132 ± 17	7.7 ± .6
	7.5	(.06 - .4)	98 ± 15	7.1 ± .6
[Gladding et al., 1973]	3.3	(.15 - .7)	103 ± 22	7.5 ± .7
	4.2	(.15 - .7)	102 ± 18	7.4 ± .6
[McClellan et al., 1971a]	3.9	0	169 ± 14	-
	4.1	0	150 ± 14	-
	4.6	0	140 ± 13	-
	5.6	0	134 ± 6	-
	5.9	0	126 ± 9	-
	6.5	0	109 ± 9	-
	6.9	0	113 ± 10	-
	7.4	0	108 ± 5	-
	8.5	(0.0 - 0.5)	103 ± 6	8.1 ± .4
[Berger et al., 1972]	8.5	(.07 - .52)	98 ± 6	7.4 ± 0.5
[Alvensleben et al., 1970a]	6.4	0	120 ± 6	-
[Bulos et al., 1970]	9	(0.0 - 0.15)	113 ± 10	9.3 ± 1.1
[Giese, 1974]	15	(0 - .3)	104 ± 10	8.7 ± .4
	13	(0 - .3)	103 ± 10	8.2 ± .3
	11	(0 - .3)	95 ± 9	6.5 ± .4
	12	(0 - .3)	99 ± 10	7.5 ± .5
	10	(0 - .3)	104 ± 10	7.8 ± .5
	8	(0 - .3)	106 ± 10	8.3 ± .5

Table 4

Slope of the $\gamma p \rightarrow \rho^{o} p$ Differential Cross Section

for Different Intervals of Momentum Transfer

Photon Energy	9 GeV		16 GeV	
Momentum Transfer Interval [Experiment]	$(0 < t < .2)$ GeV^2 [Giese, 1974]	$(0.02 < t < .5)$ GeV^2 [Ballam et al., 1973]	$(0 < t < .3)$ GeV^2 [Giese, 1974]	$(.1 < t < 1)$ GeV^2 [Anderson et al., 1970]
Slope of Cross Section, A (GeV^{-2})	8.3 ± 0.4	6.6 ± 0.3	8.7 ± 0.4	7.5 ± 0.5

Table 5

Summary of Helicity Flip Amplitudes in Vector Meson Photoproduction (taken from [Kogan, 1975])

Amplitude Ratios [a]	Estimator	$\gamma d \rightarrow pn\rho^o$	$\gamma p \rightarrow p\rho^o$		$\gamma p \rightarrow p\omega$ [b]	
		4.3 GeV	4.7 GeV	9.3 GeV	4.7 GeV	9.3 GeV
$\|T_{01}\|^2/\|T_{11}\|^2$	ρ^0_{00}	0.05 ± 0.03	0.11 ± 0.03	0.01 ± 0.03		
	ρ^N_{00}	0.07 ± 0.03	0.13 ± 0.04	0.02 ± 0.02	$0 \quad \pm 0.06$	0.11 ± 0.08
$\mathrm{Im}\ T_{01}/\|T_{11}\|$	$2\mathrm{Re}\ \rho^0_{10}$	0.14 ± 0.04	0.16 ± 0.04	0.14 ± 0.02		
	$2\mathrm{Re}\ \rho^N_{10}$	0.14 ± 0.05	0.14 ± 0.04	0.14 ± 0.02	0.25 ± 0.08	0.02 ± 0.14
	$-\mathrm{Re}\ \rho^1_{10} - \mathrm{Im}\ \rho^2_{10}$	0.11 ± 0.05	0.08 ± 0.05	0.11 ± 0.03		
$\|T_{-11}\|^2/\|T_{11}\|^2$	$\rho^1_{1-1} + \mathrm{Im}\ \rho^2_{1-1}$	0.09 ± 0.07	0.10 ± 0.06	-0.03 ± 0.07		
$\mathrm{Im}\ T_{-11}/\|T_{11}\|$	ρ^0_{1-1}	-0.14 ± 0.03	-0.08 ± 0.03	-0.12 ± 0.02		
	ρ^N_{1-1}	-0.12 ± 0.03	-0.01 ± 0.03	-0.05 ± 0.02	-0.05 ± 0.05	-0.04 ± 0.07

[a] The nucleon helicities in the amplitudes listed are $\frac{1}{2}\frac{1}{2}$ (or $-\frac{1}{2}-\frac{1}{2}$).

[b] Natural parity exchange only and $0.15 < |t| < 0.6\ \mathrm{GeV}^2$.

Table 6

Isospin Contributions to the Reaction $\gamma N \rightarrow \rho^{o} N$. See text for explanation of the methods.

Method	Experiment / Measurement	[Eisenberg et al., 1976] (4.3 GeV)	[Benz et al., 1974] (1.8 - 5.3 GeV)	[Alexander et al., 1975] (7.5 GeV)	[McClellan et al., 1971a] (6 - 8 GeV)	[Giese, 1974] (9 GeV)	[Giese, 1974] (14 - 16 GeV)
1. Comparison of $\gamma d \rightarrow \rho^{o} d$ and $\gamma p \rightarrow \rho^{o} p$.	$\left\lvert \frac{T_1}{T_0} \right\rvert$	< 0.05	< 0.12	< 0.12	< 0.07	< 0.14	< 0.03
2. Comparison of $\gamma d \rightarrow \rho^{o} d + \rho^{o} pn$ and $\gamma d \rightarrow \rho^{o} d$.	$\left\lvert \frac{T_1}{T_0} \right\rvert^2$	$0.07^{+0.10}_{-0.07}$	-	-	-	-	0 ± 0.04
3. Comparison of $\gamma d \rightarrow p_s n \rho^{o}$ and $\gamma d \rightarrow n_s p \rho^{o}$.	$2\left\lvert \frac{T_1}{T_0} \right\rvert \cos \Delta\phi$	0.02 ± 0.04	-	$0 \pm .05$	-	-	-
4. Comparison of $\gamma n \rightarrow p \rho^{-}$ and $\gamma p \rightarrow p \rho^{o}$.	$\left\lvert \frac{T_1}{T_0} \right\rvert^2$	< 0.03	< 0.05	-	-	-	-

The table is based on 1 standard deviation limit. Method 1 assumes the Regge phase for $\cos \Delta\phi$ (i.e., $\cos \Delta\phi = 0.84$). I am indebted to E. Kogan for his help in preparing this table.

Table 7

Forward Cross Section, $\left.\frac{d\sigma}{dt}\right)_0$, for the Reaction $\gamma N \rightarrow \omega N$

Experiment	2.8 GeV [Ballam et al., 1973]	4.5 GeV [Ballam et al., 1973] [Gladding et al., 1973] [Eisenberg et al., 1976]	5.7 GeV [Braccini et al., 1970]	6.8 GeV [Behrend et al., 1971] [Abramson et al., 1976]	7.5 GeV [Alexander et al., 1975]	9.3 GeV [Ballam et al., 1973]
$\lvert T_0 + T_1 \rvert^2$ (from hydrogen)	14.5 ± 5.1	13 ± 3 12.6 ± 2.4	–	~ 7.5	–	13.5 ± 2.1
$\lvert T_0 \rvert^2$ (from deuterium)	–	18.5 ± 4.5	–	~ 6.2	11.1 ± 2.3	–
$\lvert T_0 \rvert^2$ (from complex nuclei)	–	–	16 ± 3	9.6 ± 1.2	–	–
$\lvert T_0 \rvert^2$ (from eqn. (5.4) taking $\sigma(\omega N)$ from the quark model and $(\gamma_\omega^2/4\pi)$ from e^+e^- experiments)	$15.3\ \mu b/GeV^2$					

Table 8

Summary of ρ'' (1600) Properties

Experiment		M (MeV)	Γ (MeV)	I^{CG}	J^P	$\pi^+\pi^-/4\pi^\pm$	$K^+K^-/4\pi^\pm$
$\gamma A \to \rho'' A$	[Alvensleben et al., 1971] [Bulos et al., 1971]	–	–	–	–	<0.14	–
$\gamma p \to \rho'' p$	[Bingham et al., 1972] [Davier et al., 1973]	1500	500	1^{-+}	1^-	<0.20	$<.04$
$\gamma d \to \rho'' d$	[Alexander et al., 1975]	1570 ± 60	350 ± 90	–	–	–	–
$\gamma Be \to 2\pi X$ $4\pi X$	[Lee, 1975]	~ 1600	~ 500	–	–	>0.05	–
$e^+e^- \to \pi^+\pi^-\pi^+\pi^-$ $\pi^+\pi^-\pi^o\pi^o$ $\pi^+\pi^-$	[Ceradini et al., 1973]	~ 1600	~ 300	1^{-+}	1^-	not seen $\sim 10^{-2}$	–
$\pi^- p \to \rho'' n$	[Hyams et al., 1975]	~ 1590	~ 200	1^{-+}	1^-	$0.25 \pm .05$	–

Table 9

Experiments on Coherent Vector Meson Production on Complex Nucleii

Group	Photon Beam Energy (GeV)	Photon Beam Type	Number of Targets Used	Mesons Studied	References
CEA	(2 - 5)	bremsstrahlung	4	ρ	[Lanzerotti et al., 1968]
DESY-MIT	(3 - 7)	bremsstrahlung	14	ρ, ϕ	[Alvensleben et al., 1970a]
CORNELL	(4 - 9)	bremsstrahlung	10	ρ, ϕ	[McClellan et al., 1971a]
SLAC	5, 7, 9	monochromatic	8	ρ	[Bulos et al., 1969] [Williams, 1973]
DESY	5.7	bremsstrahlung	5	ω	[Braccini et al., 1970]
ROCHESTER	9	bremsstrahlung	7	ρ, ω	[Behrend et al., 1970]
	8	tagged	4	ω	[Abramson et al., 1976]

Table 10

Vector Meson Couplings, as Obtained from the e^+e^- Storage Rings

Meson	Coupling Constant $\left(\gamma_V^2/4\pi\right)$	Leptonic Width (keV)
ρ	$0.64 \pm .1$	$6.48 \pm .9$
ω	$4.60 \pm .5$	$.76 \pm .08$
ϕ	$2.83 \pm .2$	$1.34 \pm .14$
Ψ	2.6 ± 1.2	$4.8 \pm .6$
Ψ'	7.4	$2.2 \pm .3$

Table 11

Summary of the Determination of Photon Coupling Strengths

	Method	$\left(\gamma_\rho^2/4\pi\right)$	$\left(\gamma_\omega^2/4\pi\right)$	$\left(\gamma_\phi^2/4\pi\right)$	$\left(\gamma_{\rho''}^2/4\pi\right)$
1.	Storage rings	$0.64 \pm .1$	$4.60 \pm .5$	$2.83 \pm .2$	$2.8 \pm .5$
2.	Coherent Photo-production on complex nucleii	$0.61 \pm .03$ $(\eta_\rho = -.2)$	7.50 ± 1.3 $(\eta_\omega = -.2)$	10.7 ± 4.1 $(\alpha_\phi = 0)$ 5.5 ± 2.4 $(\alpha_\phi = -.25)$ 4.3 ± 2.1 $(\alpha_\phi = -.5)$	-
3.	Coherent production on deuterium at large t	$0.69 \pm .04$	-	-	-
4.	VDM with measured $d\sigma/dt)_0$ $(\gamma N \rightarrow VN)$ and $\sigma^T(VN)$ from quark model-hydrogen data	$0.67 \pm .06$	$5.3 \pm .9$ (~ 10.2)	$5.8 \pm .7$ $(\alpha_\phi = -.25)$ $6.9 \pm .8$ $(\alpha_\phi = -.5)$	-
	deuterium data	$0.70 \pm .07$	5.0 ± 1.1 (~ 11.3)	5.94 ± 1.0 $(\alpha_\phi = -.25)$ 7.14 ± 1.1 $(\alpha_\phi = -.5)$	
5.	As above, but taking $\sigma^T(\phi N) = 9mb$ (on hydrogen)	-	-	$2.8 \pm .4$ $(\alpha_\phi = -.25)$ $3.4 \pm .5$ $(\alpha_\phi = -.5)$	-
	(on deuterium)	-	-	$2.85 \pm .5$ $(\alpha_\phi = -.25)$ $3.42 \pm .5$ $(\alpha_\phi = -.5)$	-
6.	Ratio of ω/ρ production on hydrogen and deuterium and knowing $(\gamma_\rho^2/4\pi)$	-	$4.3 \pm .8$	-	3.8 ± 0.8

Table 12

Vector Meson-Nucleon Total Cross Section

Method	$\sigma(\rho N)$ (mb)	$\sigma(\omega N)$ (mb)	$\sigma(\phi N)$ (mb)
Quark model	27	27	13
Coherent production on deuterium	28.6 ± 1.4	-	-
A-dependence of coherent production	$28 \quad \pm 1.5$	25.4 ± 2.7	12.1 ± 3.0 $(\alpha=-.25)$ 9.2 ± 2.8 $(\alpha=-.5)$
VDM + $\frac{d\sigma}{dt}(\gamma N \rightarrow VN)$	28.3 ± 3.5	27.8 ± 5	9.0 ± 1.2 $(\alpha=-.25)$ 8.3 ± 1.2 $(\alpha=-.5)$

Table 13

Input Data for Compton Sum Rule

Vector Meson	$\left(\gamma_V^2/4\pi\right)$	$\left.\frac{d\sigma}{dt}\right)_0$ $(\gamma N \to VN)$ $(\mu b/GeV^2)$		
		9.3 GeV(H)	4.3 GeV(D)	7.5 GeV(D)
ρ	$0.64 \pm .05$	100 ± 10 a)	437 ± 27 c)	327 ± 11 d)
ω	$4.8 \pm .5$	13.5 ± 2 a)	69 ± 17 c)	42 ± 9 d)
ϕ	$2.8 \pm .2$	$2.49 \pm .15$ a)	11.2 ± 1.3 e)	11.2 ± 1.3 e)
ρ''	$2.8 \pm .5$	15 ± 5 b)	50 ± 10 d)	50 ± 10 d)
Forward Compton cross section $(\mu b/GeV^2)$		$0.79 \pm .03$ a)	$3.48 \pm .2$ f)	$3.0 \pm .14$ g)

a) Average of the data presented in sections 2 and 3 of this review.

b) [Wolf, 1972].

c) [Eisenberg et al., 1976].

d) [Alexander et al., 1975].

e) [McClellan et al., 1971].

f) Derived from the total cross section measurements of [Caldwell et al., 1973] using the optical theorem.

g) [Boyarski et al., 1971].

FIGURE CAPTIONS

1. A comparison of the γp total cross section with (1/200) of the average of the $\pi^+ p$ and $\pi^- p$ total cross sections.

2. The total γp cross section from threshold up to 30 GeV.

3. The total γd cross section from threshold up to 30 GeV.

4. The γn total cross section derived from the measured γd and γp cross sections. Also shown is the difference between the neutron and proton cross sections.

5. The differential cross section for Compton scattering for energies in the range (2 - 18) GeV.

6. The calculated ratio of the real to imaginary parts of the forward amplitude for the Compton scattering reaction, $\gamma p \to \gamma p$.

7. The energy dependence of the forward differential cross section, $\left.\frac{d\sigma}{dt}\right|_0$, for the Compton scattering process. The curves as calculated from the optical theorem assuming a purely imaginary amplitude (dashed line), and using the calculated real part (solid line).

8. The measured differential cross section for Compton scattering on a deuterium target, at 8 and 16 GeV.

9. The dipion mass spectrum for several regions of momentum transfer for two experiments: (a) a 9.3 GeV study of the reaction $\gamma p \to \pi^+ \pi^- p$, and (b) a 4.3 GeV experiment measuring $\gamma d \to pn\pi^+\pi^-$.

10. Diagrams describing the Söding model for photoproduction of dipion pairs. For details see text.

11. The various contributions to the $\pi^+\pi^-$ mass spectrum for the reaction $\gamma p \to \pi^+\pi^- p$ at 2.8 and 4.7 GeV, within the framework of the Söding model.

12. The total cross section for $\gamma p \rightarrow \rho^o p$ as a function of photon energy. See text for a description of curve.
13. The differential cross section for $\gamma p \rightarrow \rho^o p$ at 9 and 16 GeV.
14. The energy dependence of the forward differential cross section, $\left.\frac{d\sigma}{dt}\right|_0$. See text for a description of curve.
15. The slope of the $\gamma p \rightarrow \rho^o p$ differential cross section as a function of energy. The solid curve is the average slope for $\pi^+ p$ and $\pi^- p$ elastic scattering determined over the momentum transfer interval $(0.1 < t < 0.4\ \mathrm{GeV}^2)$.
16. The logarithmic slope of the elastic differential cross section as a function of momentum transfer for $\pi^\pm p$, $K^\pm p$ and $p^\pm p$ scattering.
17. The measured ratio of rho photoproduction from deuterium and hydrogen targets as a function of momentum transfer, for several photon energies. The solid line is a fit to the data to determine the amount of I=1 t-channel exchange amplitude (see text).
18. The differential cross section for the photoproduction of rho mesons from deuterium, showing both the total production and the coherent cross section.
19. The cross section as a function of energy for the charge exchange reaction $\gamma n \rightarrow \rho^- p$.
20. Dual Absorption Model fits to the differential cross section for rho photoproduction and Compton scattering over the energy range (4 - 18) GeV.
21. The energy dependence of the slope of the diffractive contribution to the differential cross section for $\gamma p \rightarrow \rho^o p$, $\gamma p \rightarrow \phi p$ and $\gamma p \rightarrow \gamma p$, as determined from the Dual Absorption Model fits.

22. Definition of the angles used to describe the production and decay of the rho meson in the polarized photoproduction studies.

23. Decay correlations of the rho in studies of $\gamma p \rightarrow p\pi^+\pi^-$ at 4.7 GeV with linearly polarized photons. The curves are calculated for an s-channel helicity-conserving $\gamma \rightarrow \rho^o$ transition and an incident photon polarization of 92%.

24. The parity asymmetry as a function of momentum transfer, for the reaction $\gamma p \rightarrow \rho^o p$ at 2.8, 4.7 and 9.3 GeV.

25. The rho spin density matrix elements as a function of momentum transfer, for the reaction $\gamma p \rightarrow \rho^o p$ at 4.7 GeV. The decay correlations are presented for three coordinate systems: Gottfried-Jackson, Helicity, and Adair. See text for definitions.

26. Rho spin density matrix elements in the helicity system, and the parity asymmetry as a function of momentum transfer, for the reaction $\gamma p \rightarrow \rho^o p$ at 9.3 GeV.

27. Rho decay angular correlations in the helicity system, for the reactions $\gamma d \rightarrow d\rho^o$, $\gamma d \rightarrow n_s p\rho^o$ and $\gamma d \rightarrow p_s n\rho^o$ at 4.3 GeV. The curves are calculated for an s-channel helicity-conserving $\gamma \rightarrow \rho^o$ transition and an incident photon polarization of 92%.

28. The ρ^o spin density matrix elements in the helicity system for natural and unnatural parity exchange contributions to the reaction $\gamma p \rightarrow \rho^o p$ at 9.3 GeV and $\gamma d \rightarrow pn\rho^o$ at 4.3 GeV.

29. The reaction $\gamma p \rightarrow p\pi^+\pi^-$ at 9.3 GeV. (a), (b) unnormalized moments Re $\rho^0_{10} \frac{dN}{dM_{\pi\pi}}$ and $\rho^0_{1-1} \frac{dN}{dM_{\pi\pi}}$ respectively, evaluated for ($0.2 \leq t \leq 0.8$ GeV^2). The curves were calculated from the Söding model. (c), (d) are the deviations of the measured moments of (a) and (b)

respectively, from the Söding model predictions. The curves are p-wave Breit-Wigner ρ^o shapes, normalized to the area under the experimental points.

30. The ratio of helicity flip to nonflip amplitudes in rho photoproduction and πN elastic scattering. (a), (b) $2\,\mathrm{Re}\,\rho^N_{10}$ for $\gamma p \to \rho^o p$ at 4.7 and 9.3 GeV and $|F^o_{+-}|\ |F^o_{++}|$ for $\pi N \to \pi N$ at 6 and 16 GeV/c. (c) $|F^o_{+-}|$ at 6 GeV/c and an average of $\mathrm{Im}\ T^N_{10}$ from the photoproduction experiments normalized by the VDM $\gamma\rho$ coupling strength.

31. Omega photoproduction as measured in two experiments: (a) a bubble chamber study at 9.3 GeV identifying the reaction $\gamma p \to p\pi^+\pi^-\pi^o$ and displaying the $(\pi^+\pi^-\pi^o)$ effective mass, and (b) the missing mass recoiling from the proton in a counter experiment using a tagged photon beam of 4 GeV.

32. The energy dependence of the cross section for the reaction $\gamma p \to p\omega$.

33. The differential cross section for the reaction $\gamma p \to p\omega$ at 4 and 9 GeV.

34. The ω decay angular distributions in the helicity system, and the parity asymmetry for $\gamma p \to \omega p$ at 2.8, 4.7 and 9.3 GeV, evaluated for the momentum transfer interval $(0.02 \le t \le 0.3\ \mathrm{GeV}^2)$.

35. The effective mass distribution of K^+K^- pairs in the reaction $\gamma p \to K^+K^-p$ at 9.3 GeV.

36. The energy dependence of the cross section for $\gamma p \to \phi p$.

37. The differential cross section for the reaction $\gamma p \to \phi p$: (a) a compilation of data prior to April 1975; (b) the new high statistics results of [Behrend et al., 1975] plotted for $t < 0.4\ \mathrm{GeV}^2$, with all other measurements shown for $t > 0.4\ \mathrm{GeV}^2$.

38. The differential cross section for $\gamma p \rightarrow \phi p$ measured at momentum transfer $t = 0.6\ GeV^2$, as a function of photon energy.

39. Slope of the differential cross section for the reaction $\gamma p \rightarrow \phi p$, as a function of photon energy. See text for description of curve.

40. The reaction $\gamma p \rightarrow \phi p$ at 2.8, 4.7 and 9.3 GeV. The decay angular distribution of the K^+K^- pairs in the helicity system, for the momentum transfer interval ($0.02 \leq t \leq 0.8\ GeV^2$). The curves are calculated for an s-channel helicity conserving ϕ production amplitude and for photon polarization of 92% and 77% at the two energies.

41. The differential cross section for elastic K^+p and pp scattering for fixed momentum transfer $t = 0.6\ GeV^2$, as a function of energy.

42. Total cross section for $\pi^{\pm}p$, $K^{\pm}p$ and $p^{\pm}p$ as a function of energy.

43. K^+p and pp elastic scattering. (a), (b) examples of the differential cross section measurements showing an upward curvature of the cross section at small t. (c), (d) the energy dependence of the slope of the elastic differential cross section for K^+p and pp evaluated for two regions of momentum transfer.

44. The reaction $\gamma p \rightarrow p\pi^+\pi^-$ + neutrals at 2.8, 4.7 and 9.3 GeV. The effective mass of the ($\pi^+\pi^-$ + neutrals) system for two regions of momentum transfer; (a) $t < 0.5\ GeV^2$ and (b) $0.5 \leq t \leq 1.0\ GeV^2$. The shaded region corresponds to events in which the $\pi^+\pi^-$ mass lies in the range ($0.32 \leq M_{\pi\pi} \leq 0.6$ GeV).

45. The energy dependence of the cross section for the reaction $\gamma p \rightarrow \rho'(1250)p$.

46. The differential cross section for the reaction $\gamma p \rightarrow \rho'(1250)p$ at 9.3 GeV.

47. The dipion mass distribution for the reaction $\gamma C \rightarrow \pi^+\pi^- C$ at 7 GeV photon energy.

48. The four pion mass distribution for the reaction $\gamma p \rightarrow \pi^+\pi^+\pi^-\pi^- p$ in the energy range (6 - 18) GeV.

49. The differential cross section for the reaction $\gamma p \rightarrow \rho''(1600)p$ in the energy range (6 - 18) GeV.

50. $\rho''(1600)$ decay angular distributions in the helicity system, for the reaction $\gamma p \rightarrow \rho''(1600)p$ at 9.3 GeV.

51. The cross section for $e^+e^- \rightarrow \pi^+\pi^-\pi^+\pi^-$ as a function of energy.

52. The dipion and four pion mass spectra from the reactions $\gamma Be \rightarrow \pi^+\pi^- X$ and $\gamma Be \rightarrow \pi^+\pi^+\pi^-\pi^- X$ at photon energy in the range (80 - 100) GeV.

53. Argand diagrams of the S, P, D and F wave amplitudes from the phase shift analysis of π-π scattering data.

54. The cross section for (a) $e^+e^- \rightarrow$ hadrons, (b) $e^+e^- \rightarrow \mu^+\mu^-$ and (c) $e^+e^- \rightarrow e^+e^-$ as a function of energy, in the neighborhood of the $\psi(3100)$ resonance.

55. The $(\mu^+\mu^-)$ mass distribution from the reaction (a) $\gamma p \rightarrow \mu^+\mu^- p$ for photon energy of 19 GeV, and (b) $\gamma Be \rightarrow \mu^+\mu^- X$ for photon energy in the range (80 - 100) GeV.

56. The energy dependence of the forward cross section for the reaction $\gamma p \rightarrow \psi(3100)p$.

57. The differential cross section for the reaction $\gamma p \rightarrow \psi(3100)p$ at (a) 11 GeV and (b) 19 GeV.

58. Schematic diagrams for the vector dominance model.

59. Schematic diagram for coherent vector meson photoproduction in complex nuclear targets.

60. The dipion mass distribution as a function of momentum transfer for thirteen different targets in the reaction $\gamma A \rightarrow \pi^+\pi^- A$.

61. The differential cross section for the coherent production of ϕ mesons on carbon at 8 GeV.

62. The differential cross section for the coherent production of ω mesons on beryllium and copper targets for photon energy about 8 GeV.

63. A χ^2 map of the correlation between the ratio of the real to imaginary forward ρN scattering amplitude, η_ρ, and the total ρN cross section, $\sigma(\rho N)$, as determined from an analysis of coherent rho photoproduction on 13 different nuclear targets.

64. A two-dimensional plot showing the correlation between the ratio of the real to imaginary forward ϕN scattering amplitude, η_ϕ, and the total ϕN cross section, $\sigma(\phi N)$, and the photon-phi coupling $(\gamma_\rho^2/4\pi)$. The data come from an analysis of coherent ϕ photoproduction on complex nuclear targets.

65. The ratio, R, of the total cross section for $e^+e^- \rightarrow$ hadrons to the point cross section for $e^+e^- \rightarrow \mu^+\mu^-$, as a function of energy.

66. A schematic diagram for an off-diagonal vector dominance process.

67. The ratio of the predicted Compton scattering cross section (from the measured vector meson cross sections and using the vector dominance model), to the measured Compton ($\gamma p \rightarrow \gamma p$) cross section as a function of momentum transfer for three regions of photon energy—3, 5 and 16 GeV.

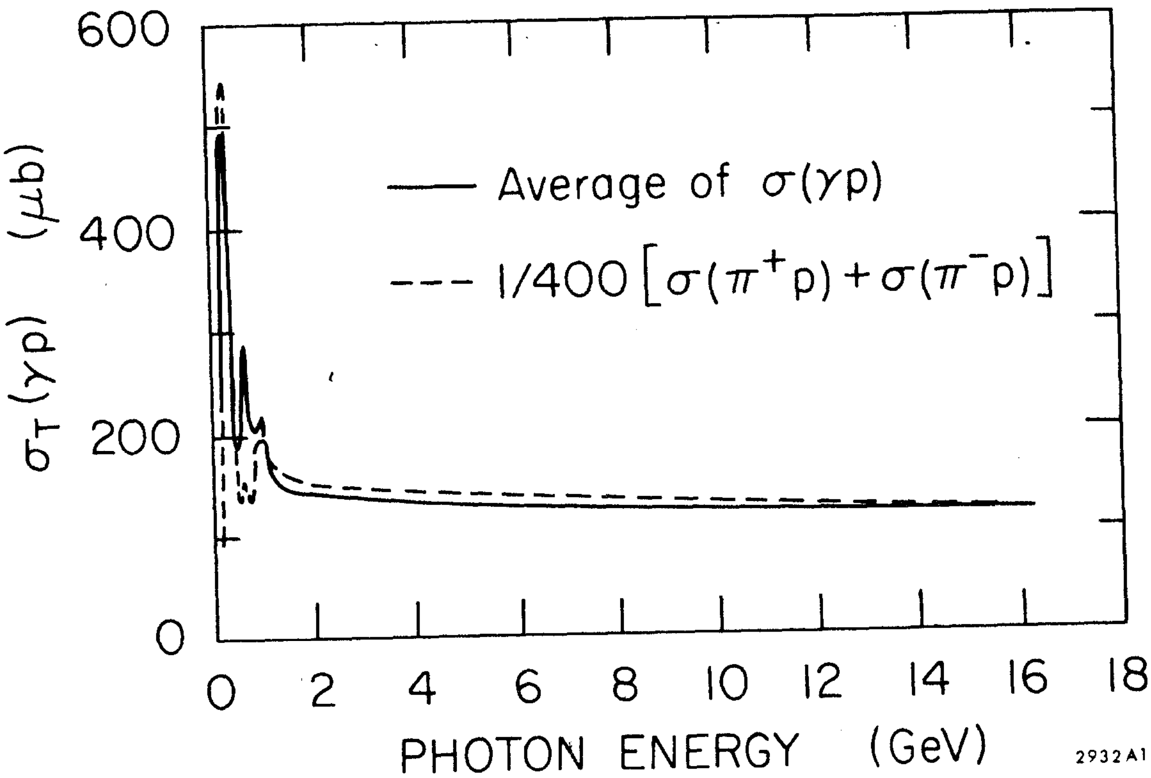
600
400
200
0
$\sigma_T(\gamma p)$ (μb)
Average of $\sigma(\gamma p)$
$1/400\,[\sigma(\pi^+p)+\sigma(\pi^-p)]$
0
2
4
6
8
10
12
14
16
18
PHOTON ENERGY (GeV)
2932A1

Fig. 1

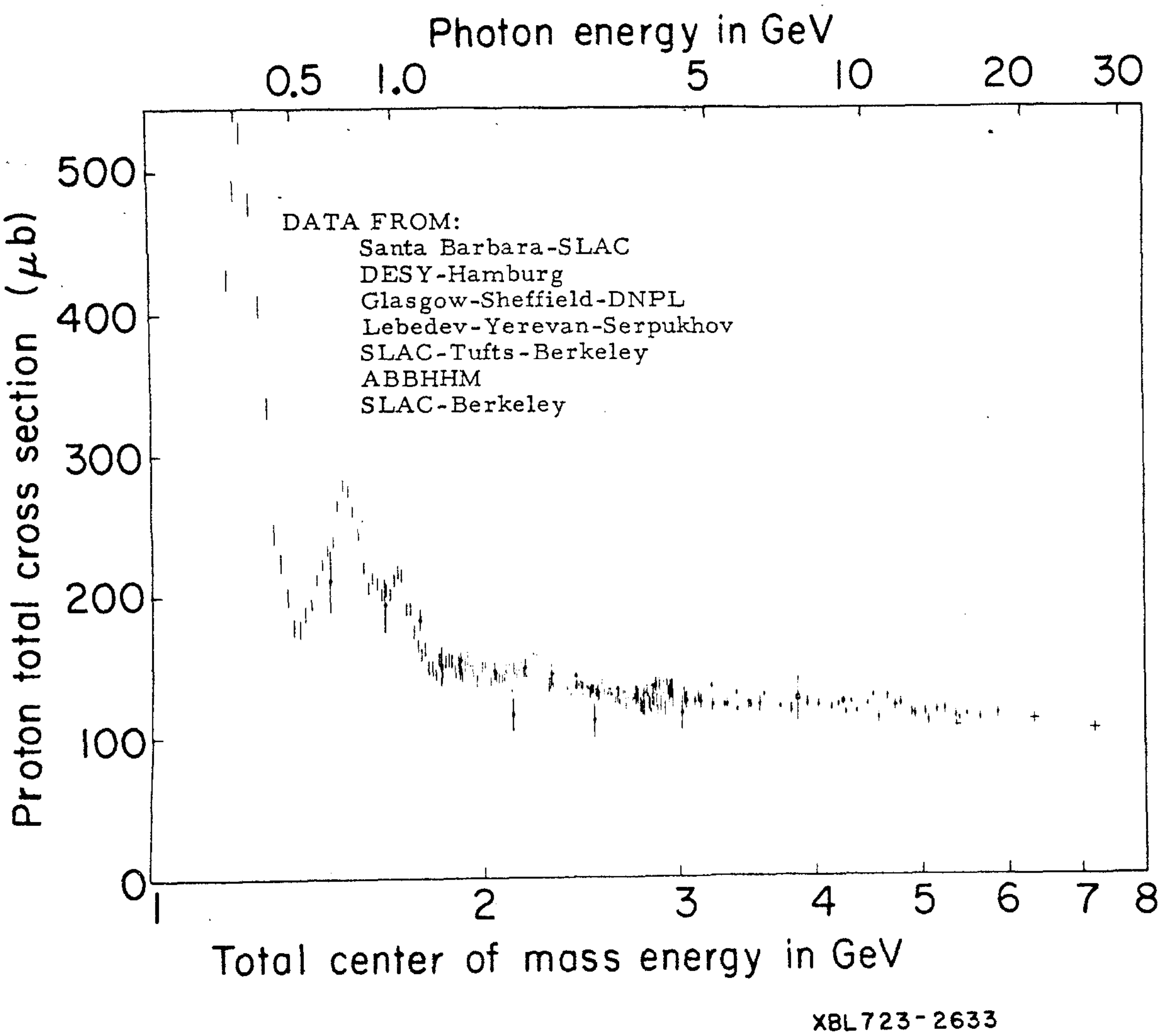
Photon energy in GeV
0.5
1.0
5
10
20
30
500
400
300
200
100
0
Proton total cross section (μb)
DATA FROM:
Santa Barbara-SLAC
DESY-Hamburg
Glasgow-Sheffield-DNPL
Lebedev-Yerevan-Serpukhov
SLAC-Tufts-Berkeley
ABBHHM
SLAC-Berkeley
1
2
3
4
5
6
7
8
Total center of mass energy in GeV
XBL723-2633

Fig. 2

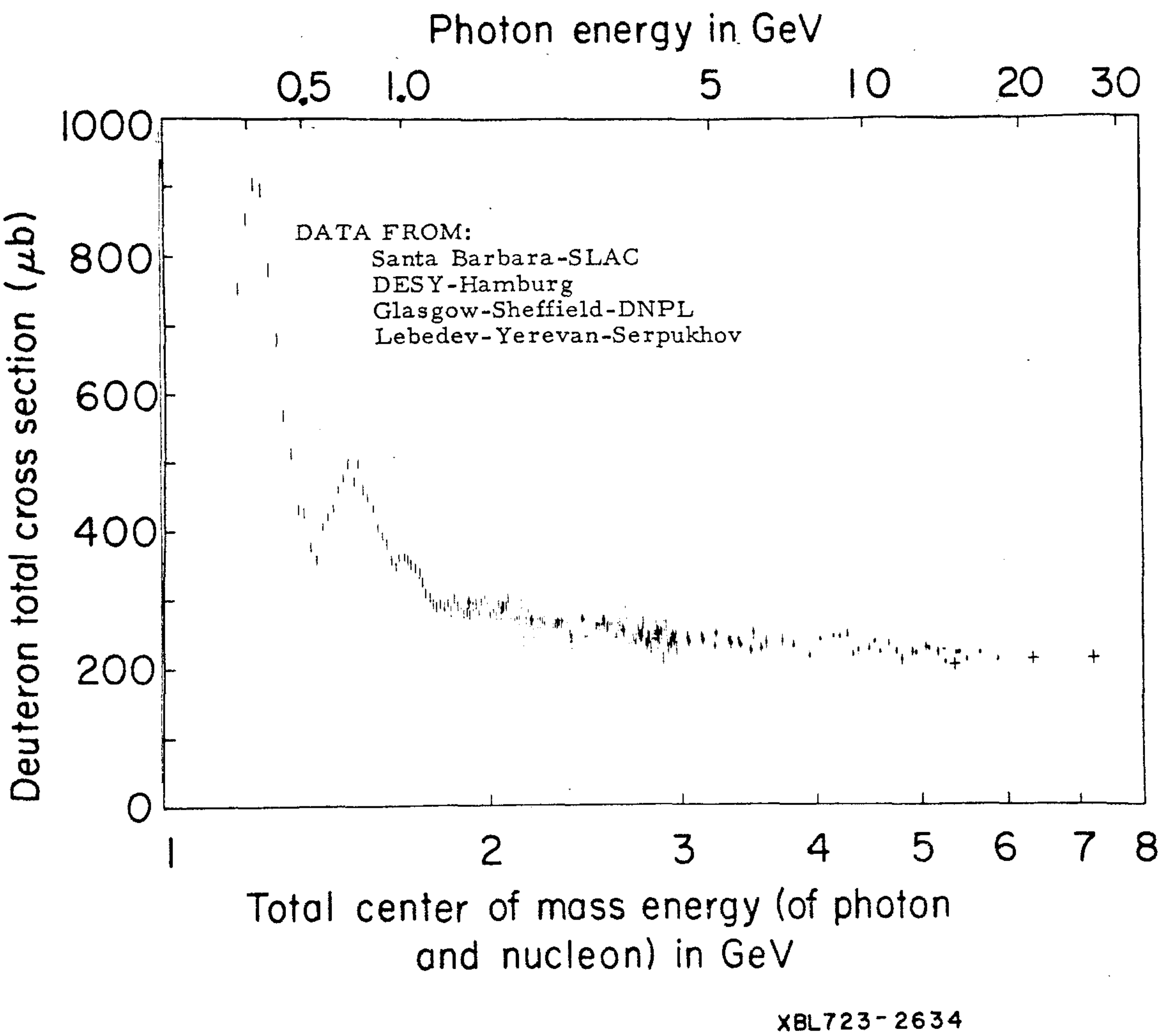

Photon energy in GeV
0.5
1.0
5
10
20
30
1000
800
600
400
200
0
Deuteron total cross section (μb)
DATA FROM:
Santa Barbara-SLAC
DESY-Hamburg
Glasgow-Sheffield-DNPL
Lebedev-Yerevan-Serpukhov
1
2
3
4
5
6
7
8
Total center of mass energy (of photon and nucleon) in GeV
XBL723-2634

Fig. 3

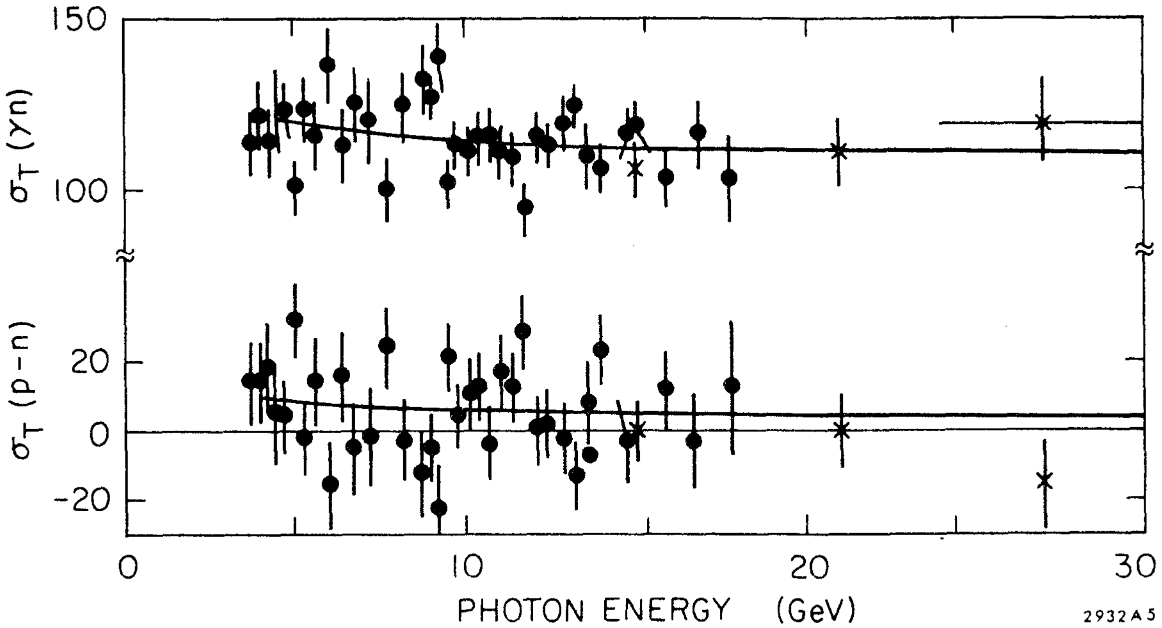
150
100
20
0
-20
σ_T (γn)
σ_T (p-n)
0
10
20
30
PHOTON ENERGY (GeV)
2932A5

Fig. 4

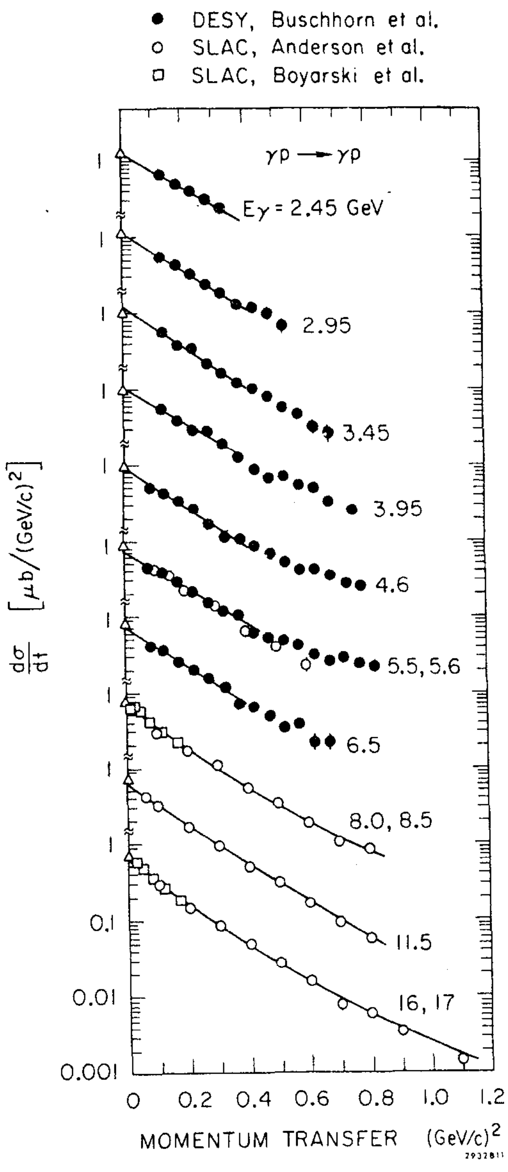
● DESY, Buschhorn et al.
○ SLAC, Anderson et al.
□ SLAC, Boyarski et al.
γp → γp
Eγ = 2.45 GeV
2.95
3.45
3.95
4.6
5.5, 5.6
6.5
8.0, 8.5
11.5
16, 17
dσ/dt [μb/(GeV/c)²]
1
0.1
0.01
0.001
0
0.2
0.4
0.6
0.8
1.0
1.2
MOMENTUM TRANSFER (GeV/c)²

Fig. 5

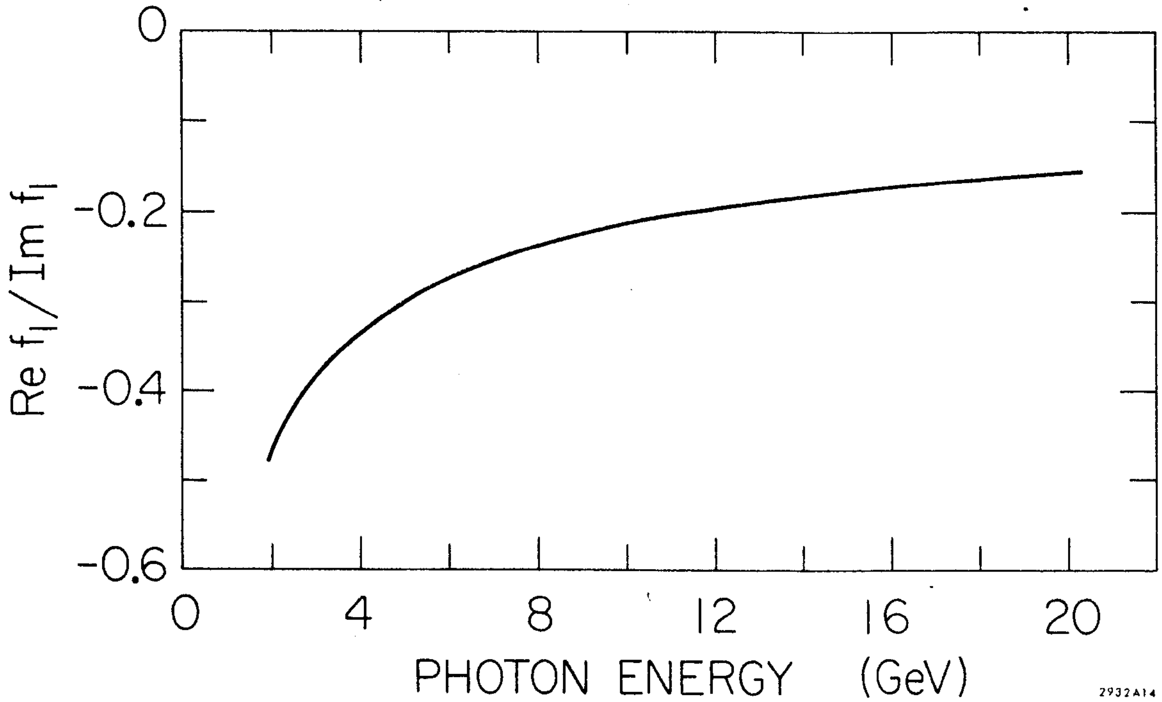

Fig. 6

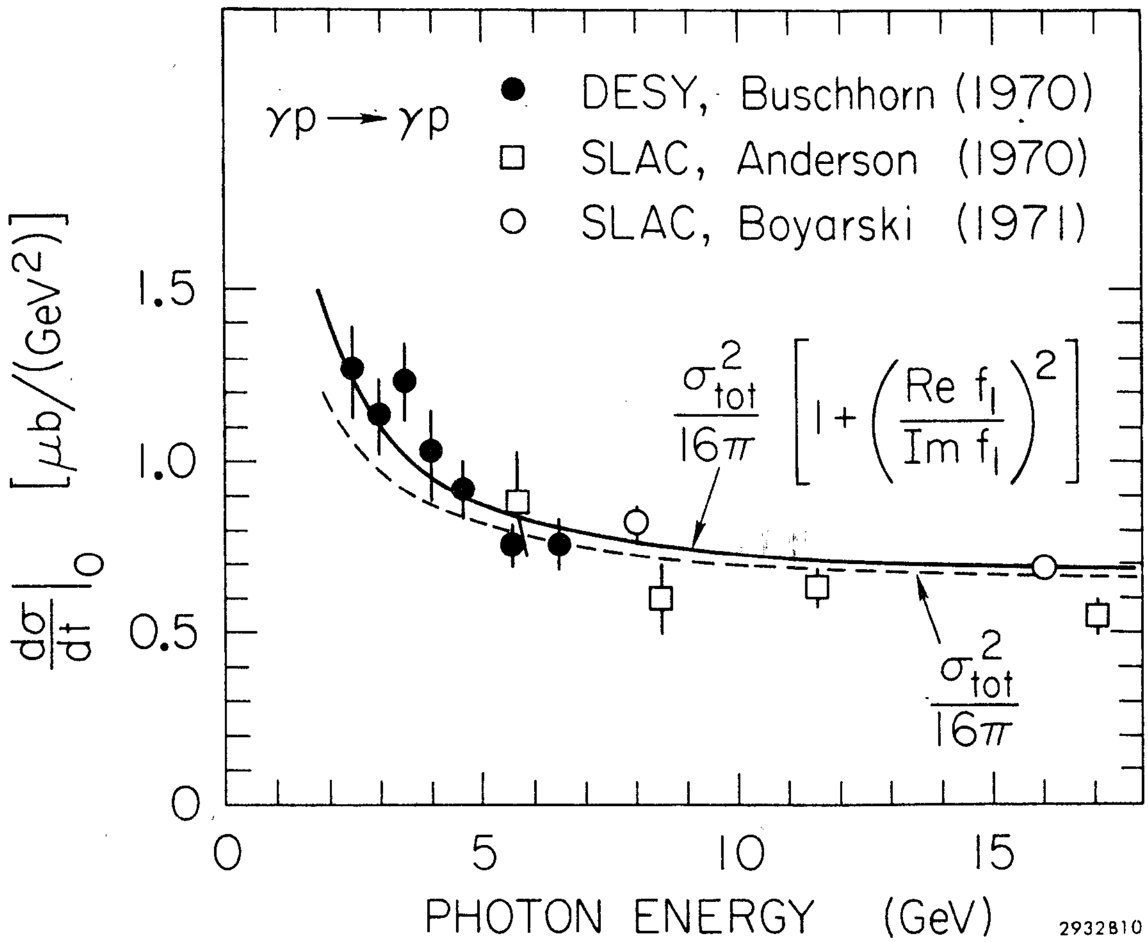

$\gamma p \to \gamma p$
DESY, Buschhorn (1970)
SLAC, Anderson (1970)
SLAC, Boyarski (1971)
$\frac{d\sigma}{dt}\Big|_0 \quad [\mu b/(GeV^2)]$
$\frac{\sigma_{tot}^2}{16\pi}\left[1+\left(\frac{Re\ f_1}{Im\ f_1}\right)^2\right]$
$\frac{\sigma_{tot}^2}{16\pi}$
PHOTON ENERGY (GeV)
0
5
10
15
0.5
1.0
1.5
2932B10

Fig. 7

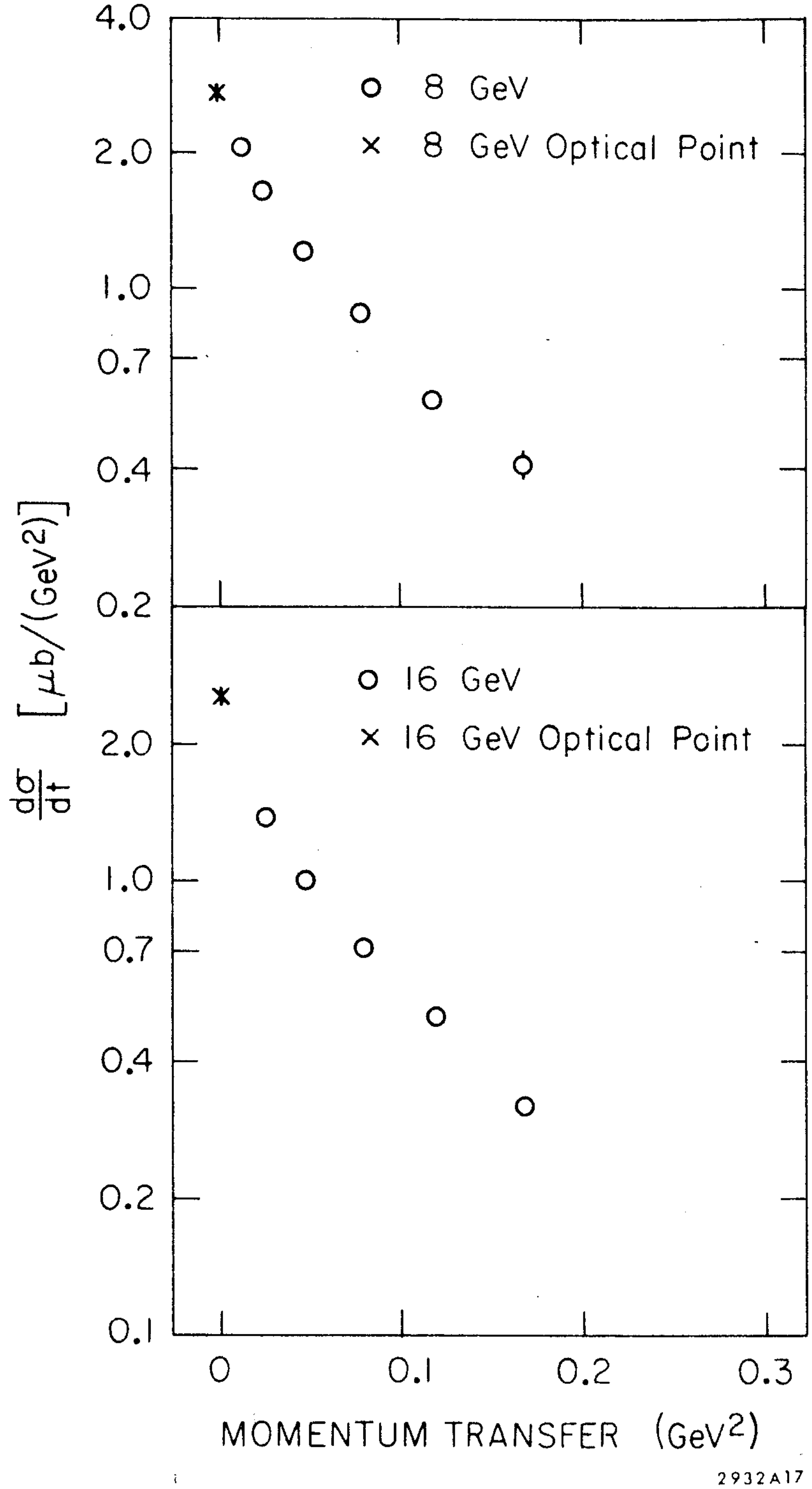

4.0
2.0
1.0
0.7
0.4
0.2
0.1
8 GeV
× 8 GeV Optical Point
16 GeV
× 16 GeV Optical Point
$\frac{d\sigma}{dt}$ [$\mu b/(GeV^2)$]
0
0.1
0.2
0.3
MOMENTUM TRANSFER (GeV^2)
2932A17

Fig. 8

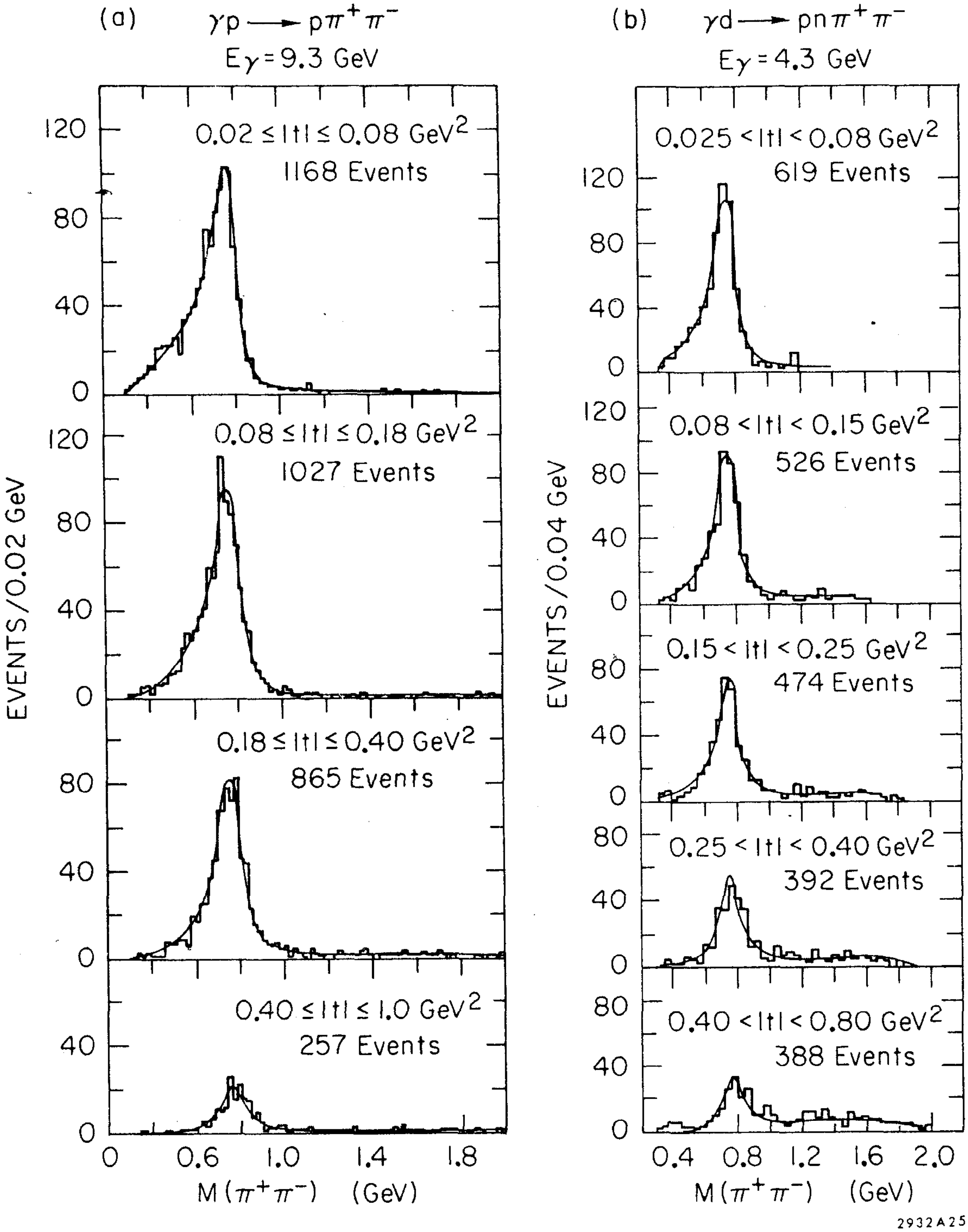
(a) $\gamma p \longrightarrow p\pi^+\pi^-$
$E_\gamma = 9.3$ GeV
$0.02 \le |t| \le 0.08$ GeV^2
1168 Events
$0.08 \le |t| \le 0.18$ GeV^2
1027 Events
$0.18 \le |t| \le 0.40$ GeV^2
865 Events
$0.40 \le |t| \le 1.0$ GeV^2
257 Events
EVENTS/0.02 GeV
$M(\pi^+\pi^-)$ (GeV)
(b) $\gamma d \longrightarrow pn\pi^+\pi^-$
$E_\gamma = 4.3$ GeV
$0.025 < |t| < 0.08$ GeV^2
619 Events
$0.08 < |t| < 0.15$ GeV^2
526 Events
$0.15 < |t| < 0.25$ GeV^2
474 Events
$0.25 < |t| < 0.40$ GeV^2
392 Events
$0.40 < |t| < 0.80$ GeV^2
388 Events
EVENTS/0.04 GeV
$M(\pi^+\pi^-)$ (GeV)
2932A25

Fig. 9

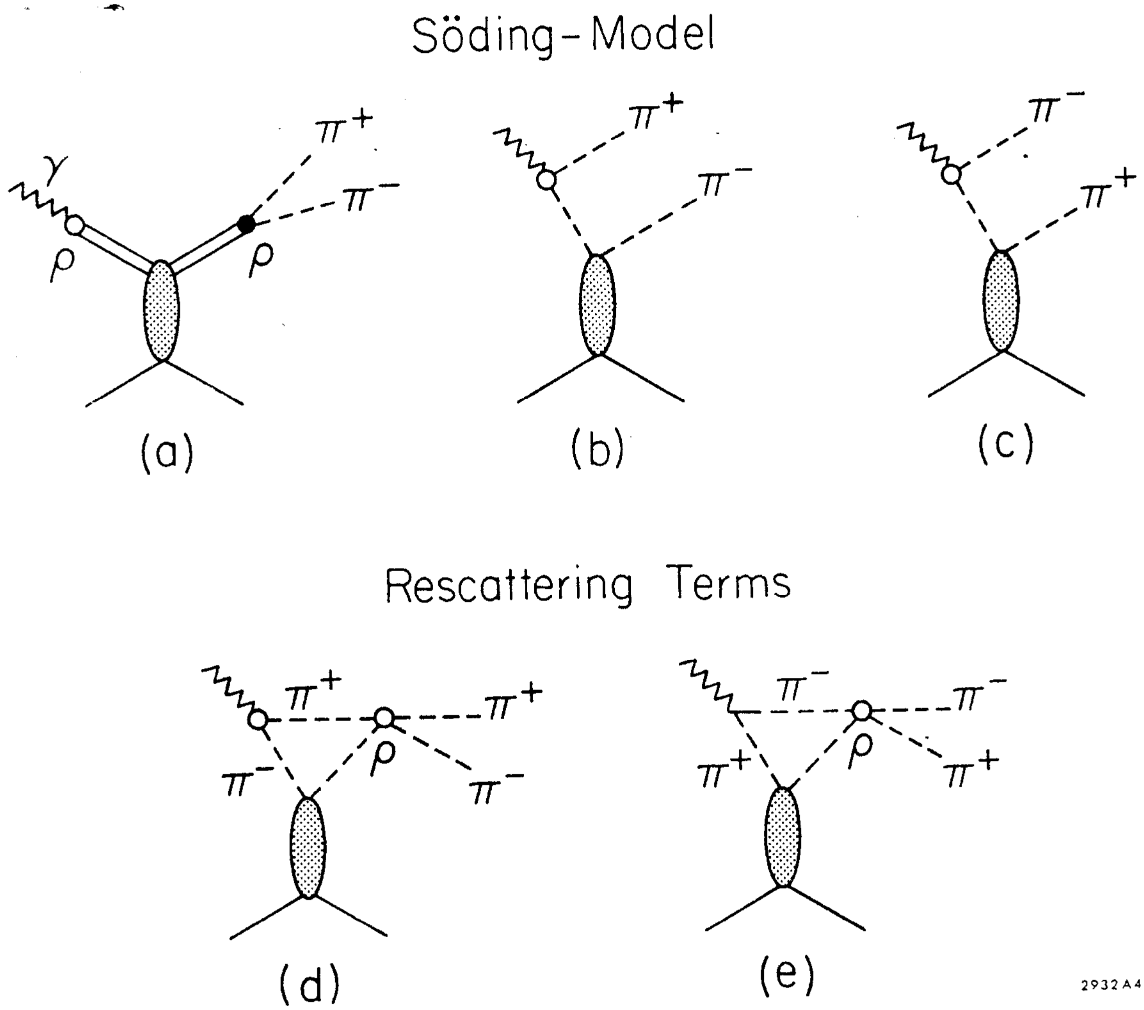

Fig. 10

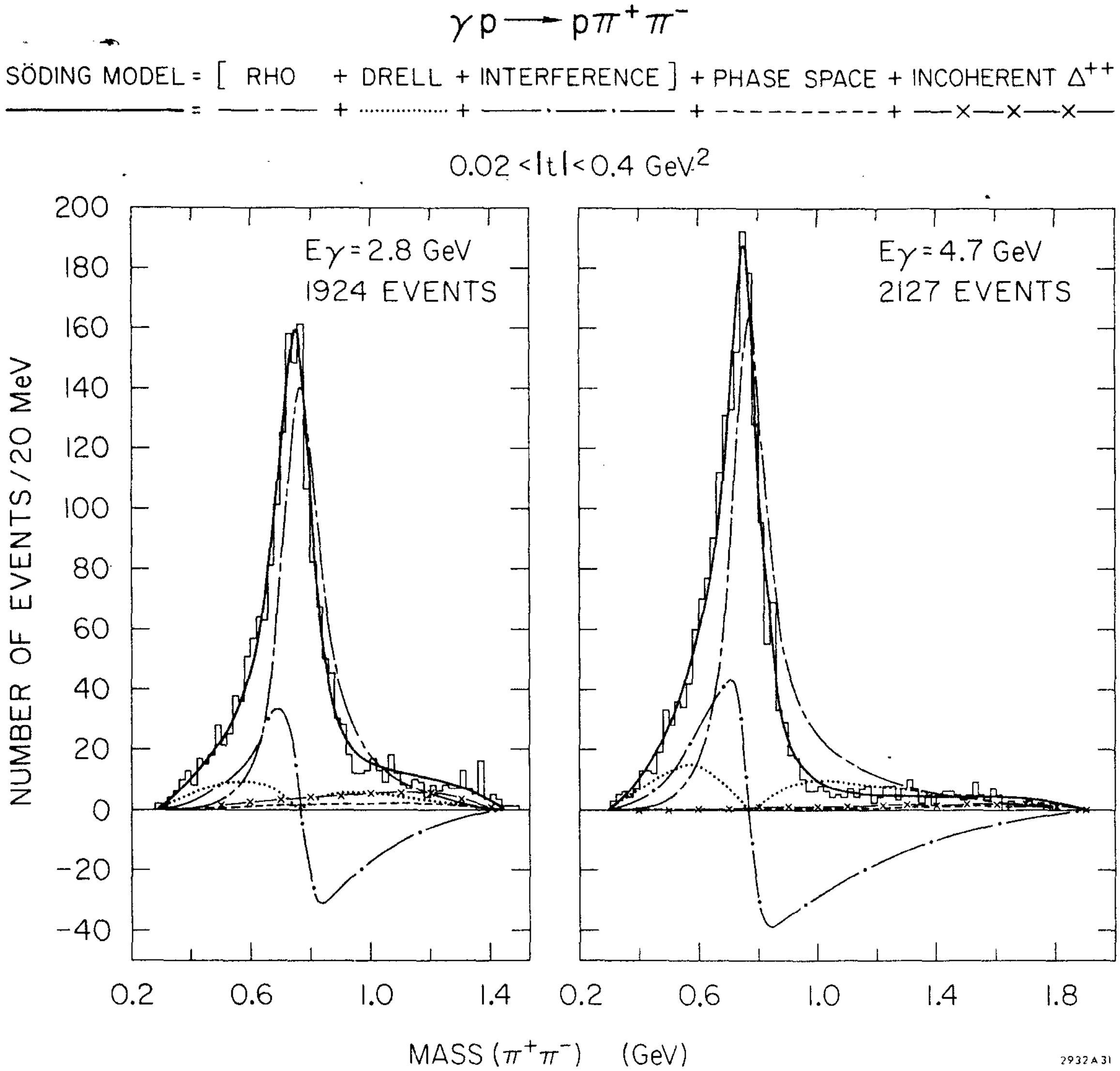

$\gamma p \longrightarrow p\pi^+\pi^-$
SÖDING MODEL = [RHO + DRELL + INTERFERENCE] + PHASE SPACE + INCOHERENT Δ^{++}
$0.02 < |t| < 0.4$ GeV^2
$E\gamma = 2.8$ GeV
1924 EVENTS
$E\gamma = 4.7$ GeV
2127 EVENTS
NUMBER OF EVENTS / 20 MeV
MASS ($\pi^+\pi^-$) (GeV)
2932A31

Fig. 11

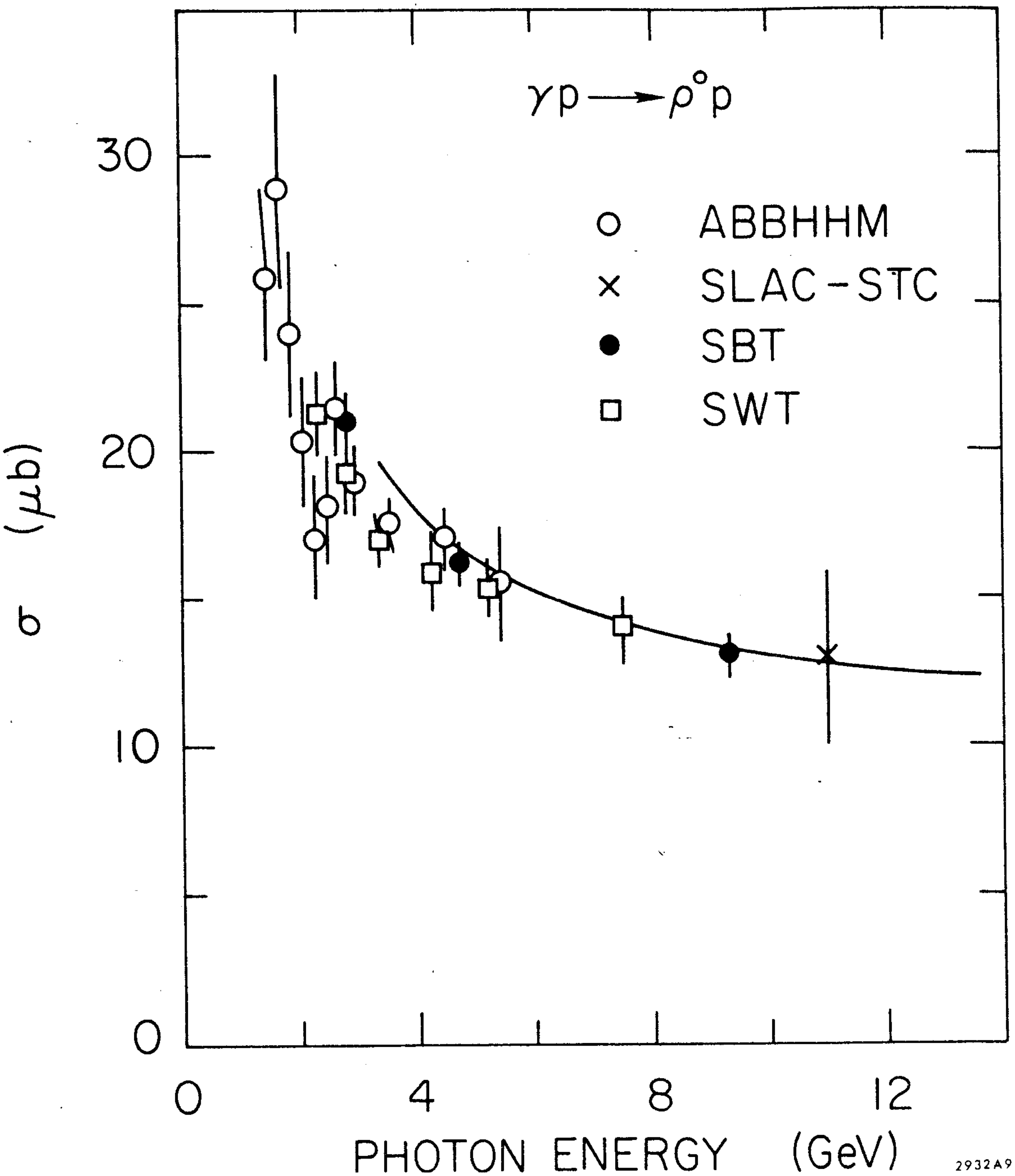

γp ⟶ ρ°p
ABBHHM
SLAC-STC
SBT
SWT
σ (μb)
30
20
10
0
0
4
8
12
PHOTON ENERGY (GeV)
2932A9

Fig. 12

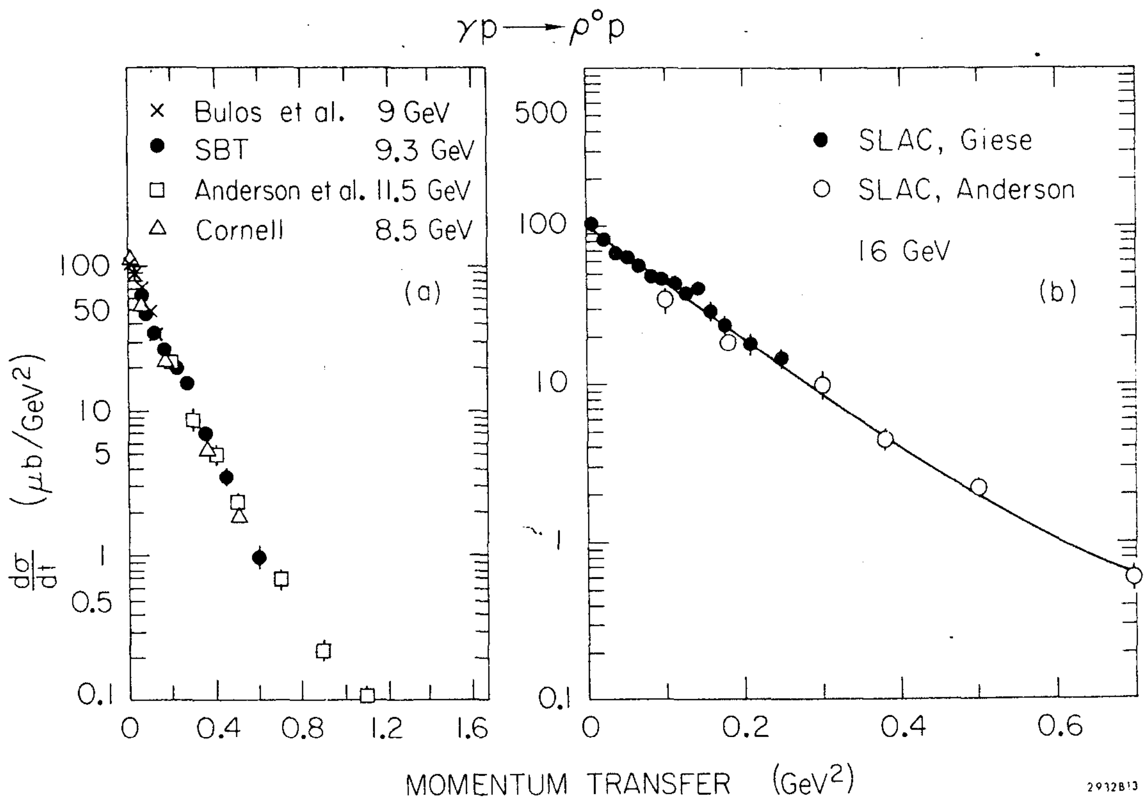

γp → ρ°p
× Bulos et al. 9 GeV
● SBT 9.3 GeV
□ Anderson et al. 11.5 GeV
△ Cornell 8.5 GeV
(a)
● SLAC, Giese
○ SLAC, Anderson
16 GeV
(b)
dσ/dt (μb/GeV²)
MOMENTUM TRANSFER (GeV²)
2932B13

Fig. 13

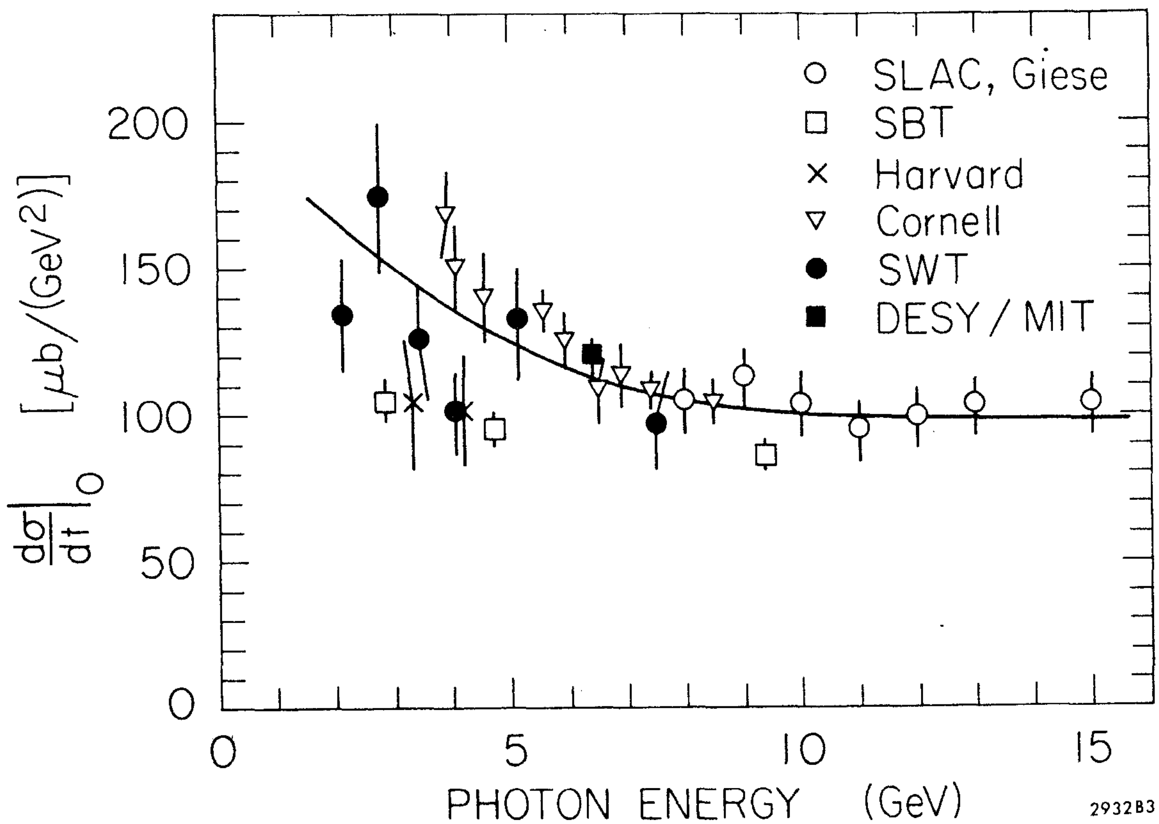

SLAC, Giese
SBT
Harvard
Cornell
SWT
DESY / MIT
200
150
100
50
0
$\frac{d\sigma}{dt}\Big|_0$ [μb/(GeV^2)]
0
5
10
15
PHOTON ENERGY (GeV)
2932B3

Fig. 14

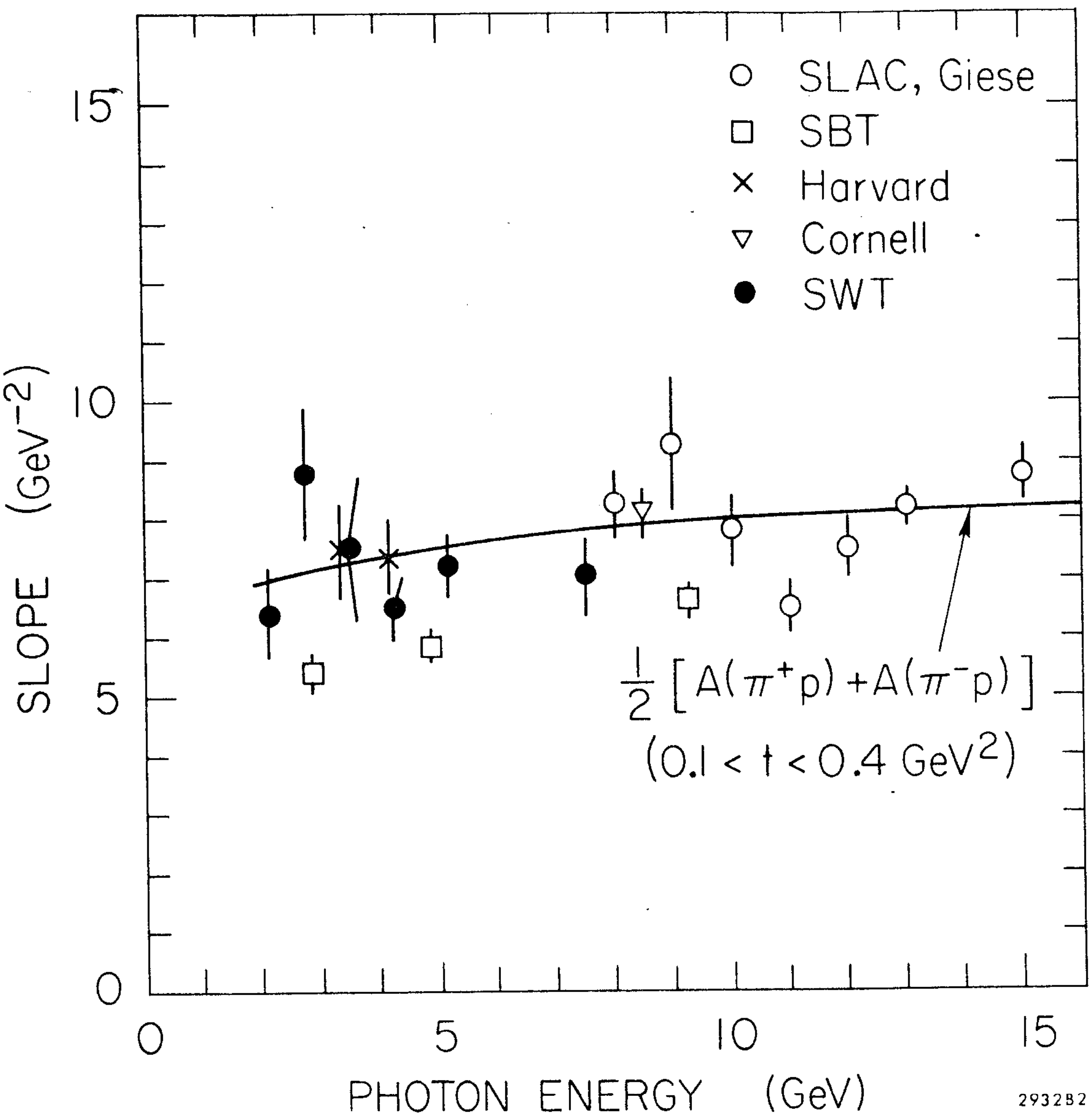

SLAC, Giese
SBT
Harvard
Cornell
SWT
SLOPE (GeV^{-2})
PHOTON ENERGY (GeV)
$\frac{1}{2}\left[A(\pi^+p)+A(\pi^-p)\right]$
$(0.1 < t < 0.4\ \mathrm{GeV}^2)$
0
5
10
15
0
5
10
15
293282

Fig. 15

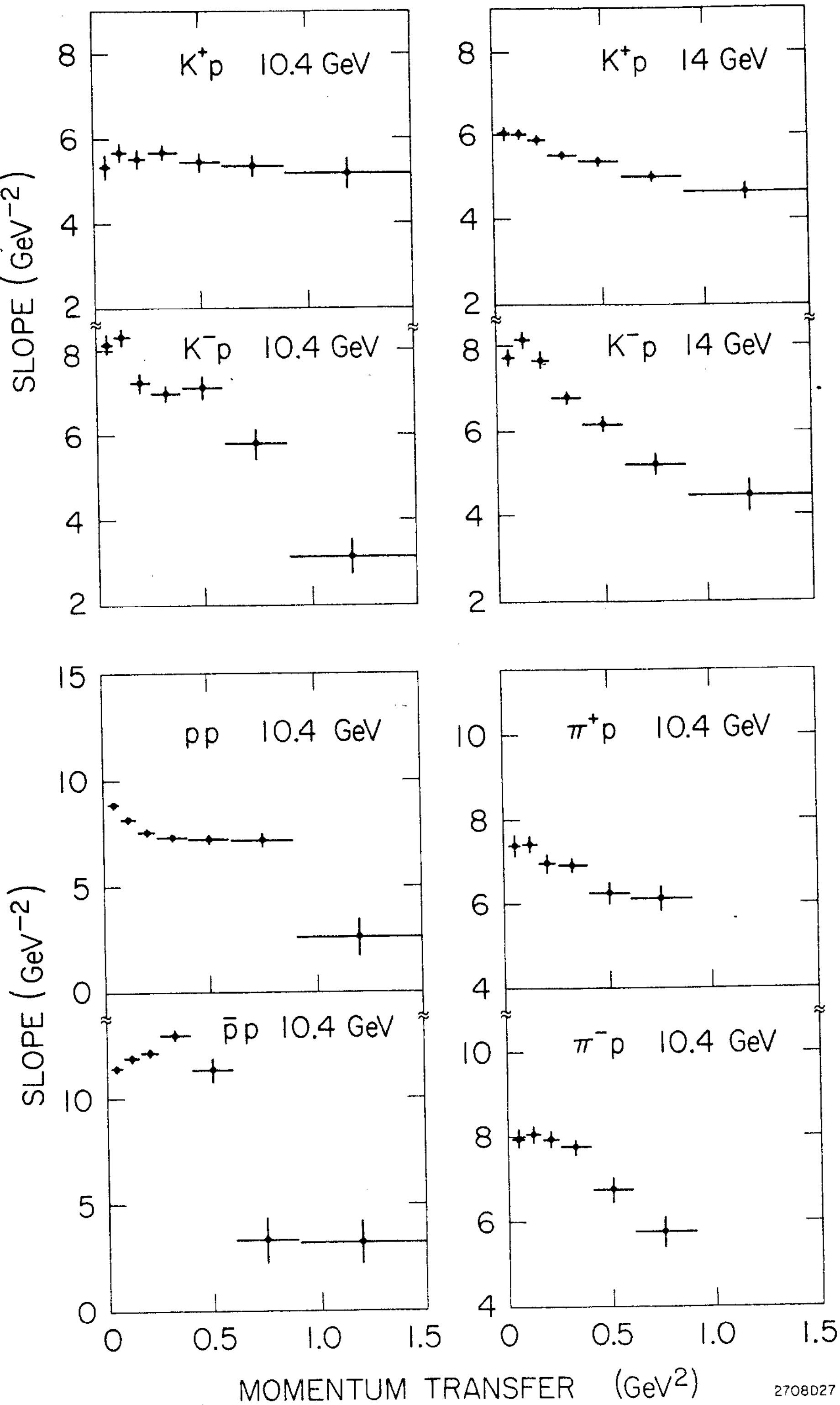
K⁺p 10.4 GeV
K⁺p 14 GeV
K⁻p 10.4 GeV
K⁻p 14 GeV
pp 10.4 GeV
π⁺p 10.4 GeV
p̄p 10.4 GeV
π⁻p 10.4 GeV
SLOPE (GeV⁻²)
MOMENTUM TRANSFER (GeV²)
2708D27

Fig. 16

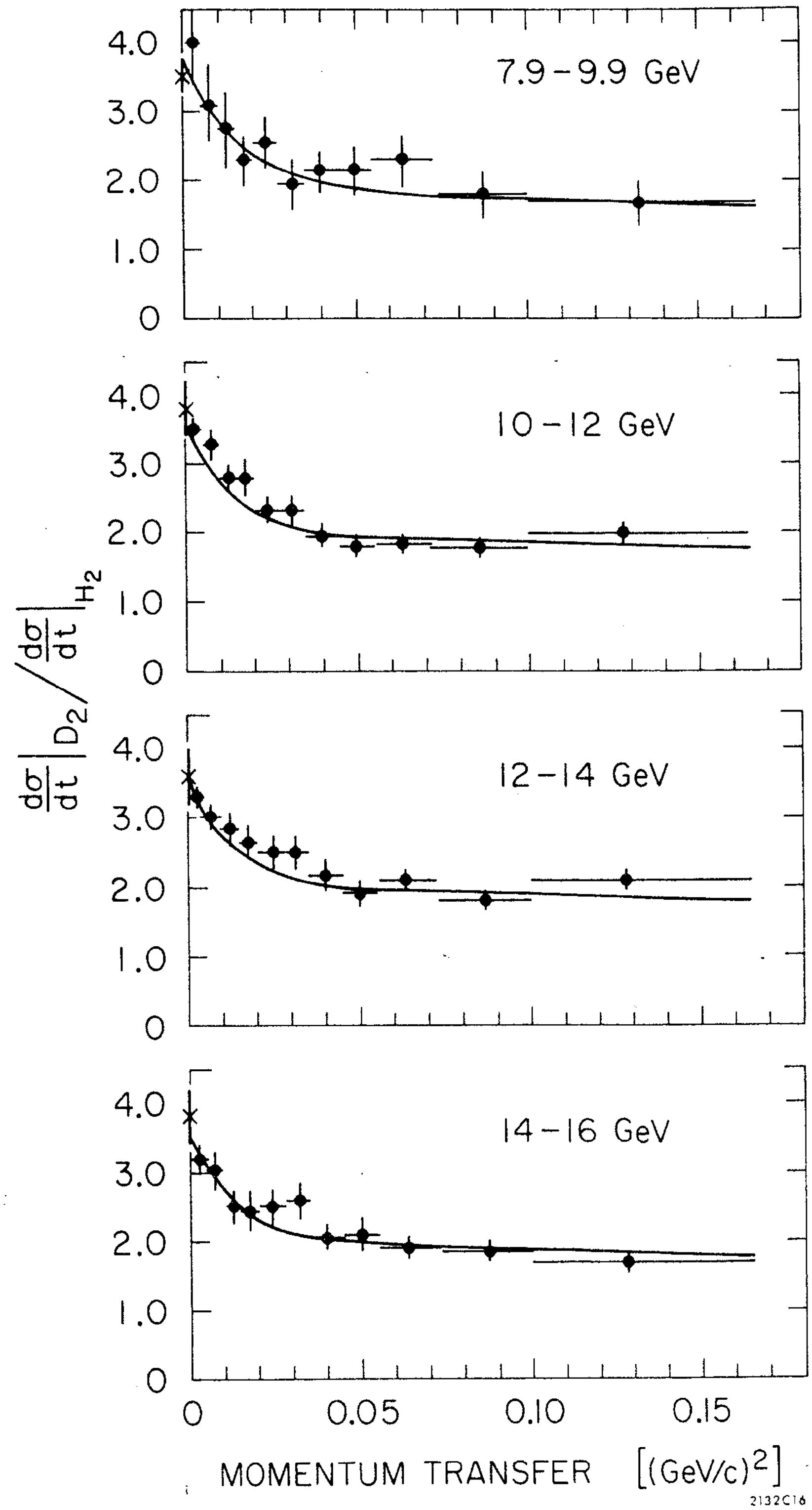

7.9 − 9.9 GeV
10 − 12 GeV
12 − 14 GeV
14 − 16 GeV
4.0
3.0
2.0
1.0
0
0
0.05
0.10
0.15
MOMENTUM TRANSFER [(GeV/c)²]
2132C16

Fig. 17

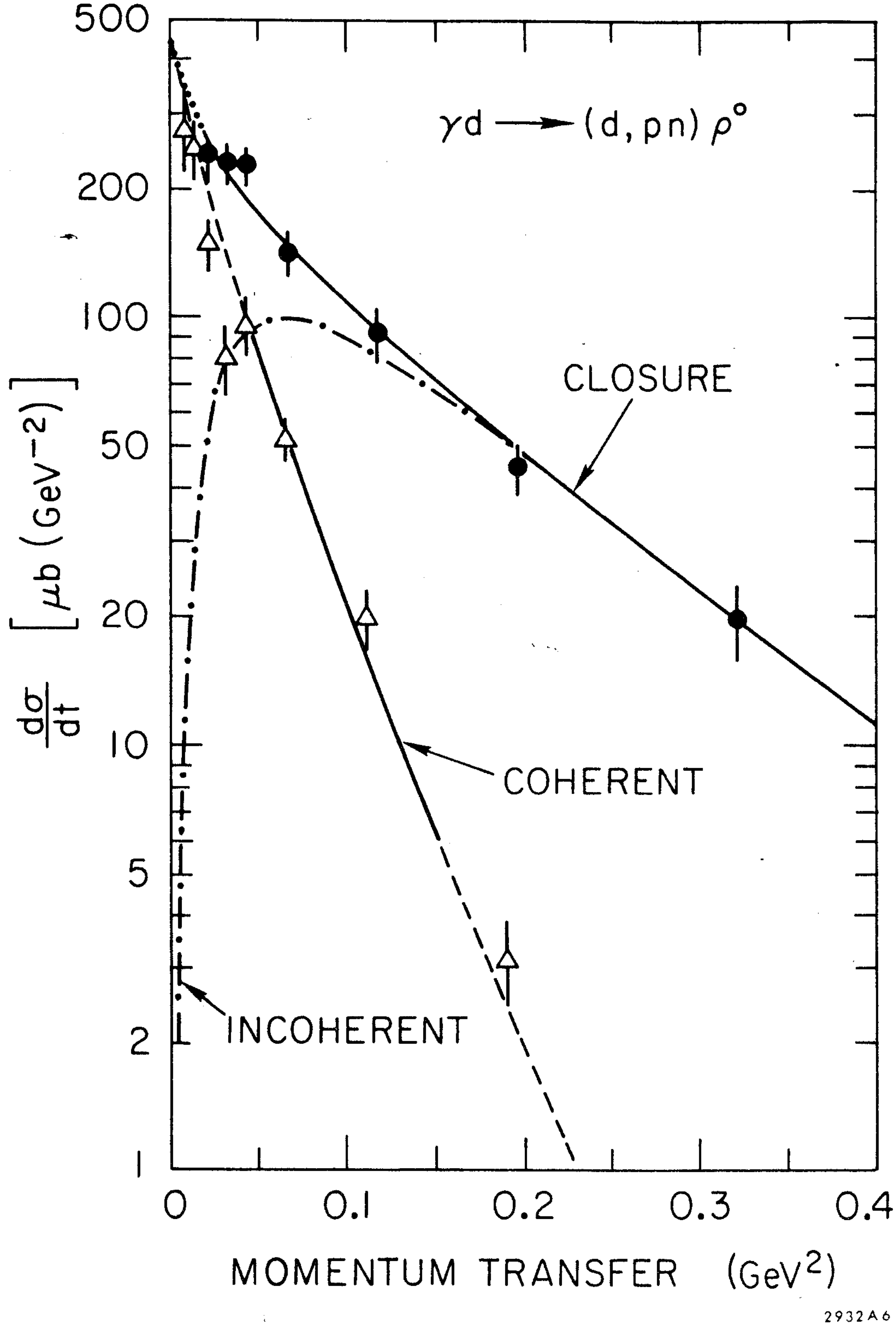

$\gamma d \longrightarrow (d, pn)\rho^{\circ}$
CLOSURE
COHERENT
INCOHERENT
$\frac{d\sigma}{dt}$ [μb (GeV^{-2})]
500
200
100
50
20
10
5
2
1
0
0.1
0.2
0.3
0.4
MOMENTUM TRANSFER (GeV^2)
2932A6

Fig. 18

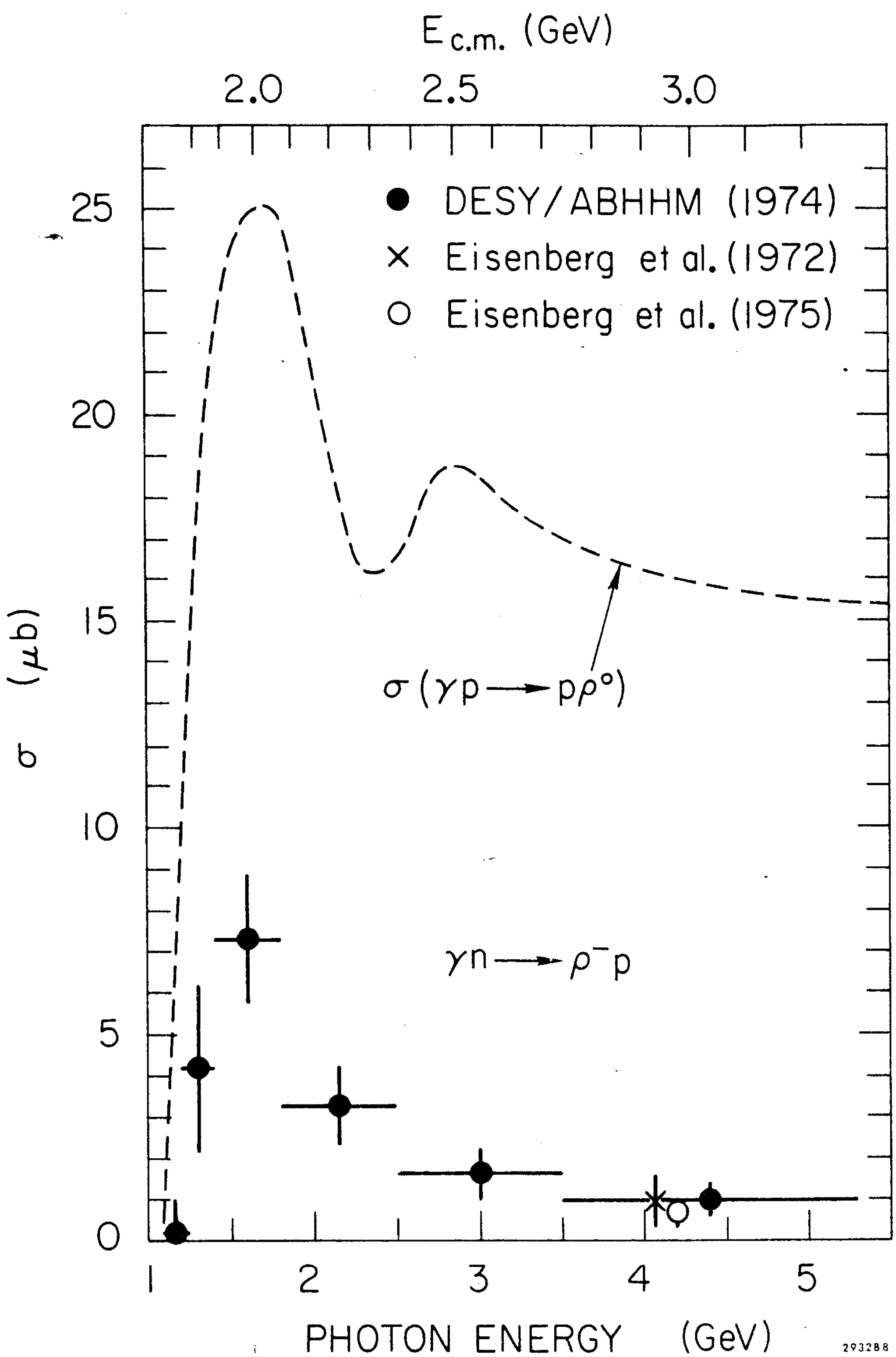

E c.m. (GeV)
2.0
2.5
3.0
DESY/ABHHM (1974)
Eisenberg et al. (1972)
Eisenberg et al. (1975)
σ (γp → pρ°)
γn → ρ⁻p
σ (μb)
25
20
15
10
5
0
1
2
3
4
5
PHOTON ENERGY (GeV)
293288

Fig. 19

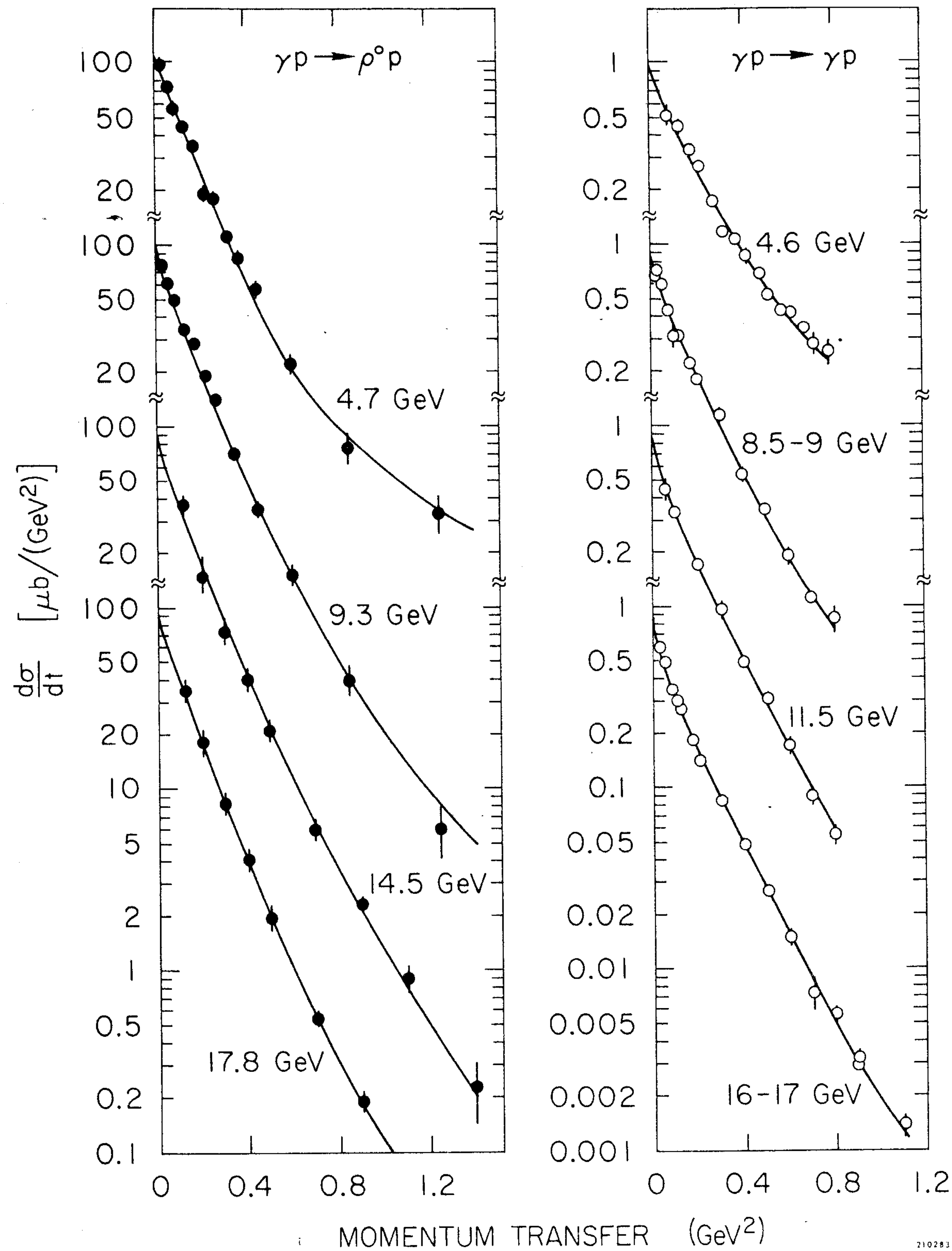

$\gamma p \rightarrow \rho^\circ p$
$\gamma p \rightarrow \gamma p$
4.7 GeV
9.3 GeV
14.5 GeV
17.8 GeV
4.6 GeV
8.5-9 GeV
11.5 GeV
16-17 GeV
$\frac{d\sigma}{dt}$ [$\mu b/(GeV^2)$]
MOMENTUM TRANSFER (GeV^2)

Fig. 20

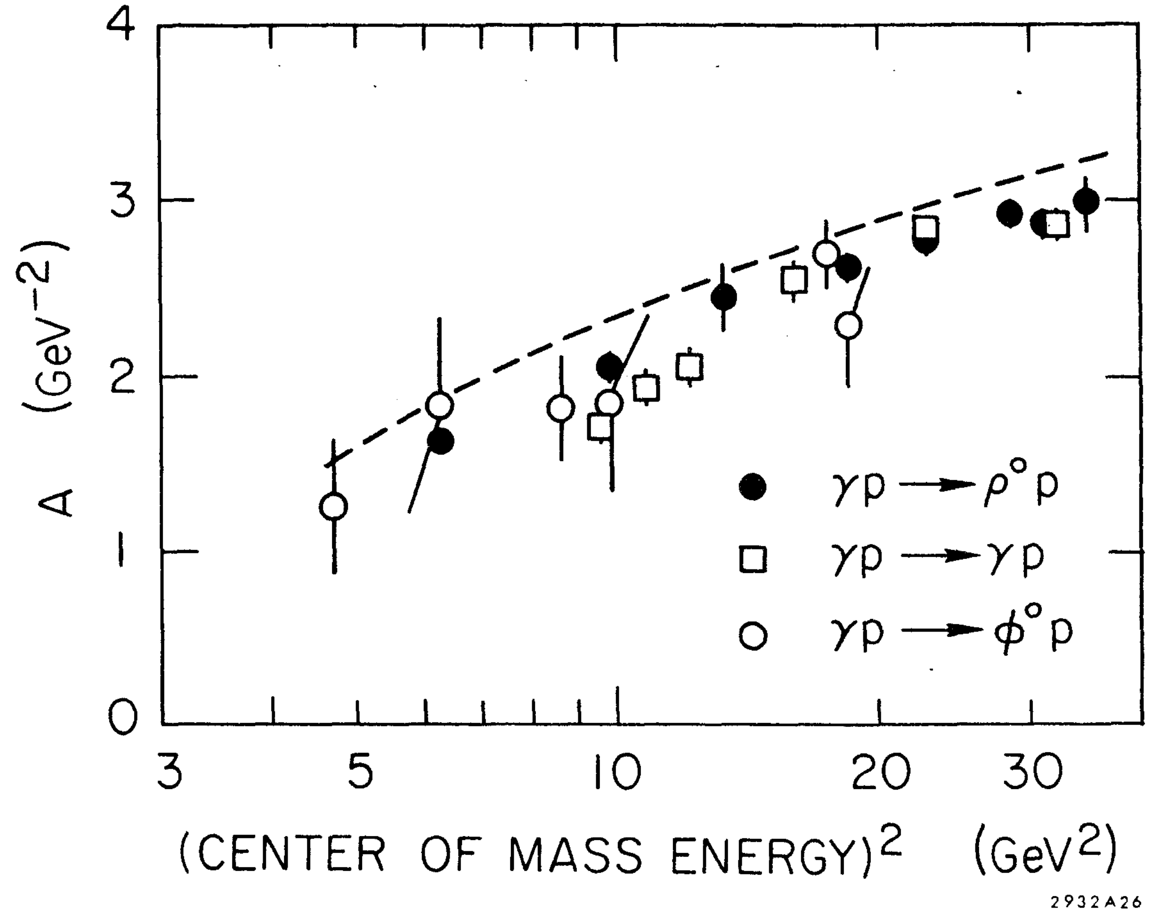
4
3
2
1
0
A (GeV^{-2})
3
5
10
20
30
(CENTER OF MASS ENERGY)^2 (GeV^2)
$\gamma p \longrightarrow \rho^\circ p$
$\gamma p \longrightarrow \gamma p$
$\gamma p \longrightarrow \phi^\circ p$
2932A26

Fig. 21

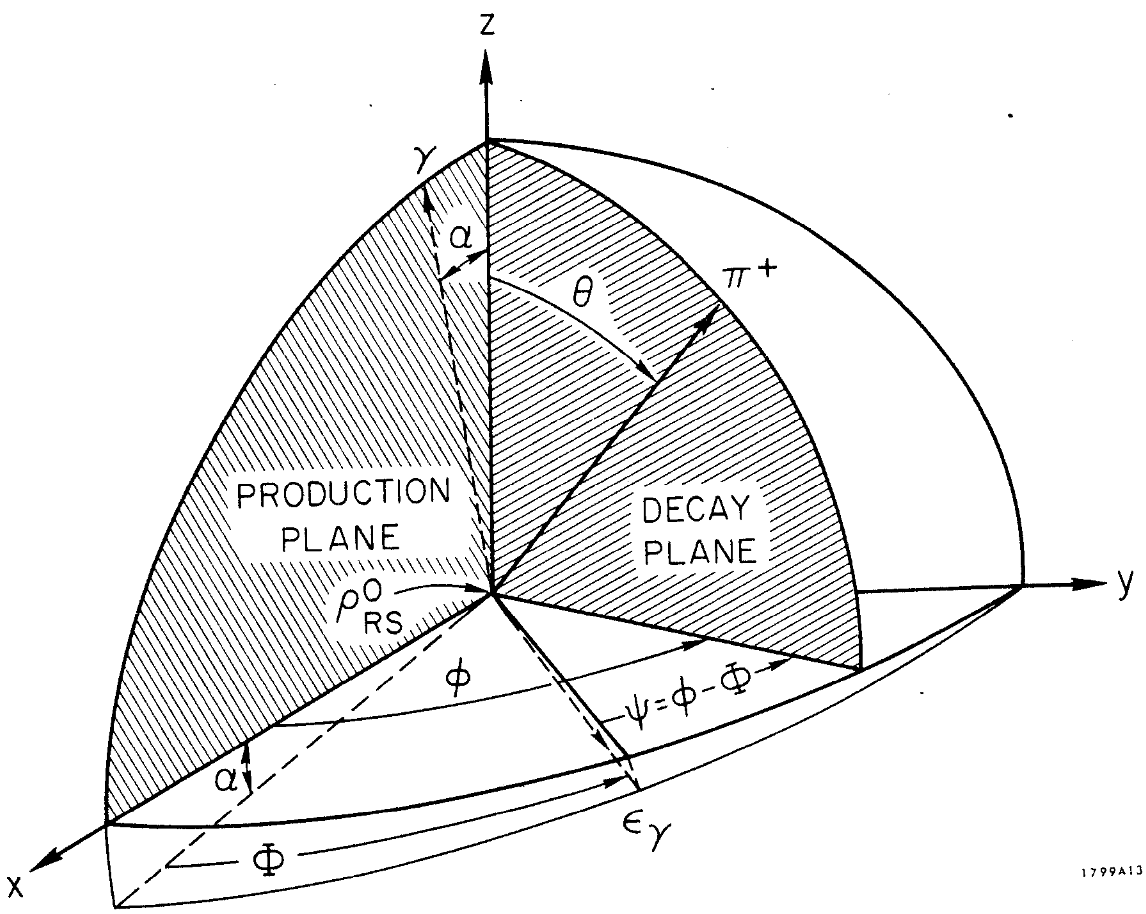
z
γ
α
θ
π⁺
PRODUCTION
PLANE
DECAY
PLANE
y
ρ^0_{RS}
φ
ψ=φ-Φ
α
ϵ_γ
Φ
x
1799A13

Fig. 22

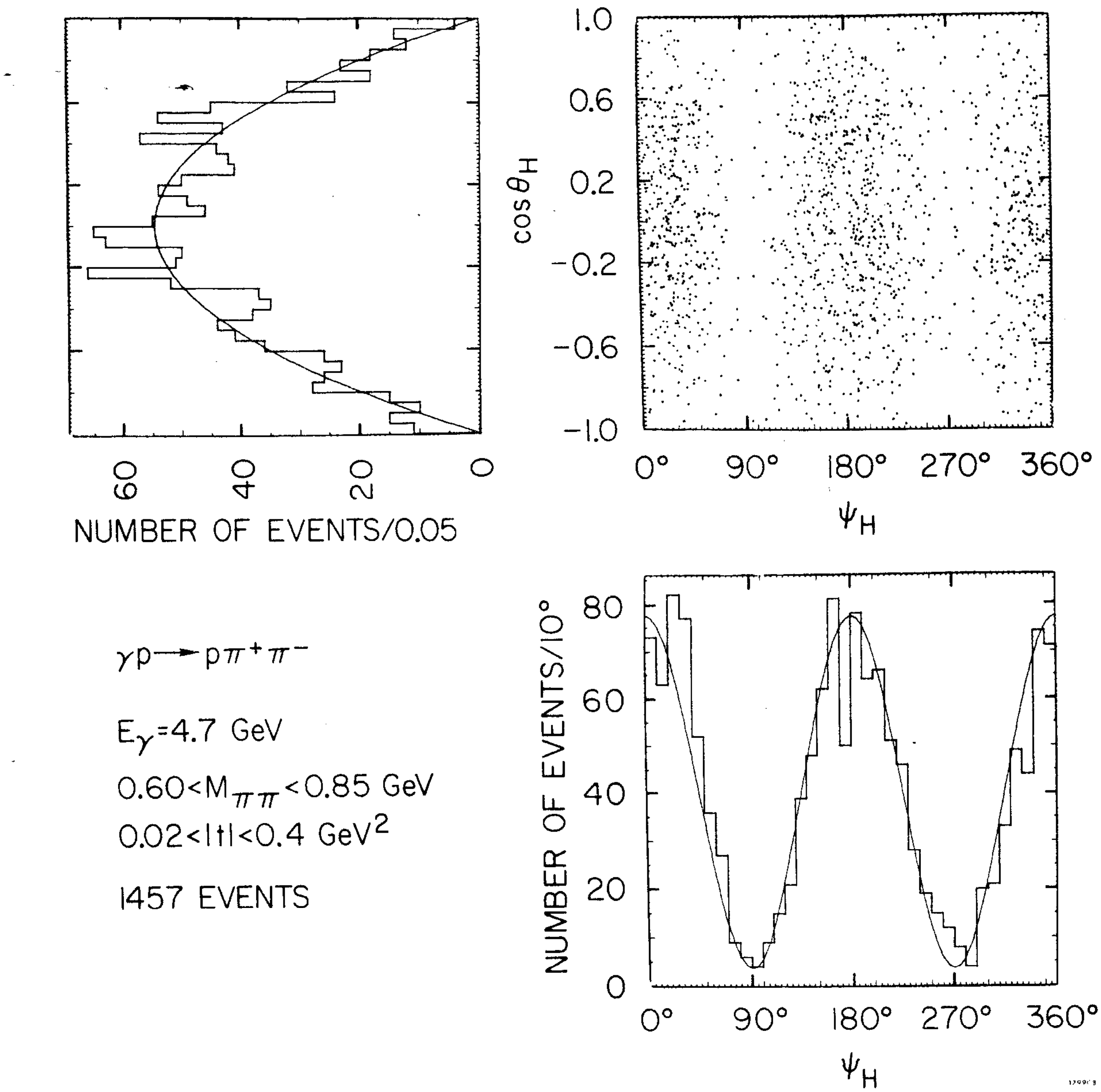

NUMBER OF EVENTS/0.05
60
40
20
0
1.0
0.6
0.2
−0.2
−0.6
−1.0
$\cos\theta_H$
0° 90° 180° 270° 360°
ψ_H
$\gamma p \rightarrow p\pi^+\pi^-$
E_γ=4.7 GeV
0.60<$M_{\pi\pi}$<0.85 GeV
0.02<|t|<0.4 GeV^2
1457 EVENTS
NUMBER OF EVENTS/10°
80
60
40
20
0
0° 90° 180° 270° 360°
ψ_H

Fig. 23

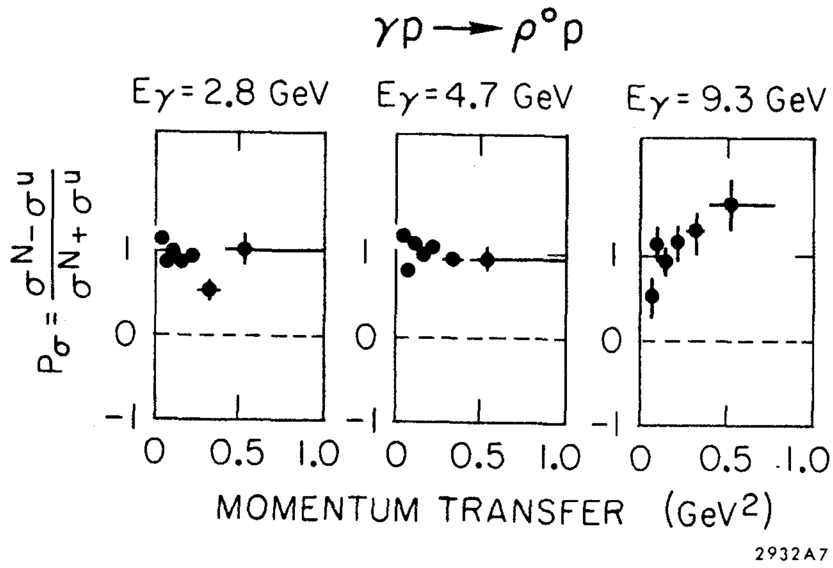

γp → ρ°p
Eγ = 2.8 GeV
Eγ = 4.7 GeV
Eγ = 9.3 GeV
Pσ = (σN − σU)/(σN + σU)
1
0
−1
0 0.5 1.0
MOMENTUM TRANSFER (GeV²)
2932A7

Fig. 24

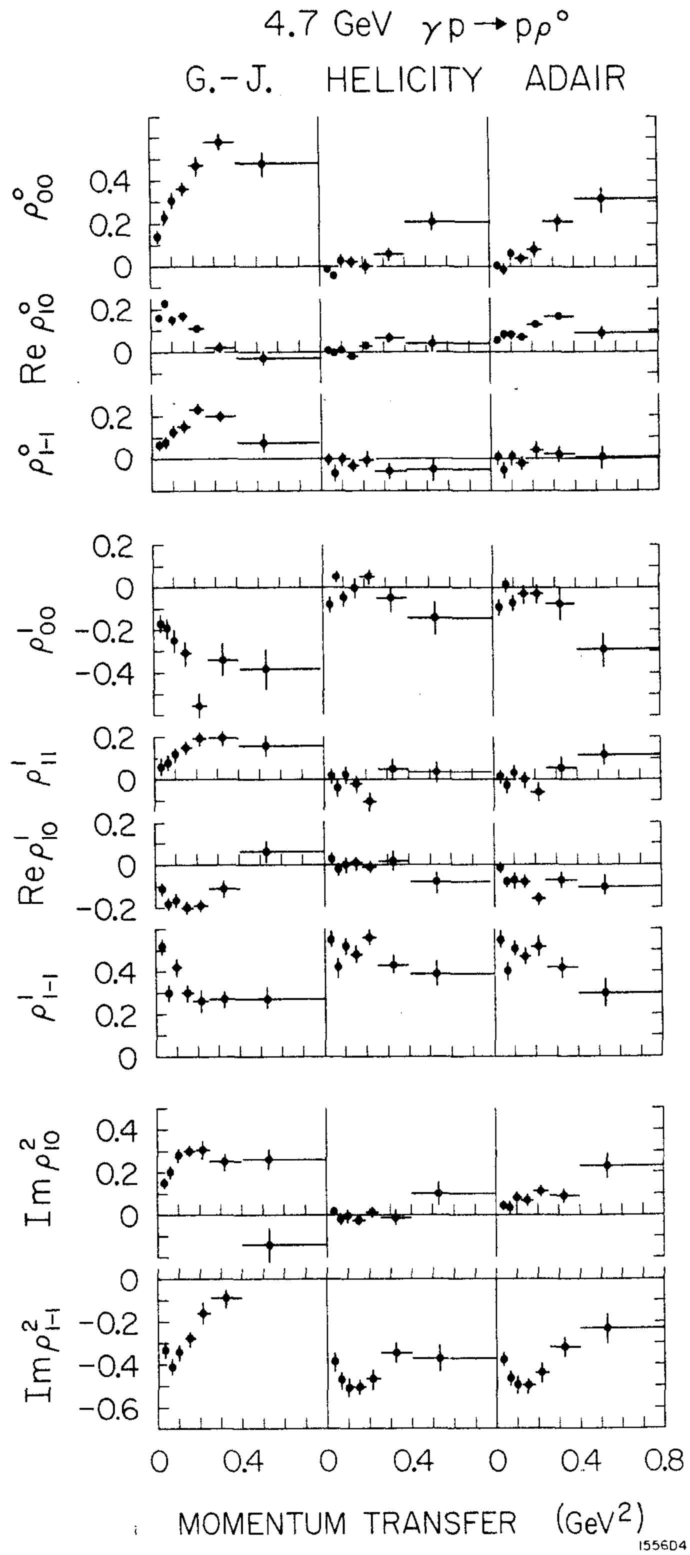
4.7 GeV $\gamma p \rightarrow p\rho^0$
G.-J.
HELICITY
ADAIR
ρ^0_{00}
$\mathrm{Re}\,\rho^0_{10}$
ρ^0_{1-1}
ρ^1_{00}
ρ^1_{11}
$\mathrm{Re}\,\rho^1_{10}$
ρ^1_{1-1}
$\mathrm{Im}\,\rho^2_{10}$
$\mathrm{Im}\,\rho^2_{1-1}$
MOMENTUM TRANSFER (GeV^2)
1556D4

Fig. 25

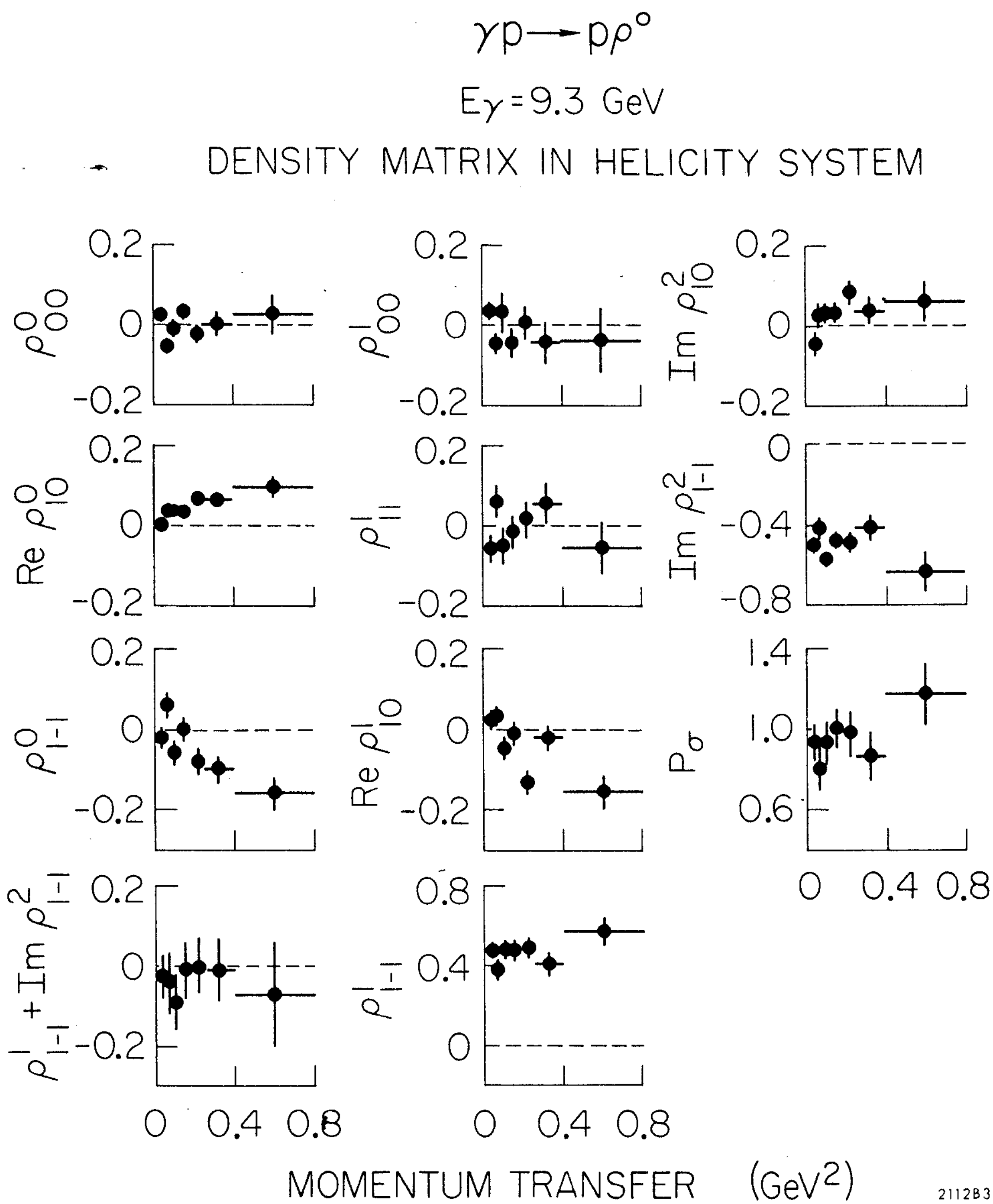
γp → pρ°
Eγ = 9.3 GeV
DENSITY MATRIX IN HELICITY SYSTEM
MOMENTUM TRANSFER (GeV²)
2112B3

Fig. 26

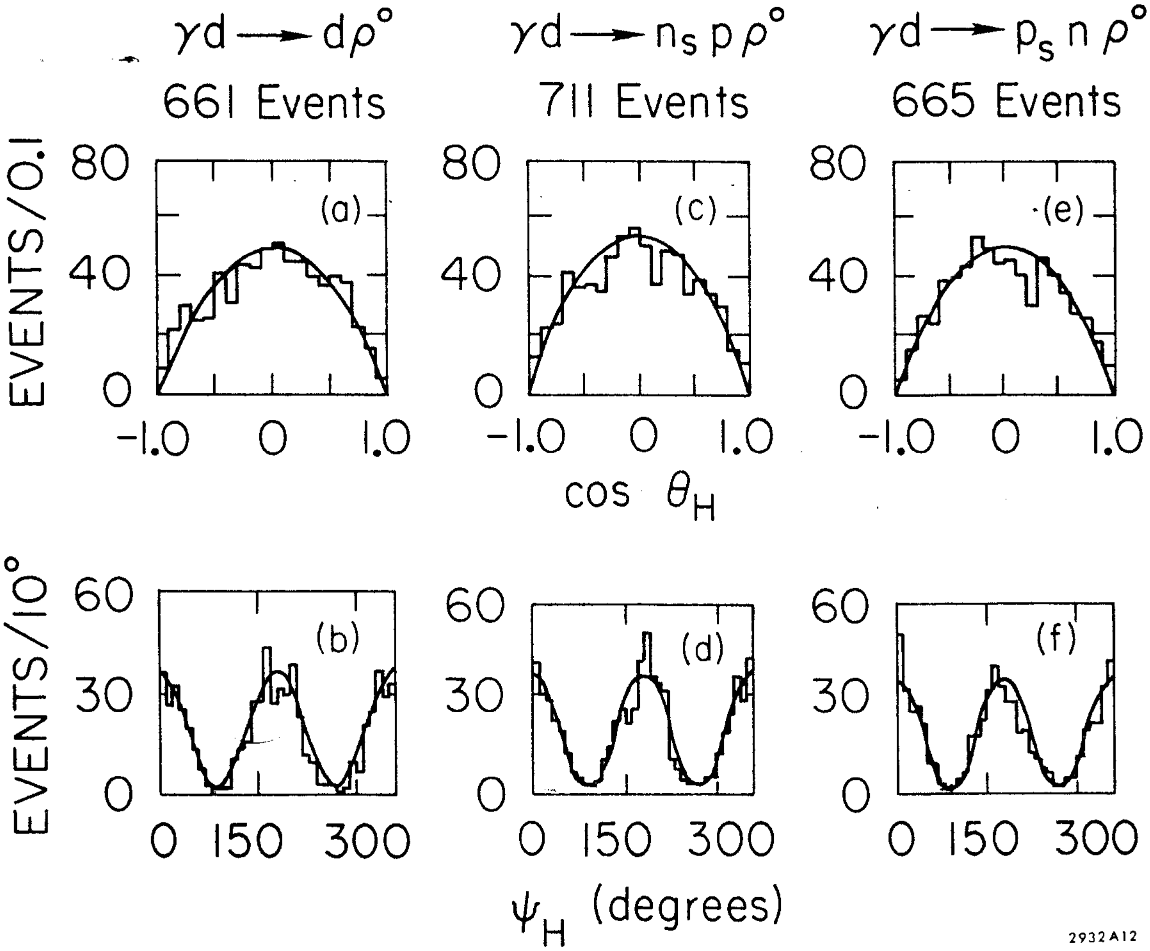
γd → dρ°
661 Events
γd → n_s p ρ°
711 Events
γd → p_s n ρ°
665 Events
EVENTS/0.1
80
40
0
(a)
(c)
(e)
-1.0
0
1.0
cos θ_H
EVENTS/10°
60
30
0
(b)
(d)
(f)
0
150
300
ψ_H (degrees)
2932A12

Fig. 27

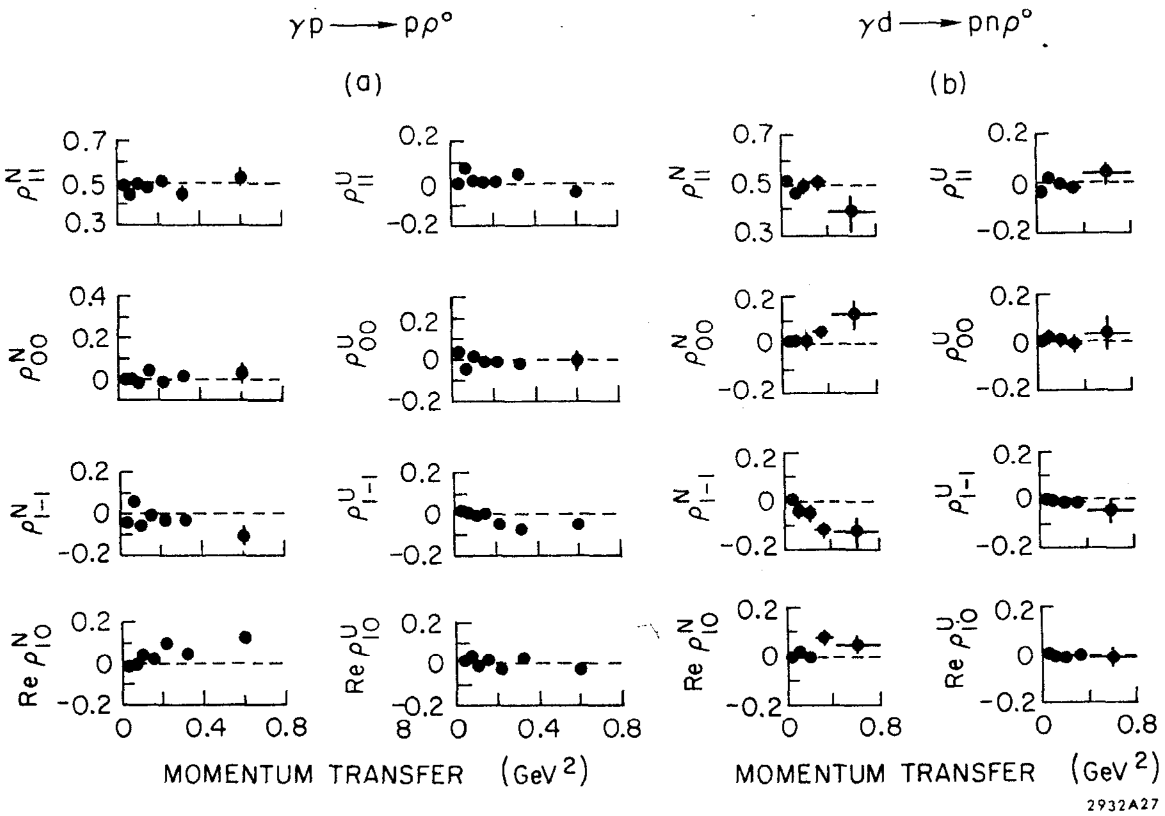
γp → pρ°
(a)
γd → pnρ°
(b)
MOMENTUM TRANSFER (GeV²)
MOMENTUM TRANSFER (GeV²)
2932A27

Fig. 28

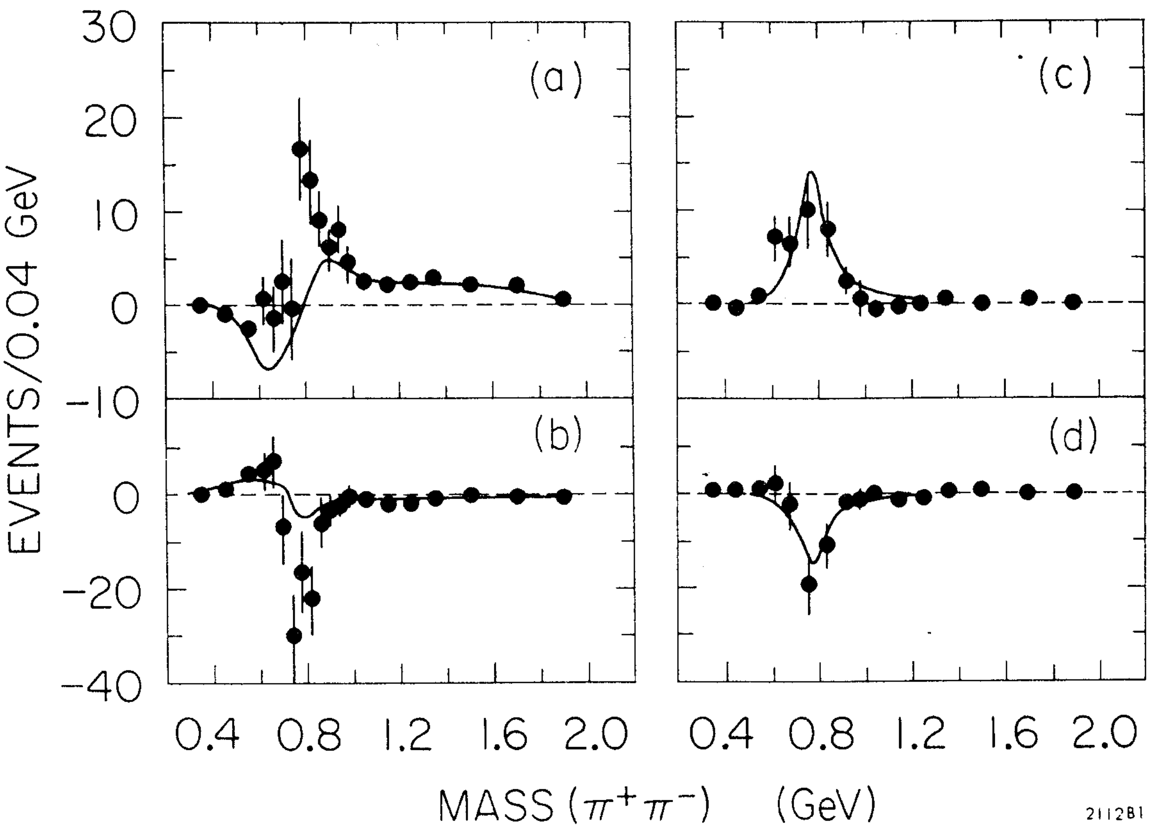

30
20
10
0
-10
0
-20
-40
(a)
(b)
(c)
(d)
EVENTS/0.04 GeV
0.4
0.8
1.2
1.6
2.0
MASS ($\pi^+\pi^-$) (GeV)
2112B1

Fig. 29

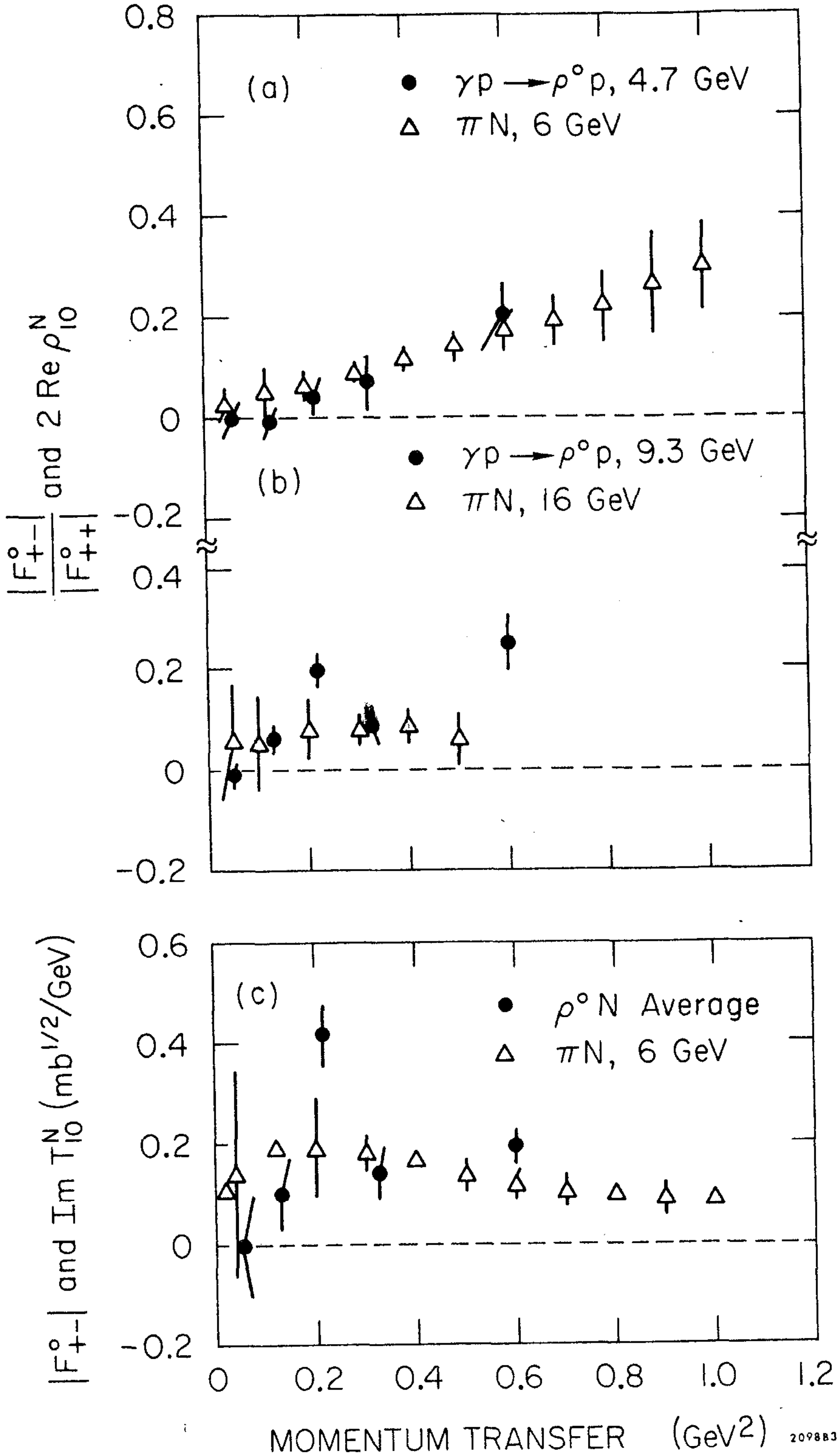

(a)
$\gamma p \rightarrow \rho^\circ p$, 4.7 GeV
πN, 6 GeV
(b)
$\gamma p \rightarrow \rho^\circ p$, 9.3 GeV
πN, 16 GeV
$\frac{|F^\circ_{+-}|}{|F^\circ_{++}|}$ and $2\,\mathrm{Re}\,\rho^N_{10}$
(c)
$\rho^\circ N$ Average
πN, 6 GeV
$|F^\circ_{+-}|$ and $\mathrm{Im}\,T^N_{10}$ (mb$^{1/2}$/GeV)
MOMENTUM TRANSFER (GeV^2)
0.8
0.6
0.4
0.2
0
−0.2
0.4
0.2
0
−0.2
0.6
0.4
0.2
0
−0.2
0
0.2
0.4
0.6
0.8
1.0
1.2
209883

Fig. 30

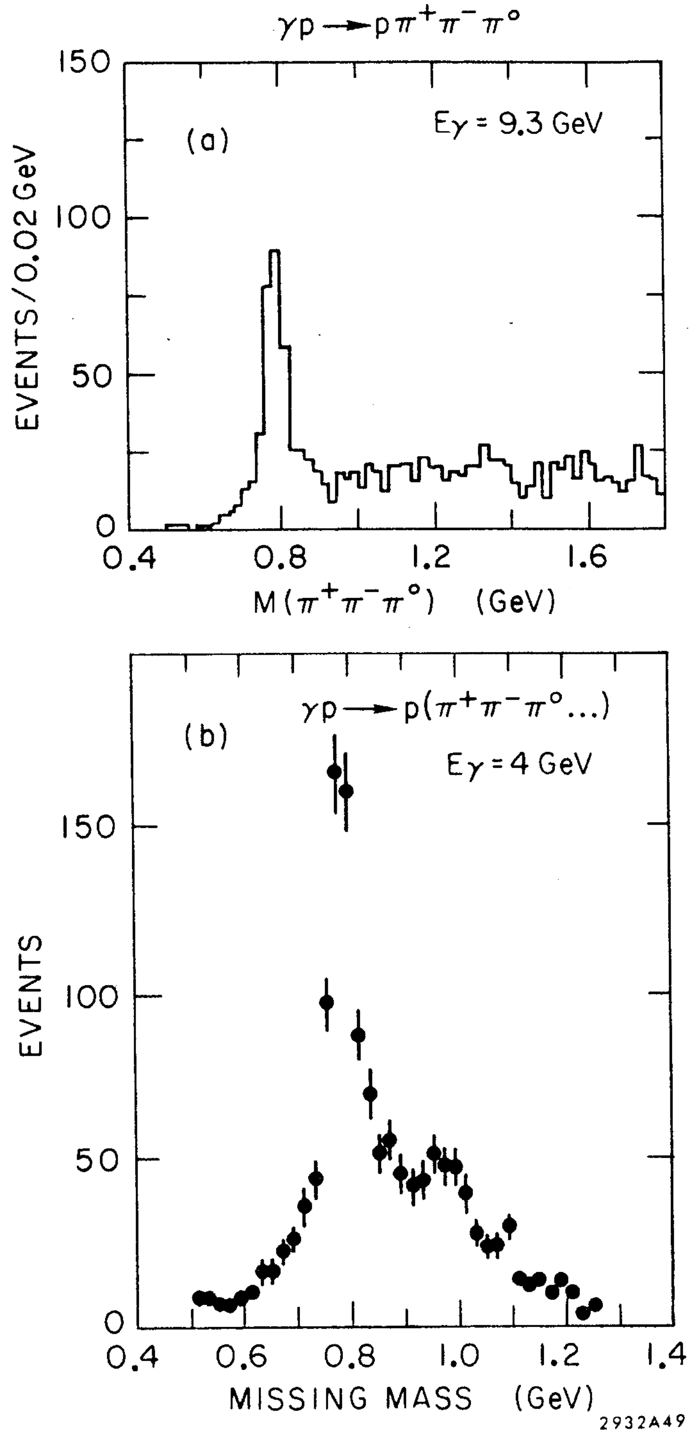

γp → pπ⁺π⁻π°
150
100
50
0
(a)
Eγ = 9.3 GeV
EVENTS/0.02 GeV
0.4
0.8
1.2
1.6
M(π⁺π⁻π°) (GeV)
(b)
γp → p(π⁺π⁻π°...)
Eγ = 4 GeV
EVENTS
150
100
50
0
0.4
0.6
0.8
1.0
1.2
1.4
MISSING MASS (GeV)
2932A49

Fig. 31

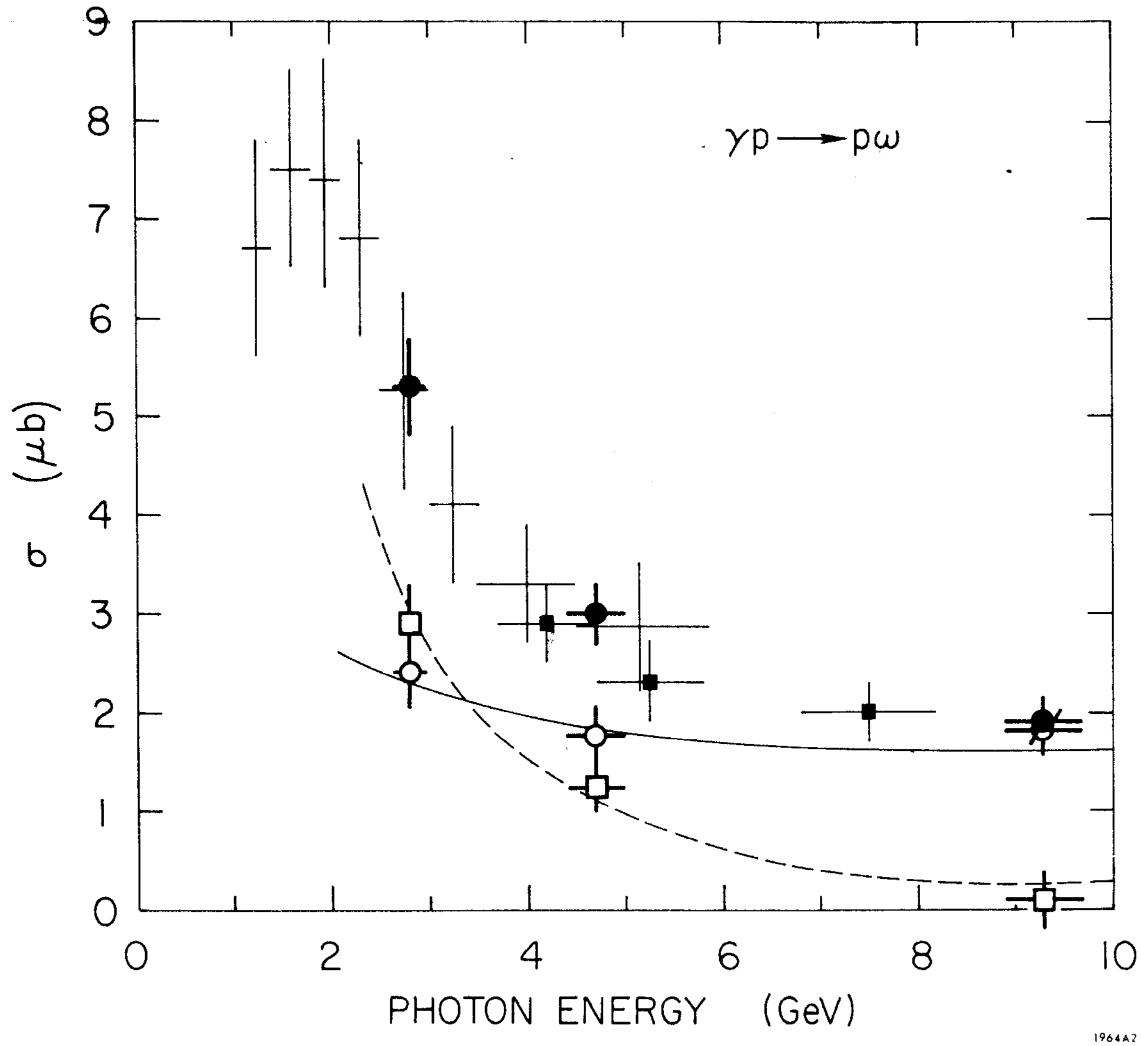

Fig. 32

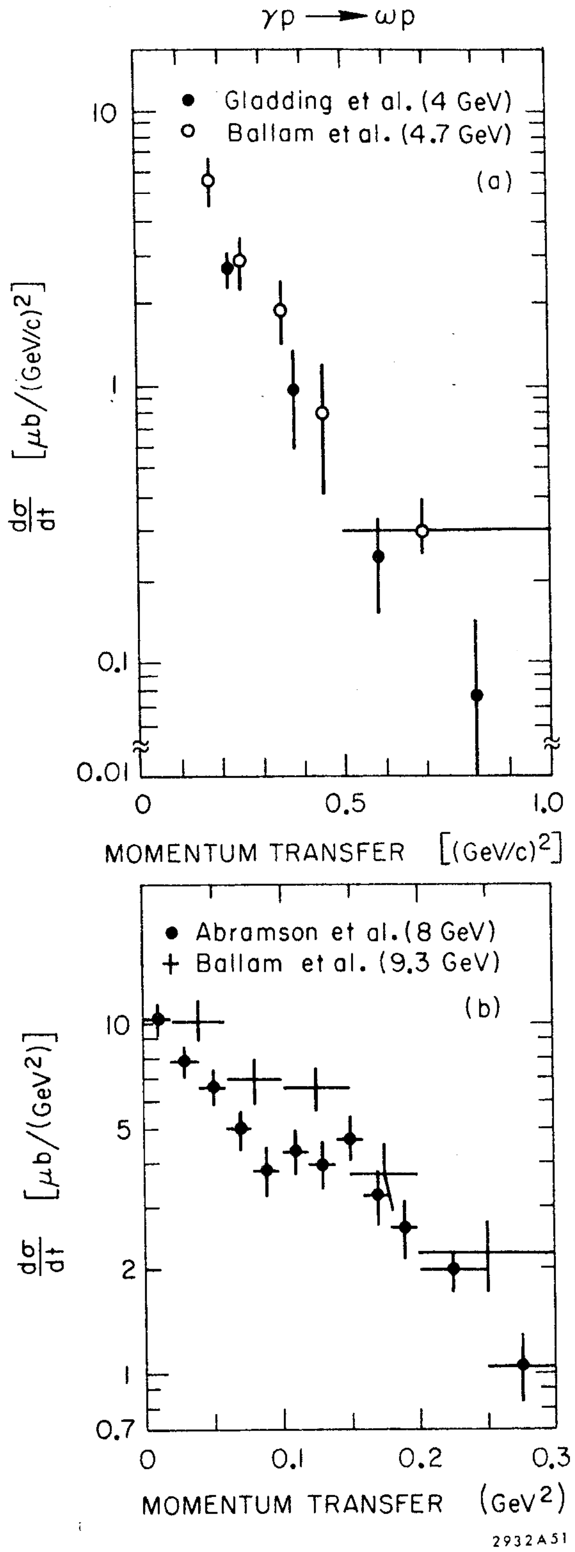
γp → ωp
Gladding et al. (4 GeV)
Ballam et al. (4.7 GeV)
(a)
dσ/dt [μb/(GeV/c)^2]
10
1
0.1
0.01
0
0.5
1.0
MOMENTUM TRANSFER [(GeV/c)^2]
Abramson et al. (8 GeV)
Ballam et al. (9.3 GeV)
(b)
dσ/dt [μb/(GeV^2)]
10
5
2
1
0.7
0
0.1
0.2
0.3
MOMENTUM TRANSFER (GeV^2)
2932A51

Fig. 33

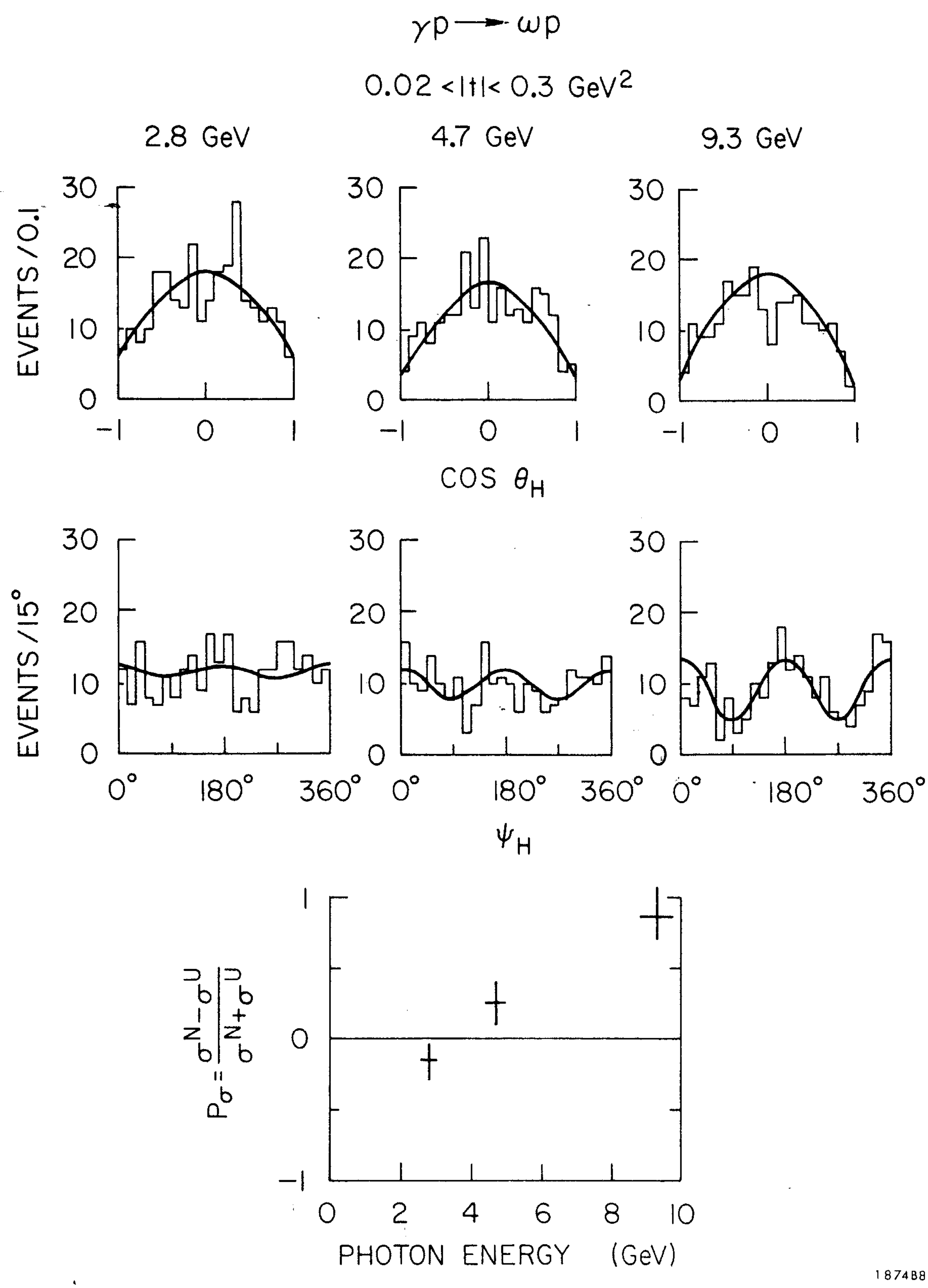

$\gamma p \to \omega p$
$0.02 < |t| < 0.3$ GeV^2
2.8 GeV
4.7 GeV
9.3 GeV
EVENTS / 0.1
COS θ_H
EVENTS / 15°
ψ_H
$P_\sigma = \frac{\sigma^N - \sigma^U}{\sigma^N + \sigma^U}$
PHOTON ENERGY (GeV)
187488

Fig. 34

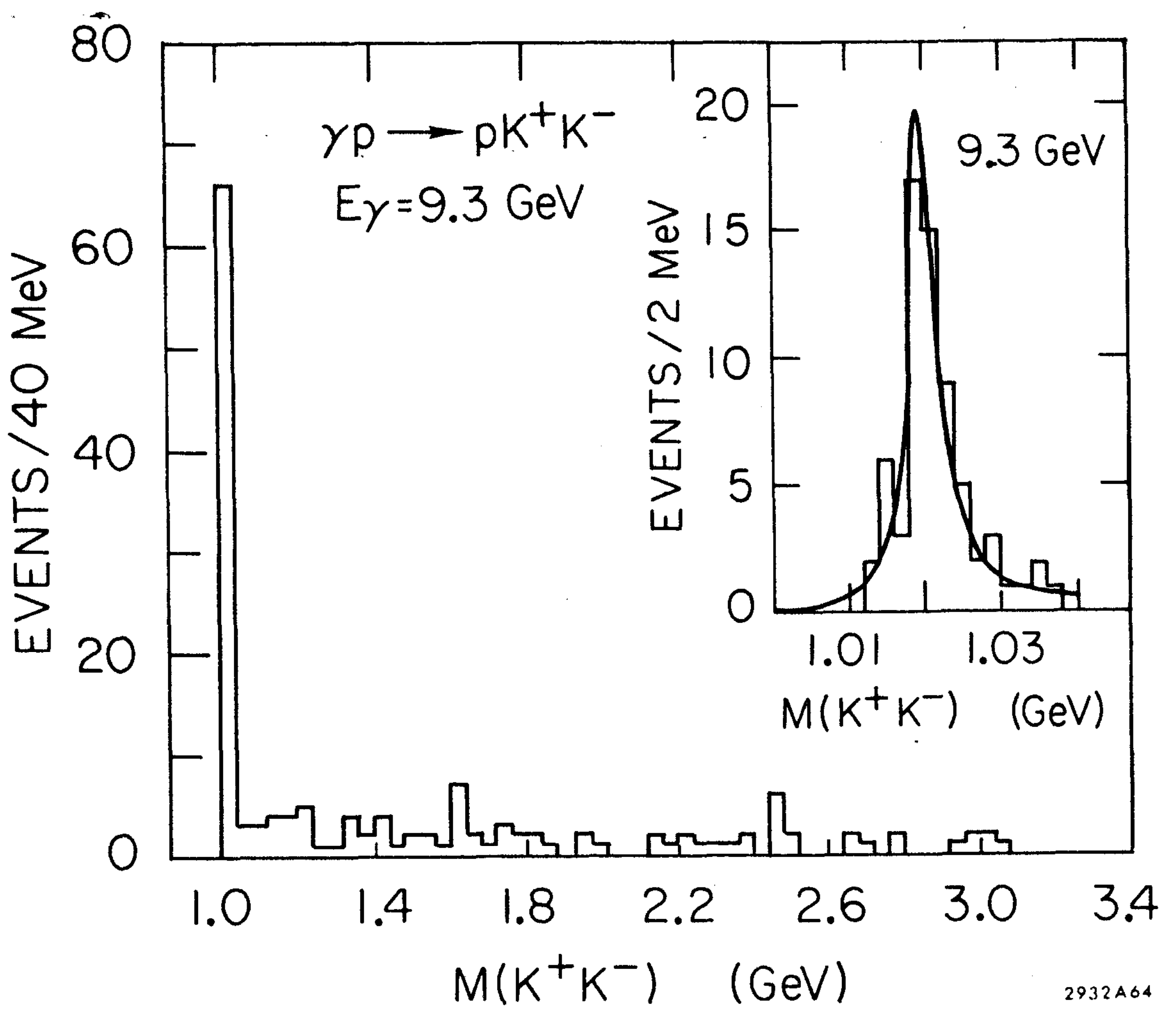

$\gamma p \rightarrow pK^+K^-$
$E\gamma$=9.3 GeV
9.3 GeV
EVENTS/2 MeV
EVENTS/40 MeV
M(K+K−) (GeV)
M(K+K−) (GeV)
2932A64

Fig. 35

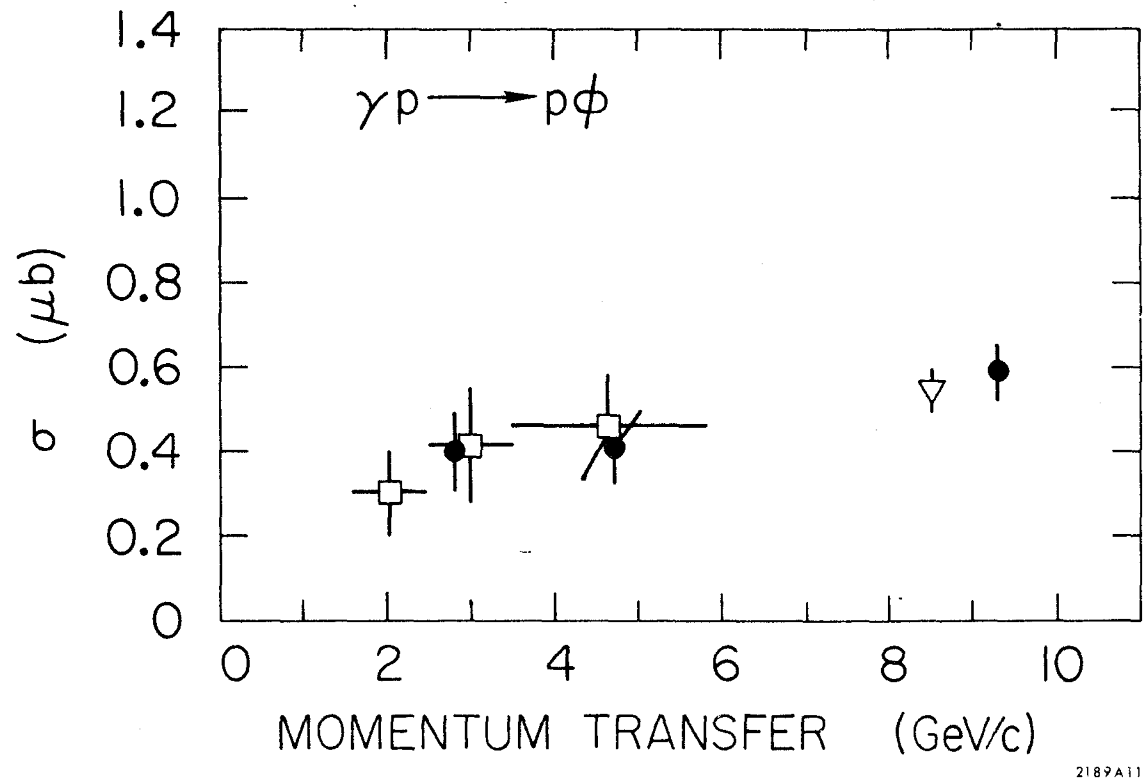
1.4
1.2
1.0
0.8
0.6
0.4
0.2
0
σ (μb)
γp ⟶ pφ
0
2
4
6
8
10
MOMENTUM TRANSFER (GeV/c)
2189A11

Fig. 36

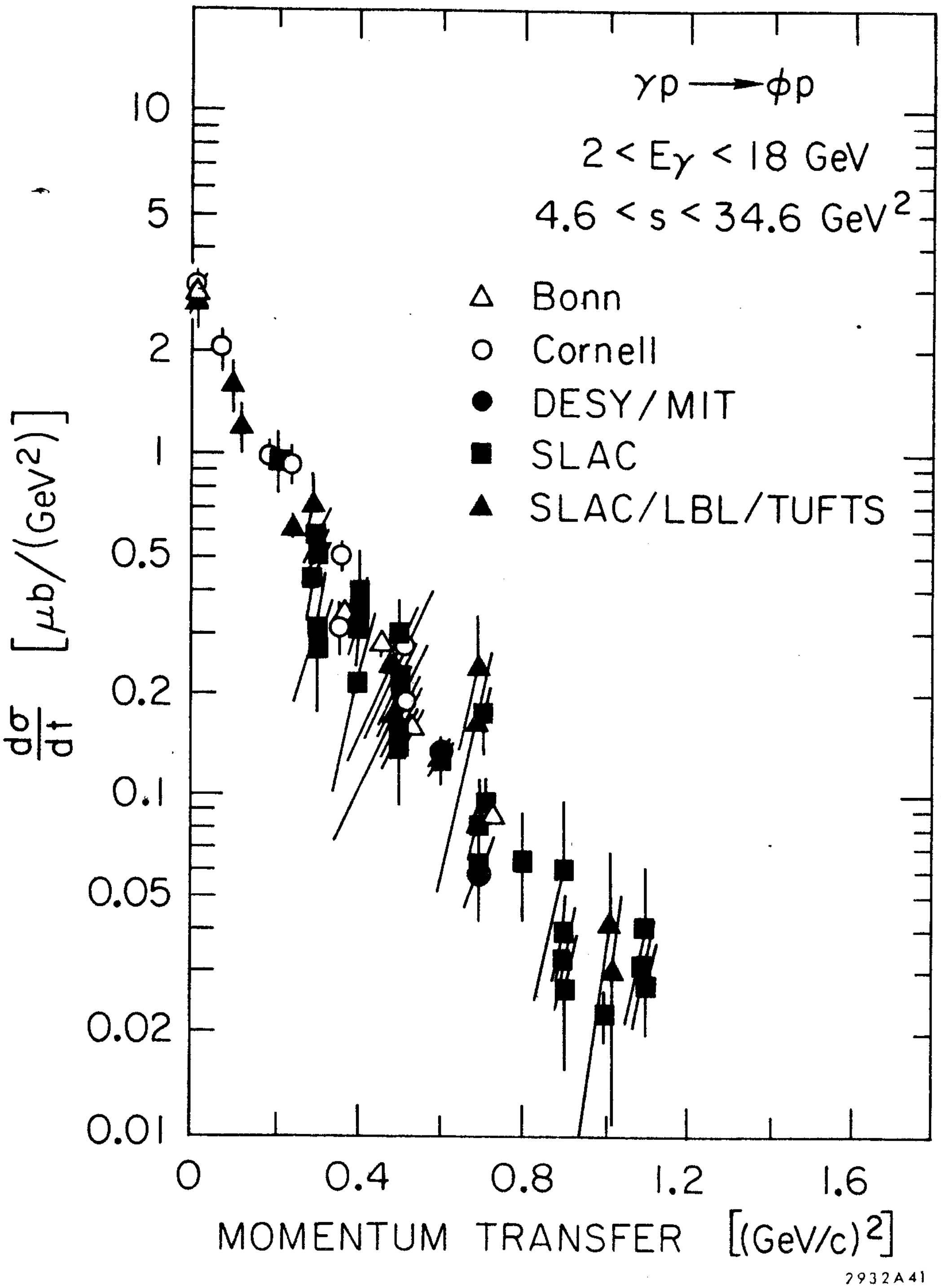
γp → φp
2 < Eγ < 18 GeV
4.6 < s < 34.6 GeV²
Bonn
Cornell
DESY/MIT
SLAC
SLAC/LBL/TUFTS
dσ/dt [μb/(GeV²)]
10
5
2
1
0.5
0.2
0.1
0.05
0.02
0.01
0
0.4
0.8
1.2
1.6
MOMENTUM TRANSFER [(GeV/c)²]
2932A41

Fig. 37a

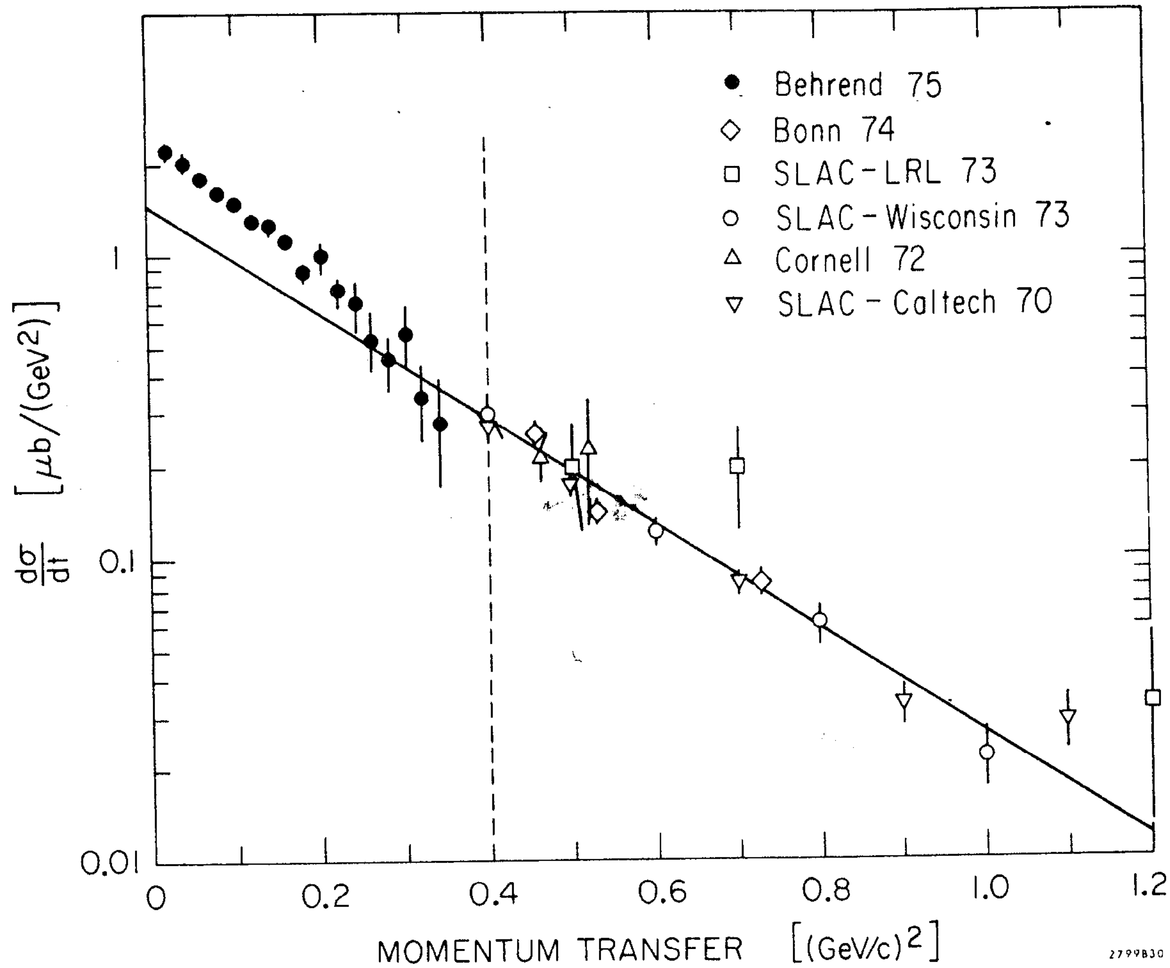
Behrend 75
Bonn 74
SLAC-LRL 73
SLAC-Wisconsin 73
Cornell 72
SLAC-Caltech 70
$\frac{d\sigma}{dt}$ [μb/(GeV^2)]
1
0.1
0.01
0
0.2
0.4
0.6
0.8
1.0
1.2
MOMENTUM TRANSFER [(GeV/c)^2]
2799B30

Fig. 37b

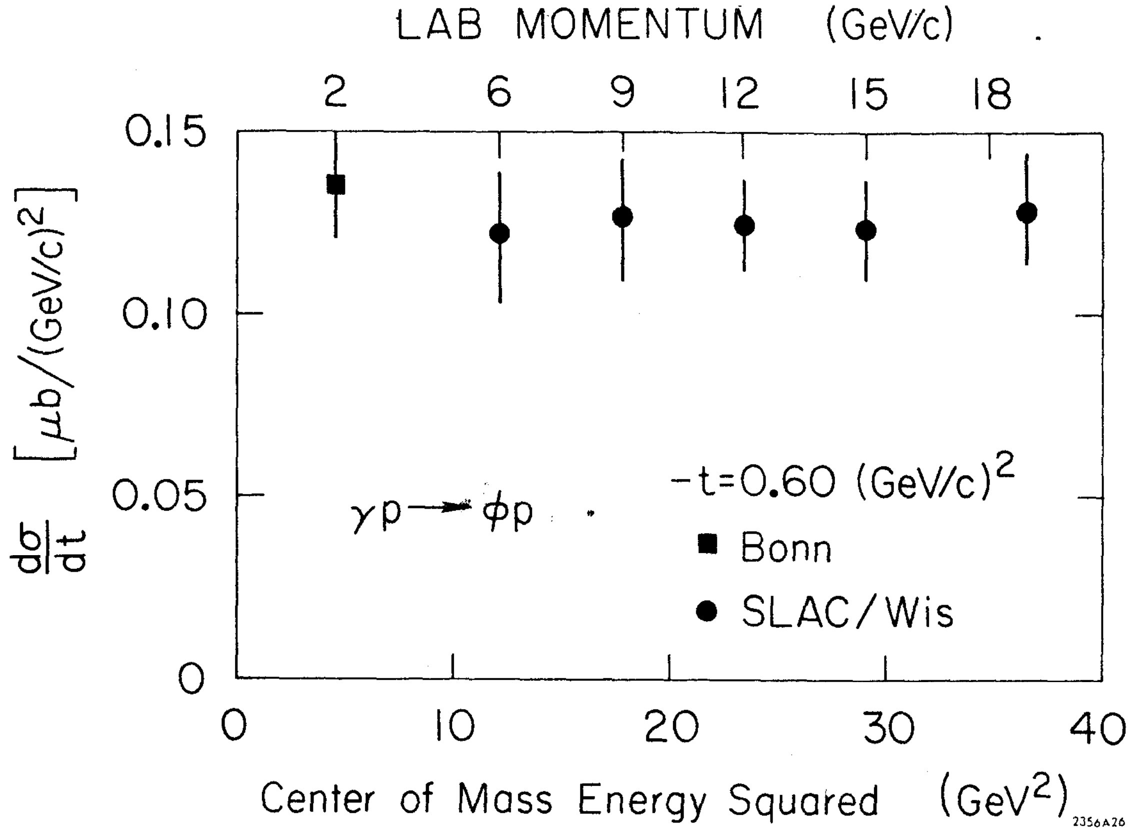
LAB MOMENTUM (GeV/c)
2
6
9
12
15
18
0.15
0.10
0.05
0
$\frac{d\sigma}{dt}$ $[\mu b/(GeV/c)^2]$
$\gamma p \longrightarrow \phi p$
$-t=0.60\ (GeV/c)^2$
Bonn
SLAC/Wis
0
10
20
30
40
Center of Mass Energy Squared (GeV^2)
2356A26

Fig. 38

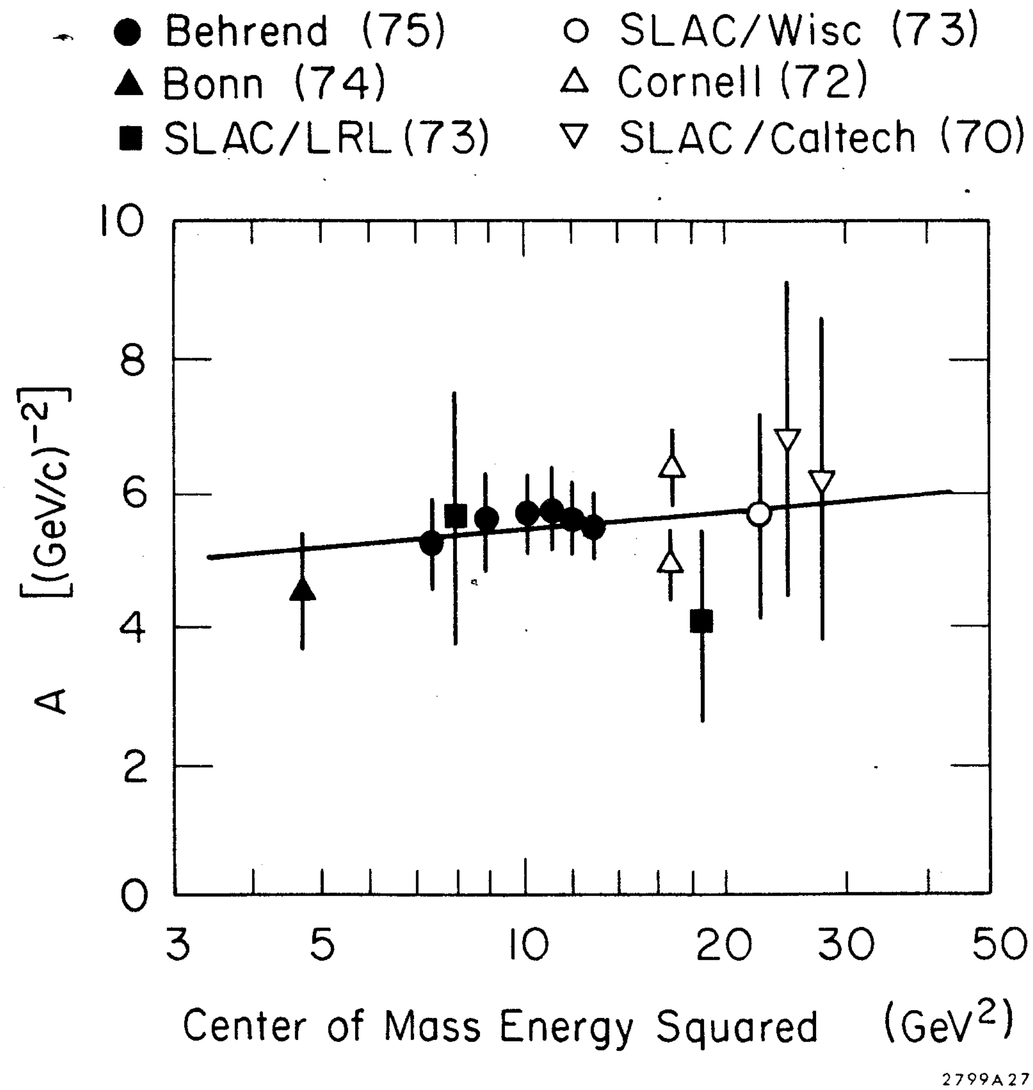
● Behrend (75)
▲ Bonn (74)
■ SLAC/LRL (73)
○ SLAC/Wisc (73)
△ Cornell (72)
▽ SLAC/Caltech (70)
10
8
6
4
2
0
A [(GeV/c)$^{-2}$]
3
5
10
20
30
50
Center of Mass Energy Squared (GeV^2)
2799A27

Fig. 39

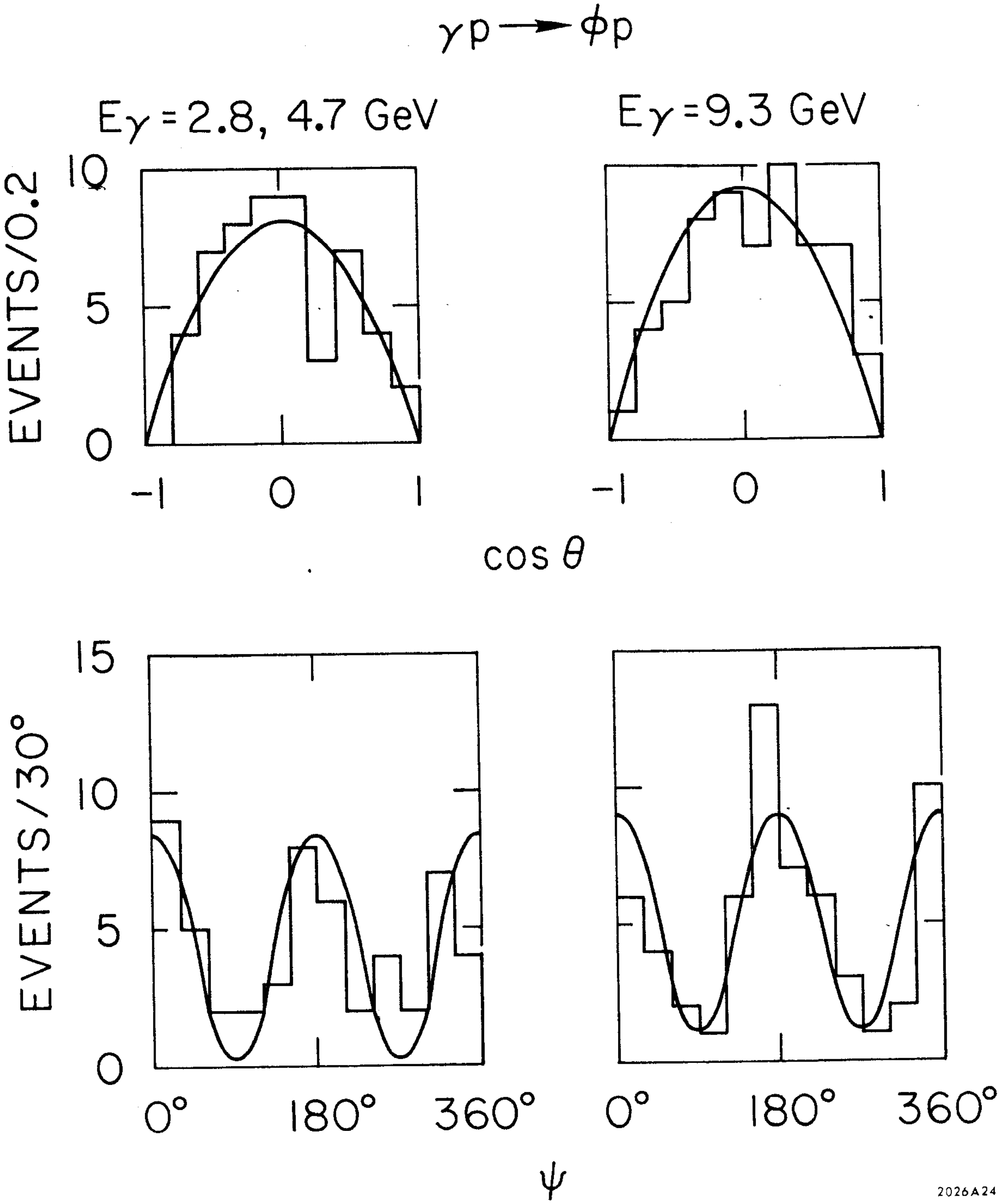
γp → φp
Eγ = 2.8, 4.7 GeV
Eγ = 9.3 GeV
EVENTS/0.2
10
5
0
−1
0
1
cos θ
EVENTS/30°
15
10
5
0
0°
180°
360°
ψ
2026A24

Fig. 40

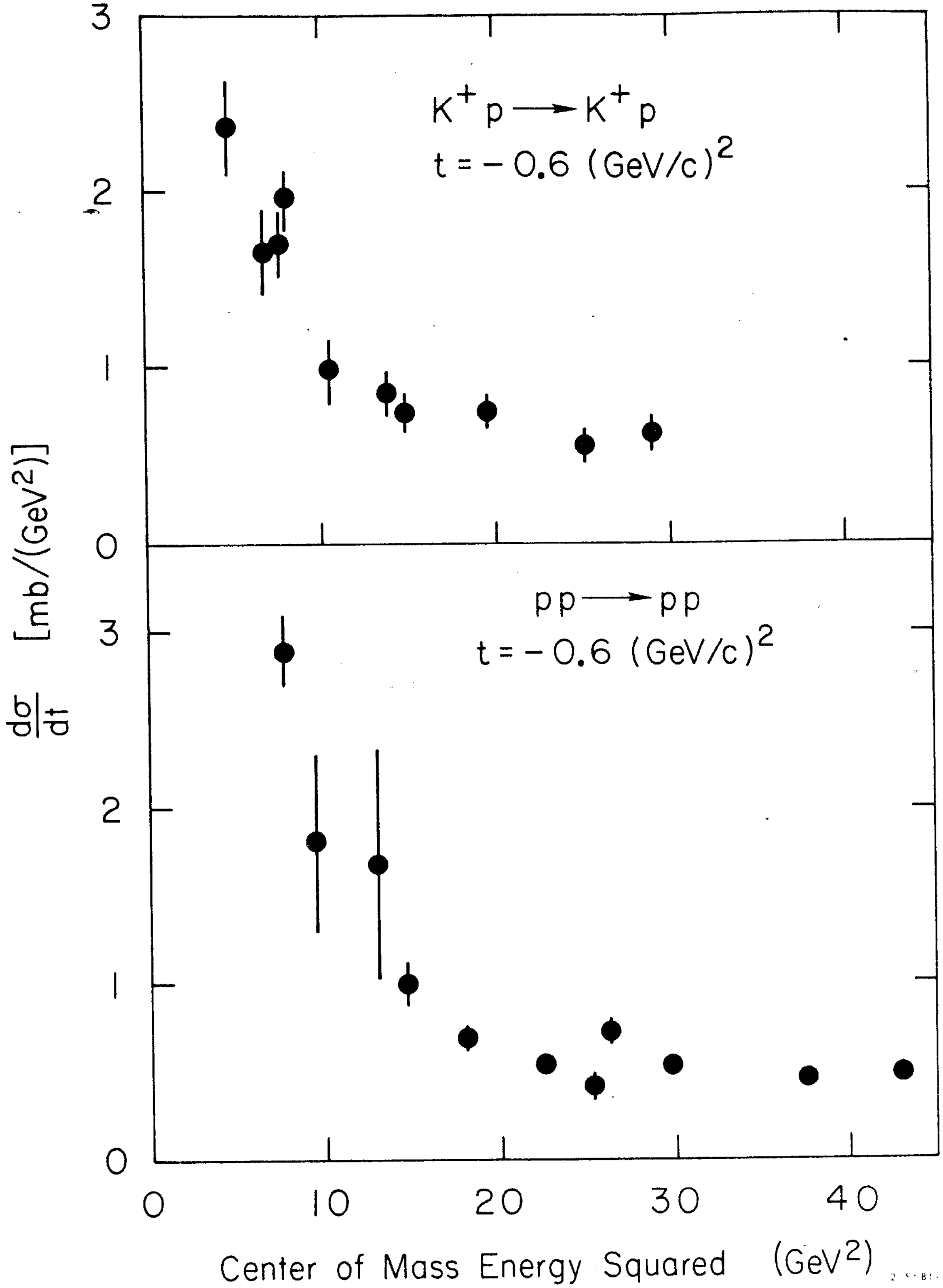
K+ p → K+ p
t = −0.6 (GeV/c)2
p p → p p
t = −0.6 (GeV/c)2
dσ/dt [mb/(GeV2)]
Center of Mass Energy Squared (GeV2)
0
1
2
3
0
1
2
3
0
10
20
30
40

Fig. 41

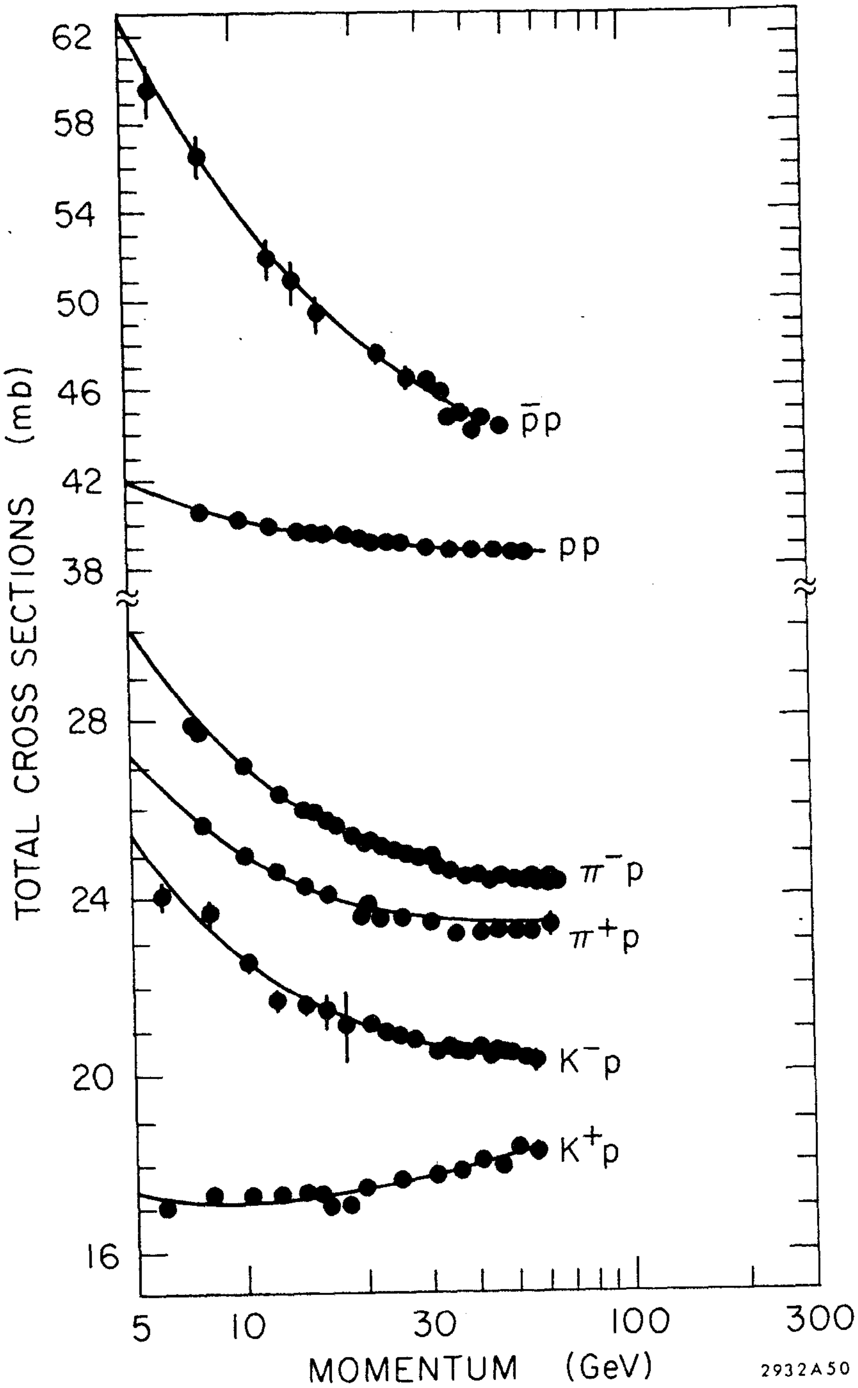
TOTAL CROSS SECTIONS (mb)
62
58
54
50
46
42
38
28
24
20
16
5
10
30
100
300
MOMENTUM (GeV)
$\bar{p}p$
pp
π^-p
π^+p
K^-p
K^+p
2932A50

Fig. 42

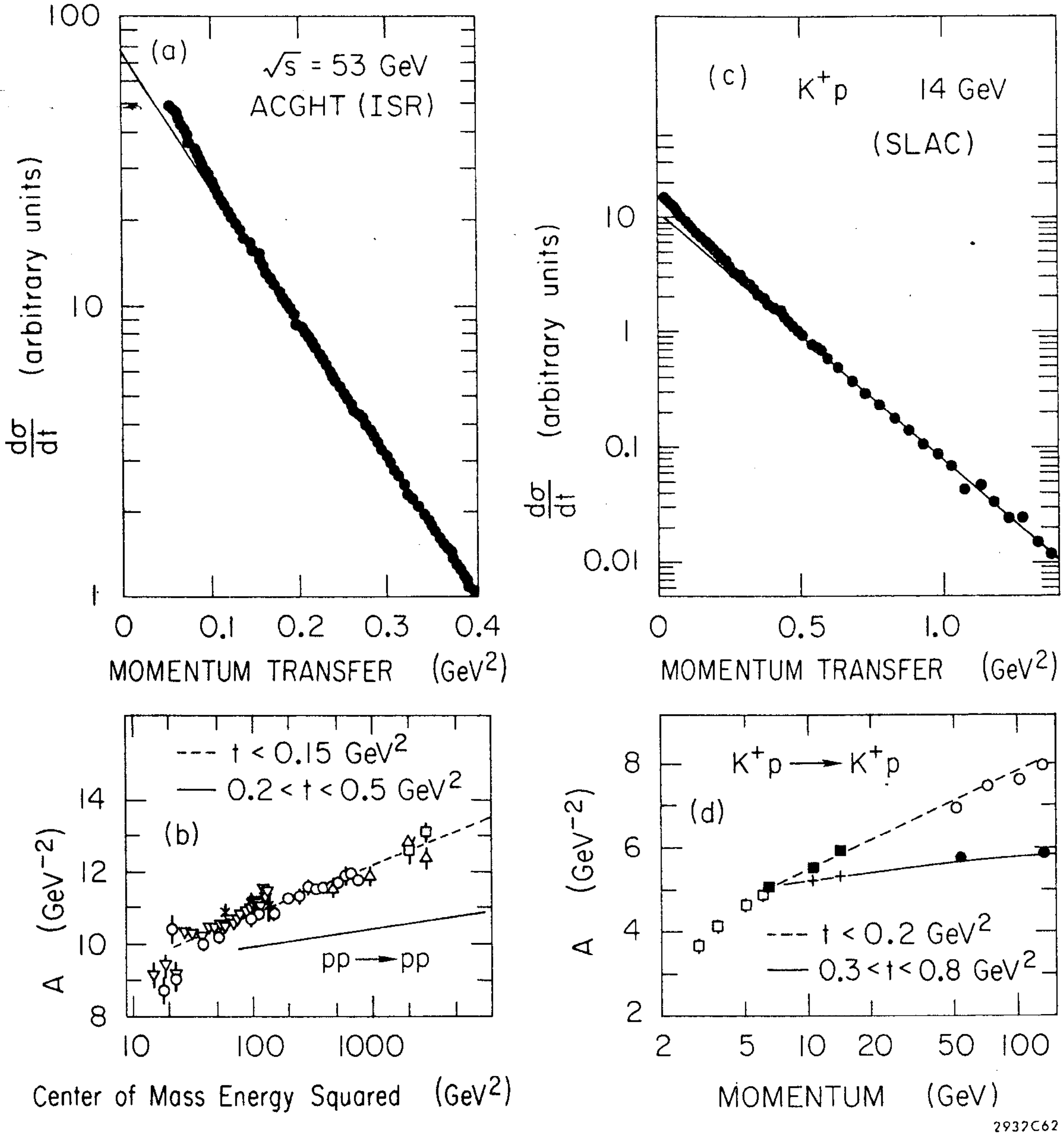

(a)
$\sqrt{s}$ = 53 GeV
ACGHT (ISR)
$\frac{d\sigma}{dt}$ (arbitrary units)
100
10
1
0
0.1
0.2
0.3
0.4
MOMENTUM TRANSFER (GeV^2)
(c) K^+p 14 GeV
(SLAC)
$\frac{d\sigma}{dt}$ (arbitrary units)
10
1
0.1
0.01
0
0.5
1.0
MOMENTUM TRANSFER (GeV^2)
--- $t < 0.15$ GeV^2
— $0.2 < t < 0.5$ GeV^2
(b)
pp → pp
A (GeV^{-2})
14
12
10
8
10
100
1000
Center of Mass Energy Squared (GeV^2)
$K^+p \rightarrow K^+p$
(d)
--- $t < 0.2$ GeV^2
— $0.3 < t < 0.8$ GeV^2
A (GeV^{-2})
8
6
4
2
2
5
10
20
50
100
MOMENTUM (GeV)
2937C62

Fig. 43

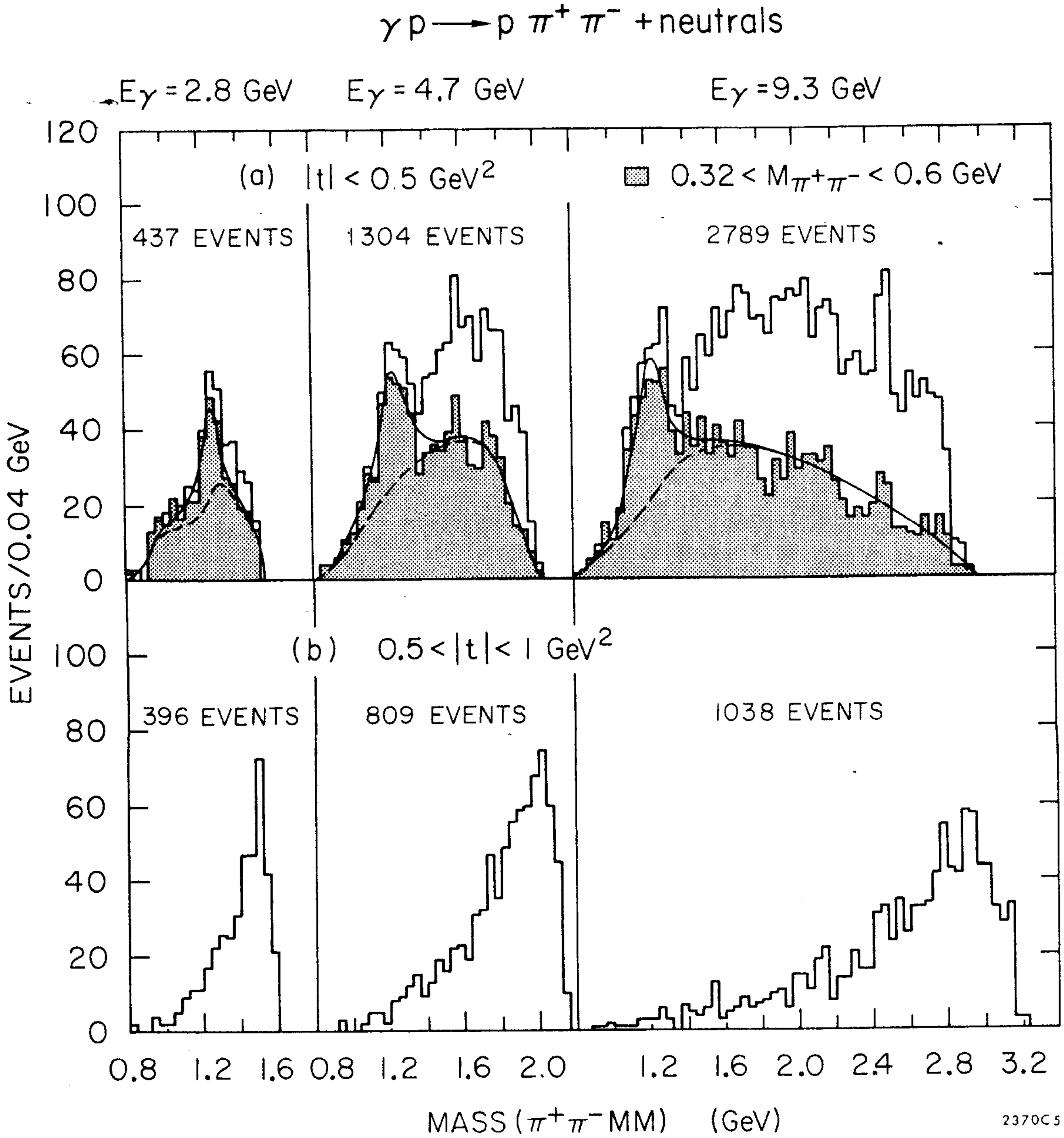

$\gamma p \longrightarrow p\, \pi^+ \pi^-$ + neutrals
$E\gamma$ = 2.8 GeV
$E\gamma$ = 4.7 GeV
$E\gamma$ = 9.3 GeV
(a) $|t| < 0.5$ GeV^2
$0.32 < M_{\pi^+\pi^-} < 0.6$ GeV
437 EVENTS
1304 EVENTS
2789 EVENTS
(b) $0.5 < |t| < 1$ GeV^2
396 EVENTS
809 EVENTS
1038 EVENTS
EVENTS/0.04 GeV
0
20
40
60
80
100
120
0.8
1.2
1.6
2.0
2.4
2.8
3.2
MASS ($\pi^+\pi^-$MM) (GeV)
2370C5

Fig. 44

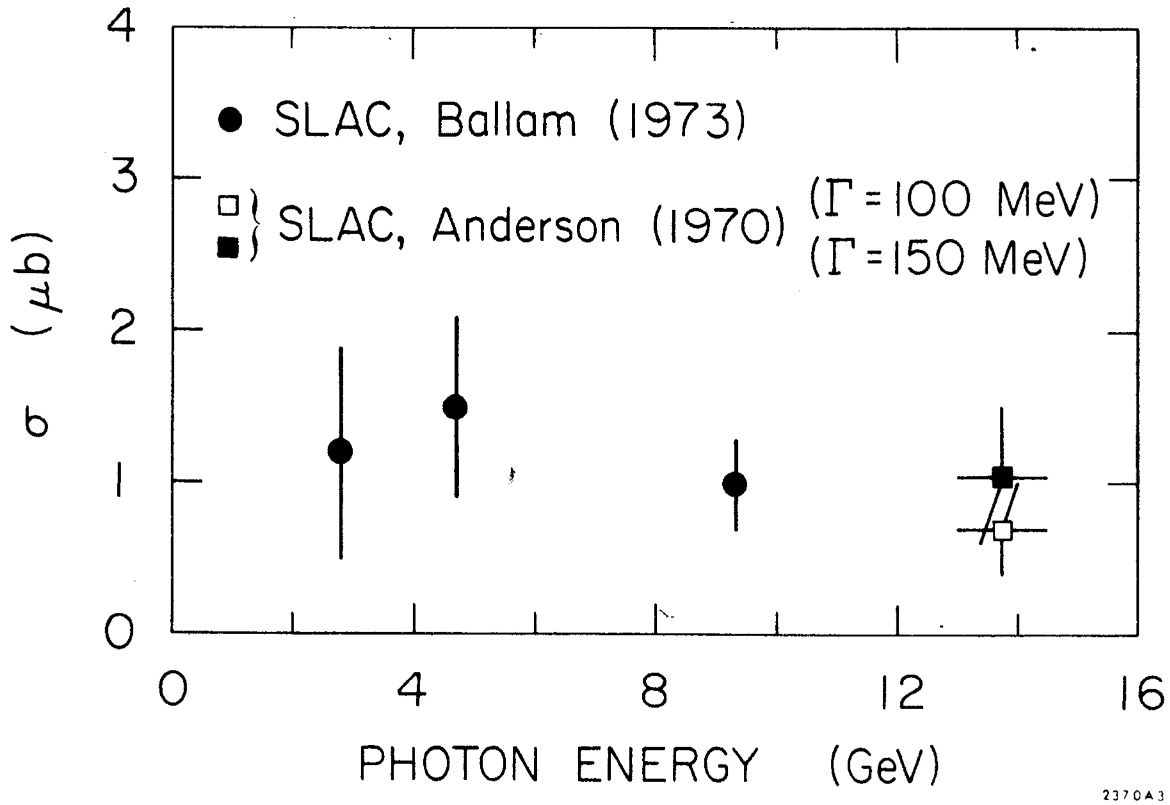
SLAC, Ballam (1973)
SLAC, Anderson (1970)
(Γ = 100 MeV)
(Γ = 150 MeV)
σ (μb)
PHOTON ENERGY (GeV)
0
1
2
3
4
0
4
8
12
16
2370A3

Fig. 45

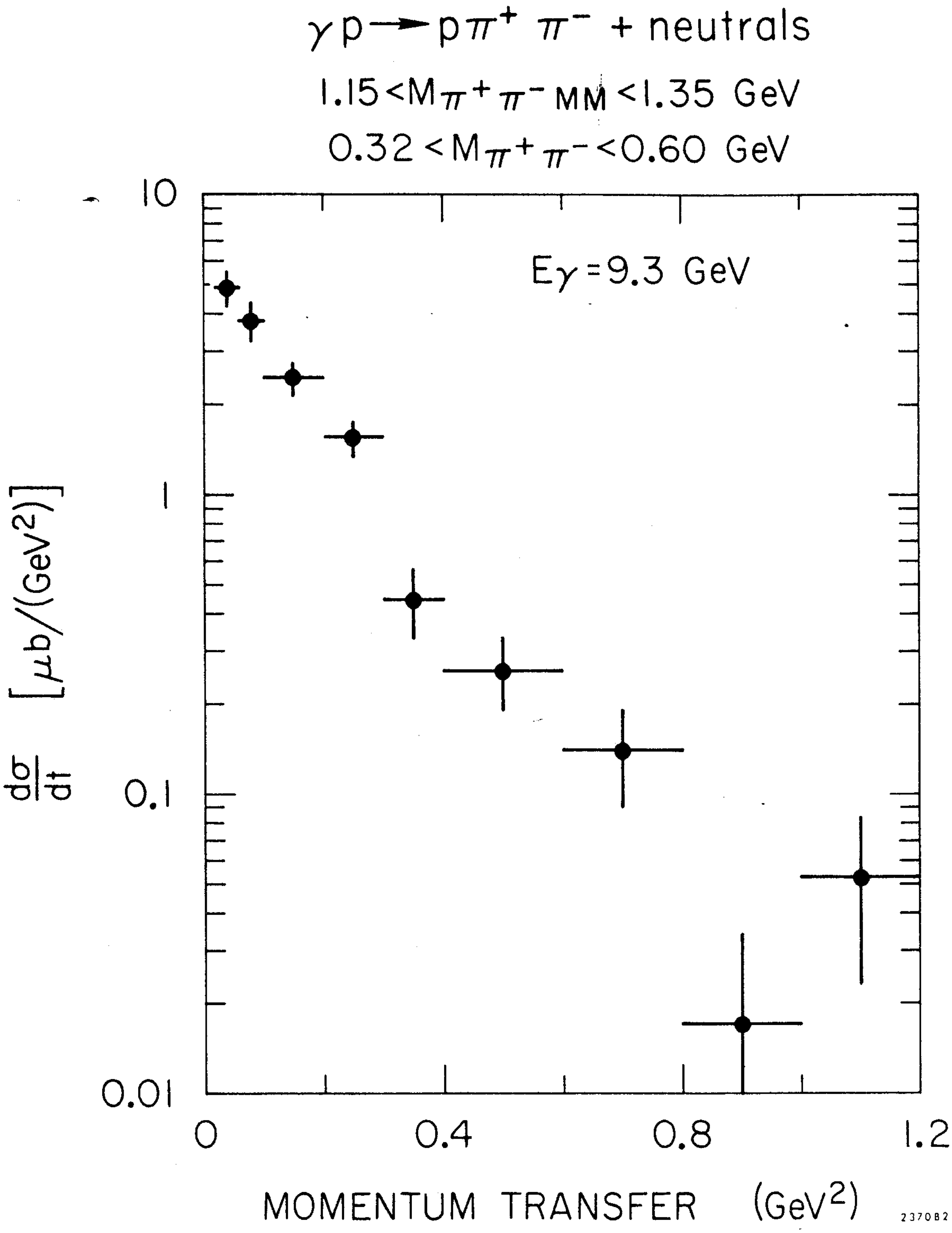

$\gamma p \rightarrow p\pi^+\pi^-$ + neutrals
$1.15 < M_{\pi^+\pi^- MM} < 1.35$ GeV
$0.32 < M_{\pi^+\pi^-} < 0.60$ GeV
$E\gamma = 9.3$ GeV
$\frac{d\sigma}{dt}$ [$\mu b/(GeV^2)$]
10
1
0.1
0.01
0
0.4
0.8
1.2
MOMENTUM TRANSFER (GeV^2)
237082

Fig. 46

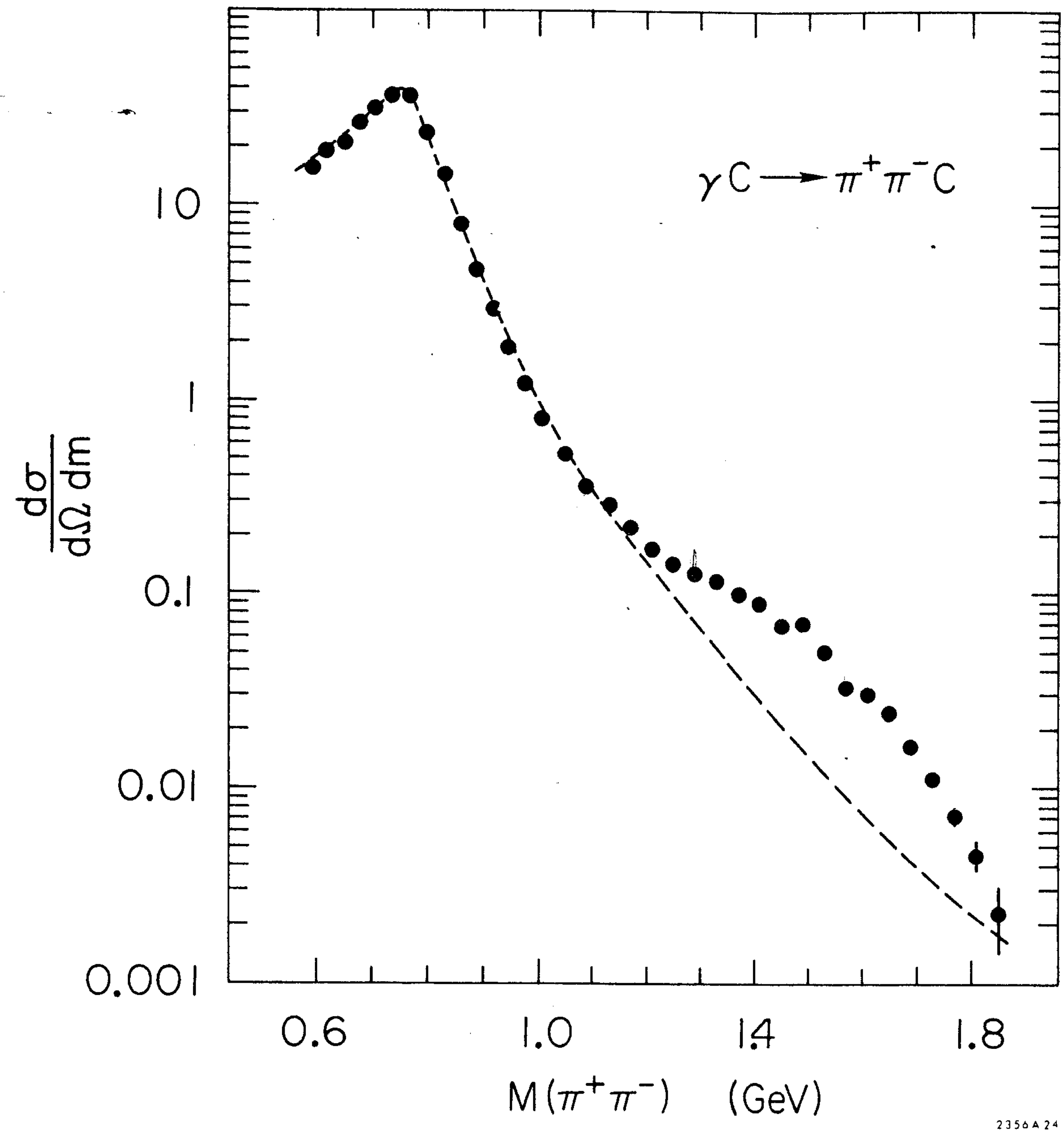

$\gamma C \longrightarrow \pi^+\pi^- C$
$\frac{d\sigma}{d\Omega\, dm}$
10
1
0.1
0.01
0.001
0.6
1.0
1.4
1.8
$M(\pi^+\pi^-)$ (GeV)
2356A24

Fig. 47

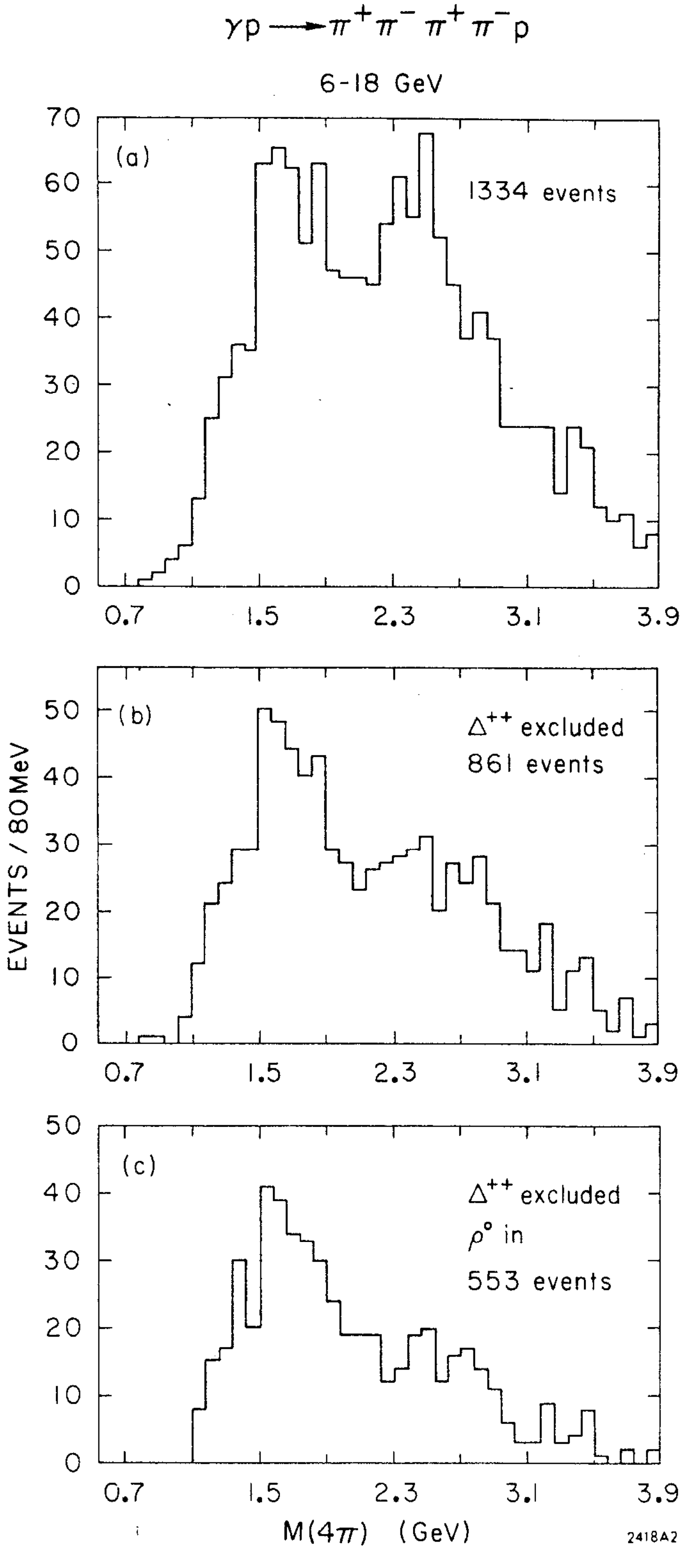

$\gamma p \longrightarrow \pi^+\pi^-\pi^+\pi^- p$
6-18 GeV
(a)
1334 events
(b)
Δ^{++} excluded
861 events
(c)
Δ^{++} excluded
ρ° in
553 events
EVENTS / 80MeV
0.7
1.5
2.3
3.1
3.9
M(4π) (GeV)
2418A2

Fig. 48

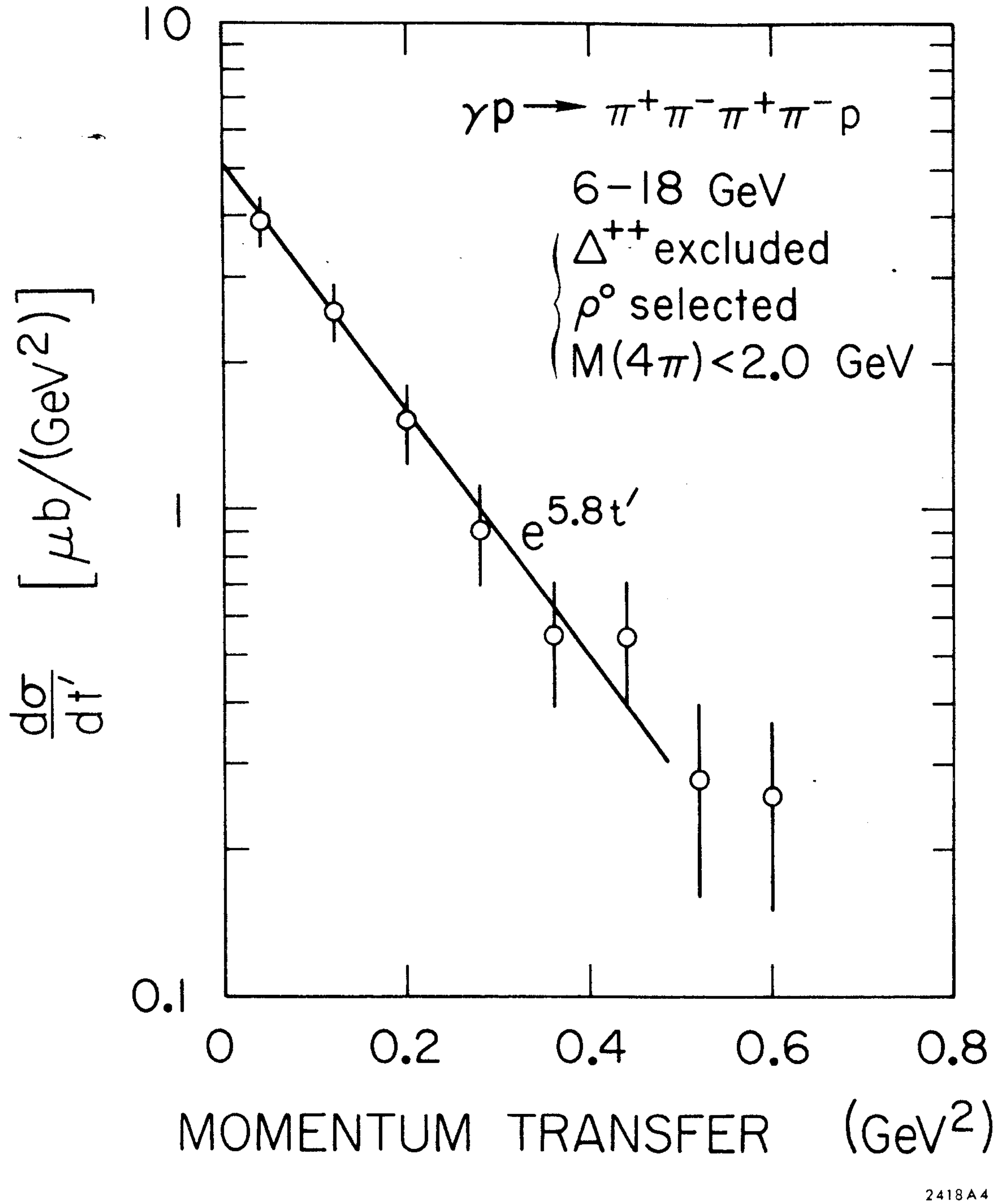
10
1
0.1
0
0.2
0.4
0.6
0.8
$\gamma p \rightarrow \pi^+\pi^-\pi^+\pi^- p$
6–18 GeV
Δ^{++} excluded
ρ^0 selected
$M(4\pi)<2.0$ GeV
$e^{5.8t'}$
$\frac{d\sigma}{dt'}$ [$\mu b/(GeV^2)$]
MOMENTUM TRANSFER (GeV^2)
2418A4

Fig. 49

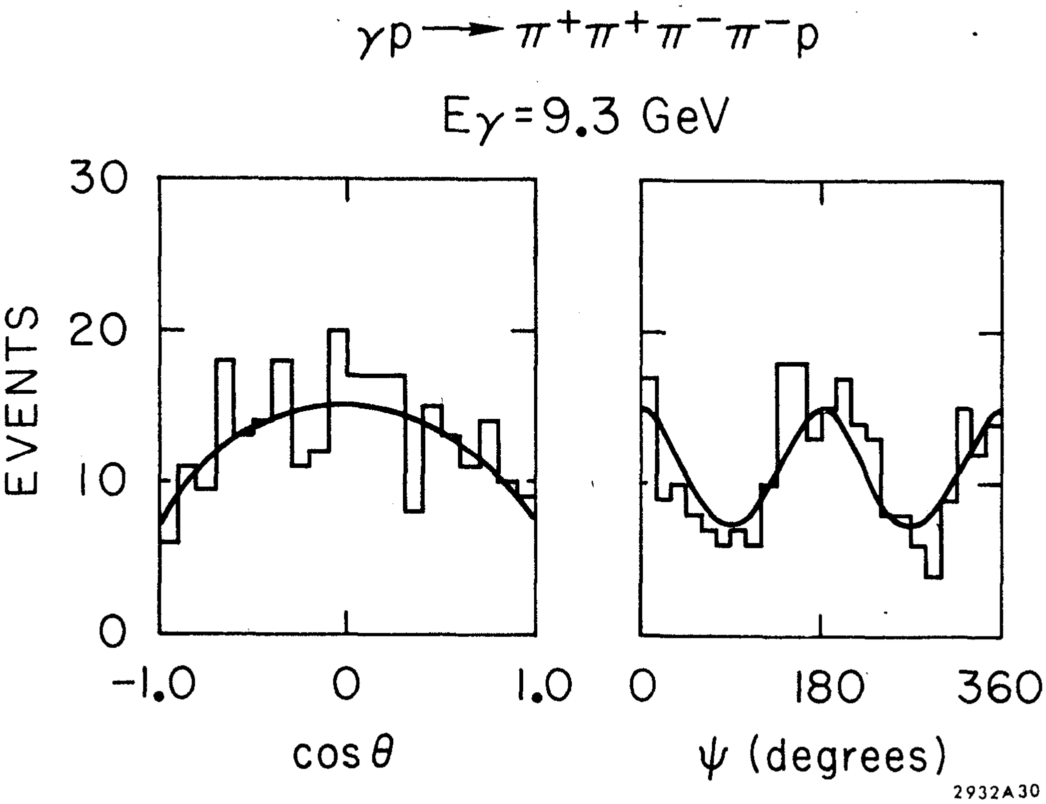
γp ⟶ π⁺π⁺π⁻π⁻p
Eγ = 9.3 GeV
EVENTS
30
20
10
0
−1.0
0
1.0
cos θ
0
180
360
ψ (degrees)
2932A30

Fig. 50

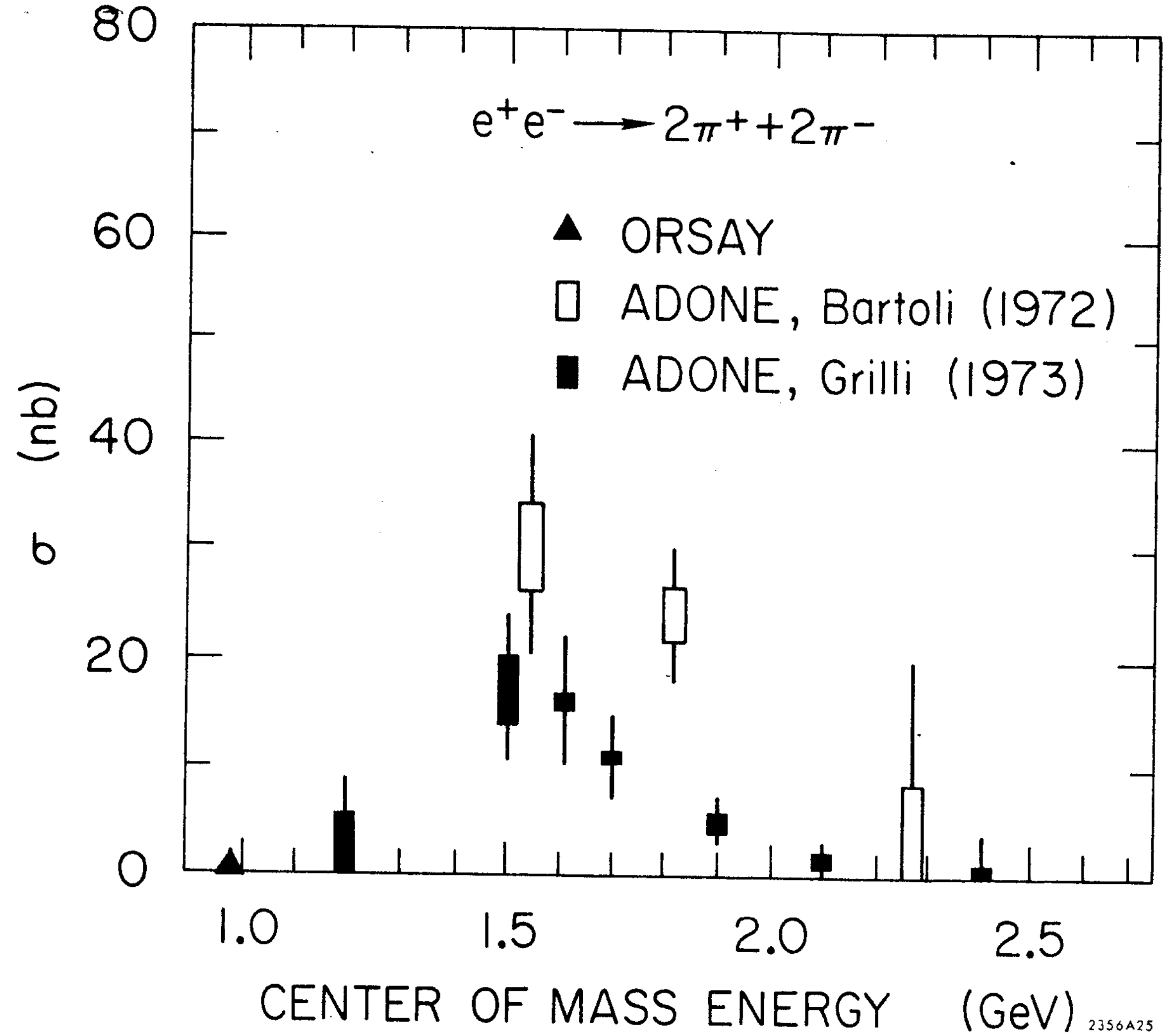

$e^+e^- \longrightarrow 2\pi^+ + 2\pi^-$
ORSAY
ADONE, Bartoli (1972)
ADONE, Grilli (1973)
σ (nb)
0
20
40
60
80
1.0
1.5
2.0
2.5
CENTER OF MASS ENERGY (GeV)
2356A25

Fig. 51

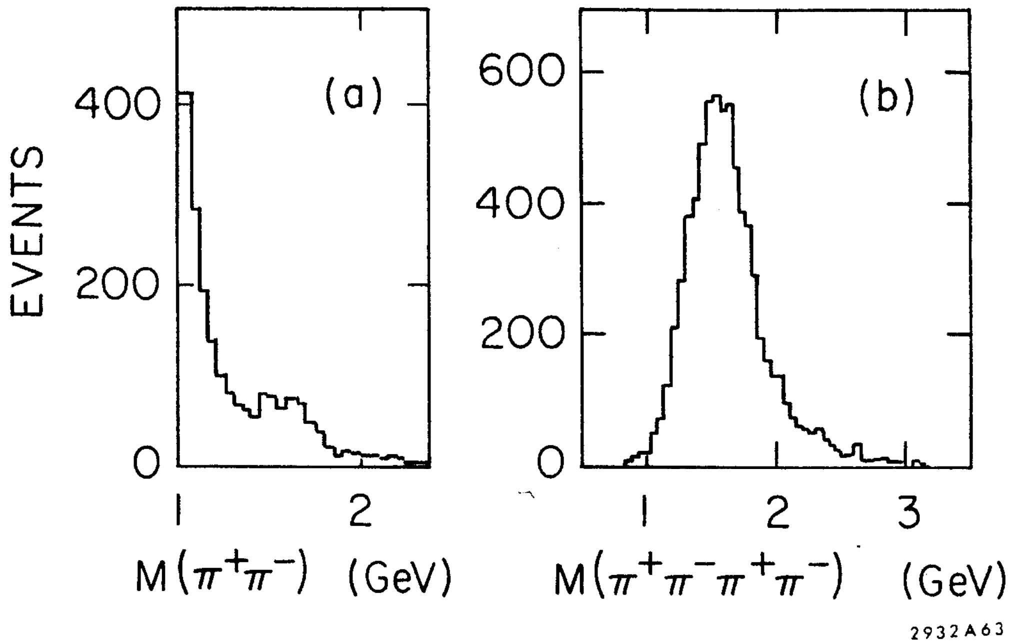

EVENTS
400
200
0
(a)
1
2
$M(\pi^+\pi^-)$ (GeV)
600
400
200
0
(b)
1
2
3
$M(\pi^+\pi^-\pi^+\pi^-)$ (GeV)
2932A63

Fig. 52

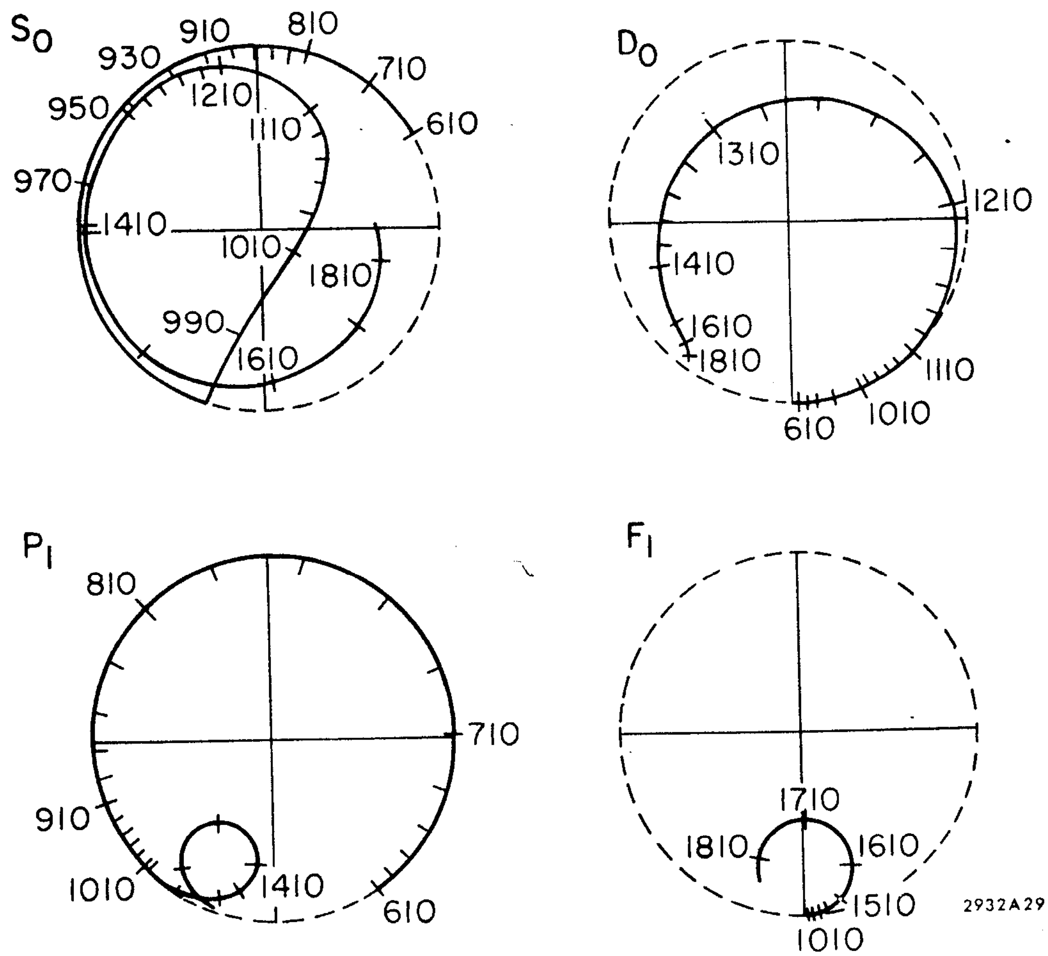

S_0
910
810
930
710
950
1210
610
1110
970
1410
1010
1810
990
1610
D_0
1310
1210
1410
1610
1810
1110
610
1010
P_1
810
710
910
1010
1410
610
F_1
1710
1810
1610
1510
1010
2932A29

Fig. 53

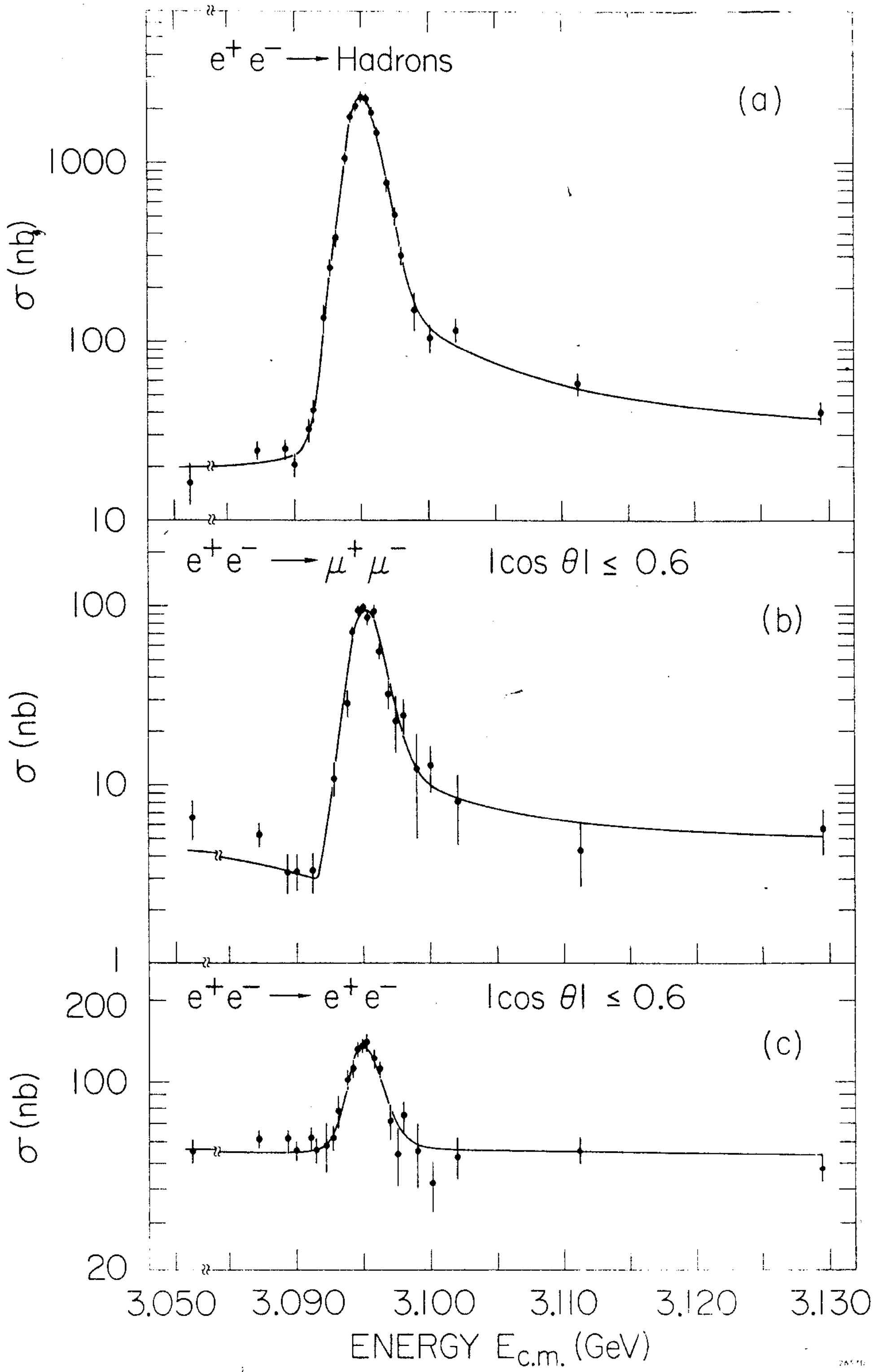

e+ e− → Hadrons
(a)
1000
100
10
σ (nb)
e+e− → μ+μ− |cos θ| ≤ 0.6
(b)
100
10
1
σ (nb)
e+e− → e+e− |cos θ| ≤ 0.6
(c)
200
100
20
σ (nb)
3.050
3.090
3.100
3.110
3.120
3.130
ENERGY Ec.m. (GeV)

Fig. 54

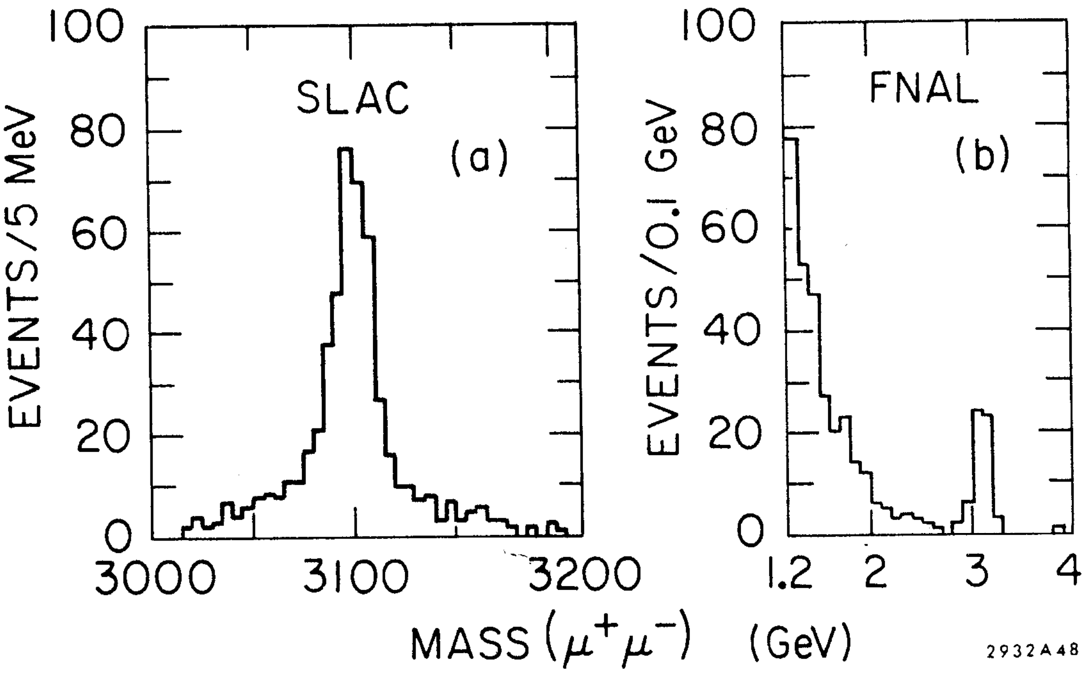

SLAC
(a)
EVENTS/5 MeV
100
80
60
40
20
0
3000
3100
3200
FNAL
(b)
EVENTS/0.1 GeV
1.2
2
3
4
MASS ($\mu^+\mu^-$) (GeV)
2932A48

Fig. 55

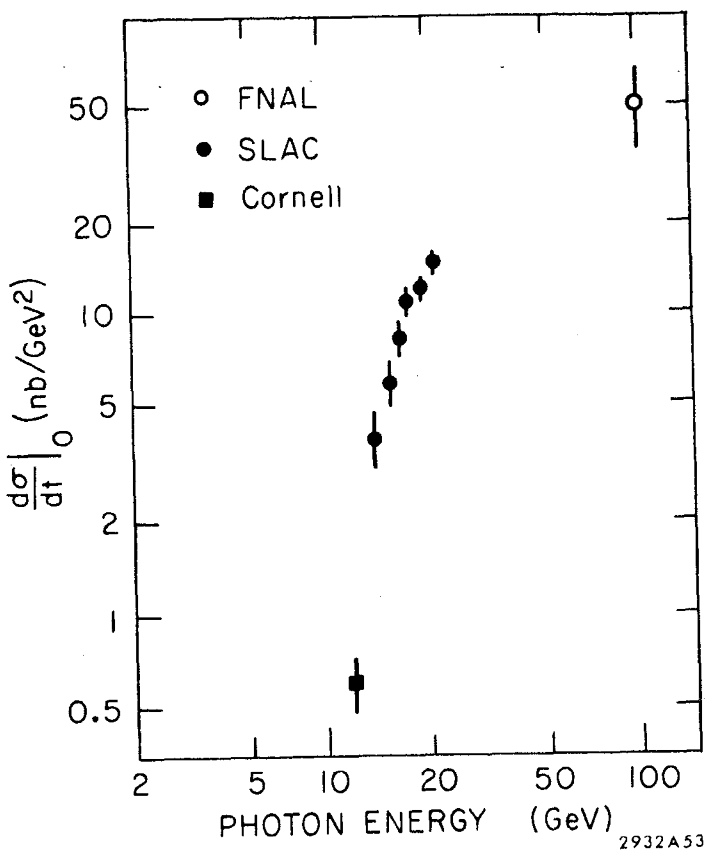

FNAL
SLAC
Cornell
50
20
10
5
2
1
0.5
$\frac{d\sigma}{dt}\Big|_0$ (nb/GeV^2)
2
5
10
20
50
100
PHOTON ENERGY (GeV)
2932A53

Fig. 56

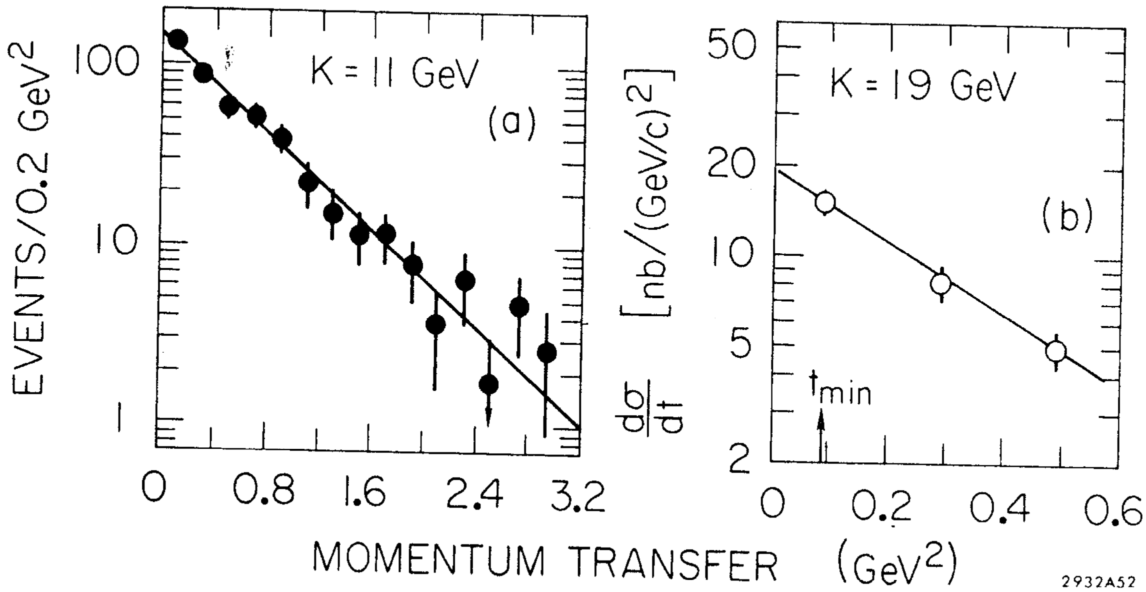

EVENTS/O.2 GeV^2
100
10
1
K = 11 GeV
(a)
0
0.8
1.6
2.4
3.2
$\frac{d\sigma}{dt}$ [nb/(GeV/c)^2]
50
20
10
5
2
K = 19 GeV
(b)
t_{min}
0
0.2
0.4
0.6
MOMENTUM TRANSFER (GeV^2)
2932A52

Fig. 57

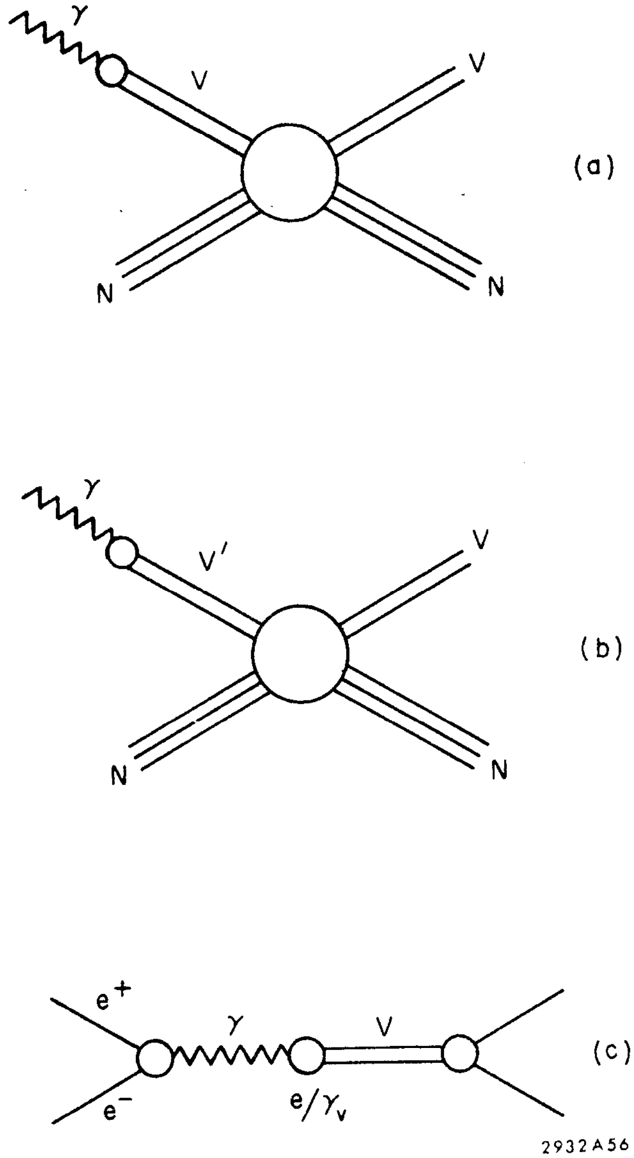

Fig. 58

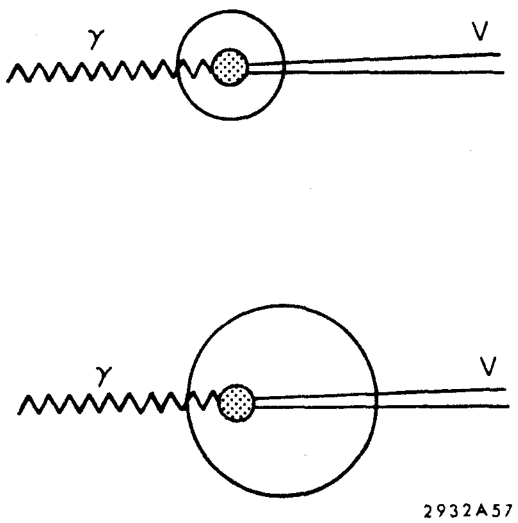

Fig. 59

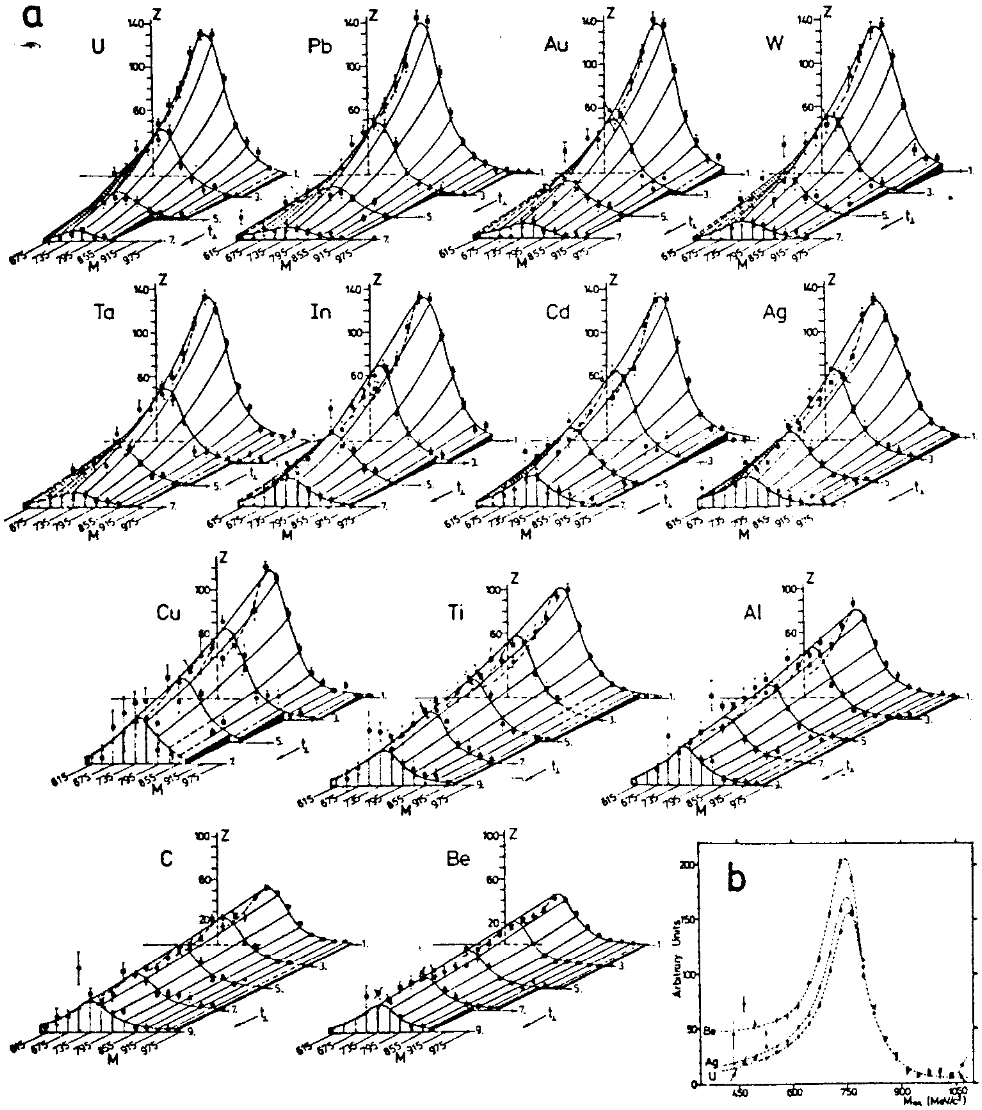

1729A11

Fig. 60

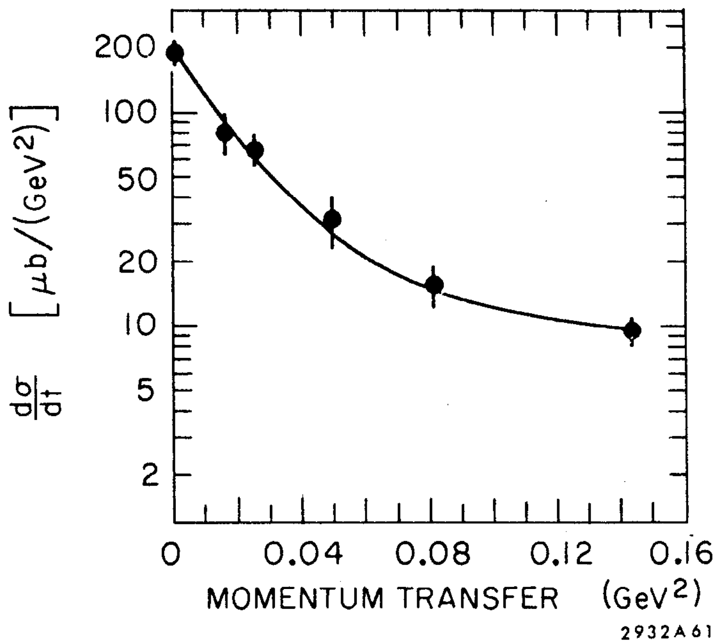

200
100
50
20
10
5
2
$\frac{d\sigma}{dt}$ [μb/(GeV²)]
0
0.04
0.08
0.12
0.16
MOMENTUM TRANSFER (GeV²)
2932A61

Fig. 61

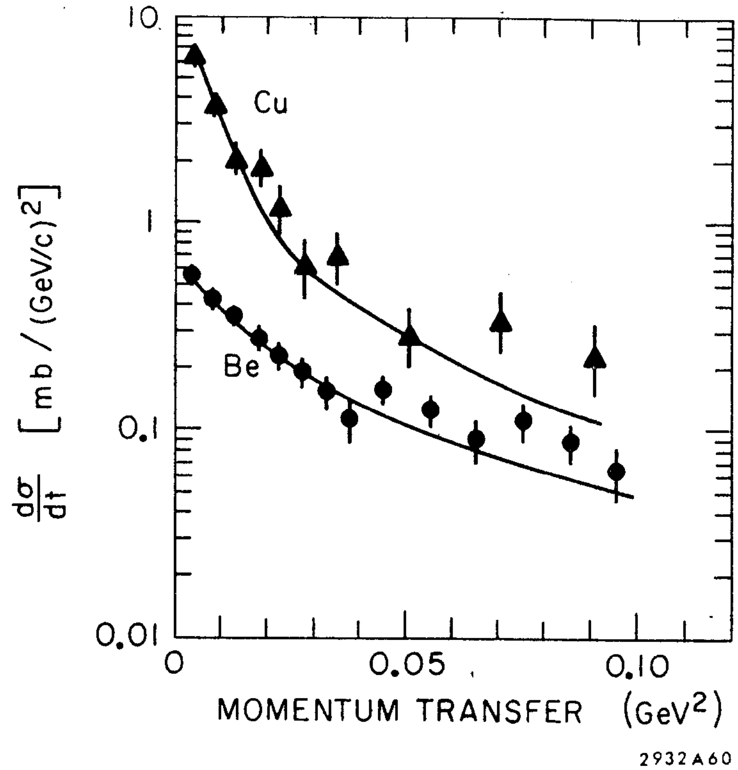
10
1
0.1
0.01
0
0.05
0.10
Cu
Be
dσ/dt [mb / (GeV/c)2]
MOMENTUM TRANSFER (GeV2)
2932A60

Fig. 62

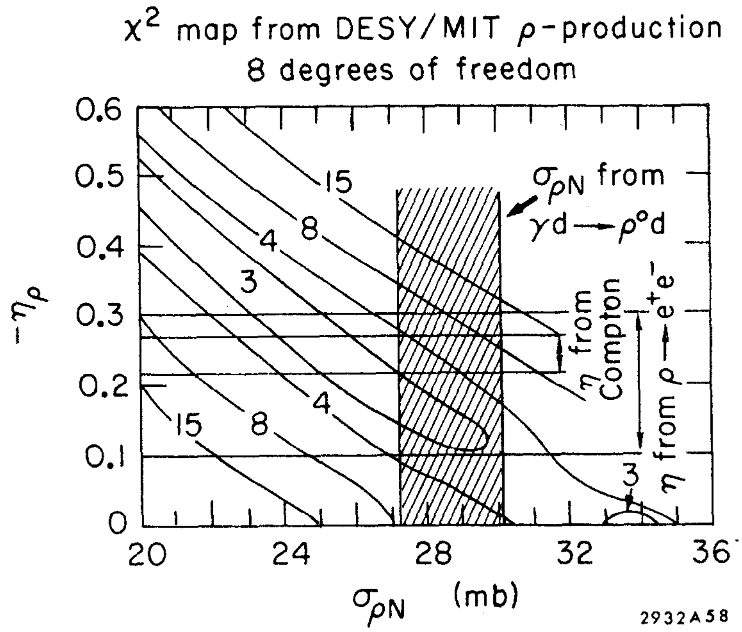

χ^2 map from DESY/MIT ρ-production
8 degrees of freedom
0.6
0.5
0.4
0.3
0.2
0.1
0
$-\eta_\rho$
15
8
4
3
4
8
15
3
$\sigma_{\rho N}$ from
$\gamma d \to \rho^o d$
η from Compton
η from $\rho \to e^+e^-$
20
24
28
32
36
$\sigma_{\rho N}$ (mb)
2932A58

Fig. 63

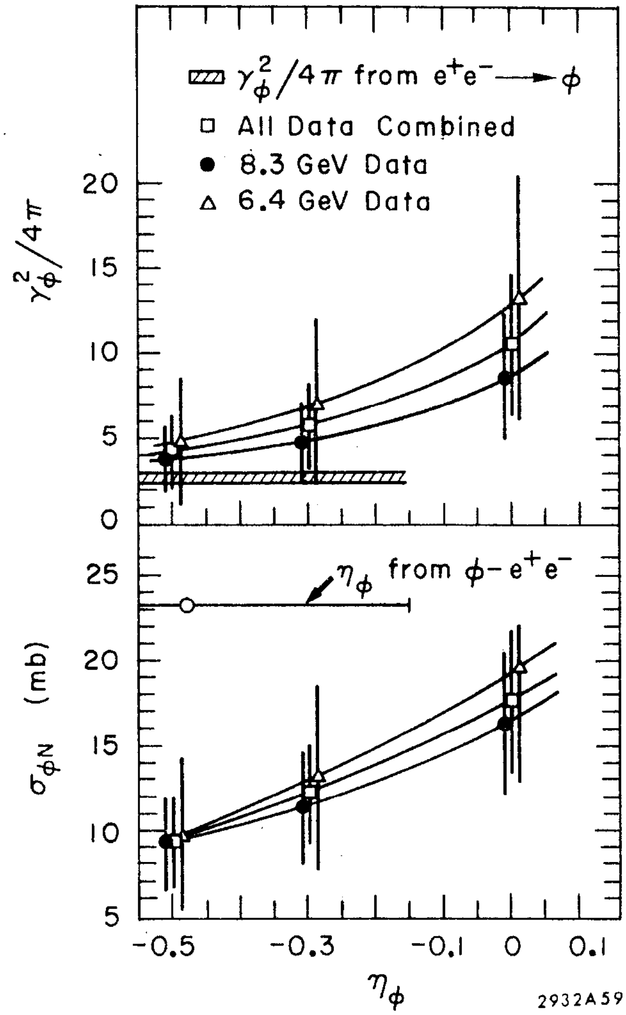

$\gamma_\phi^2/4\pi$ from $e^+e^- \to \phi$
All Data Combined
8.3 GeV Data
6.4 GeV Data
$\gamma_\phi^2/4\pi$
20
15
10
5
0
η_ϕ from $\phi - e^+e^-$
25
20
15
10
5
$\sigma_{\phi N}$ (mb)
−0.5
−0.3
−0.1
0
0.1
η_ϕ
2932A59

Fig. 64

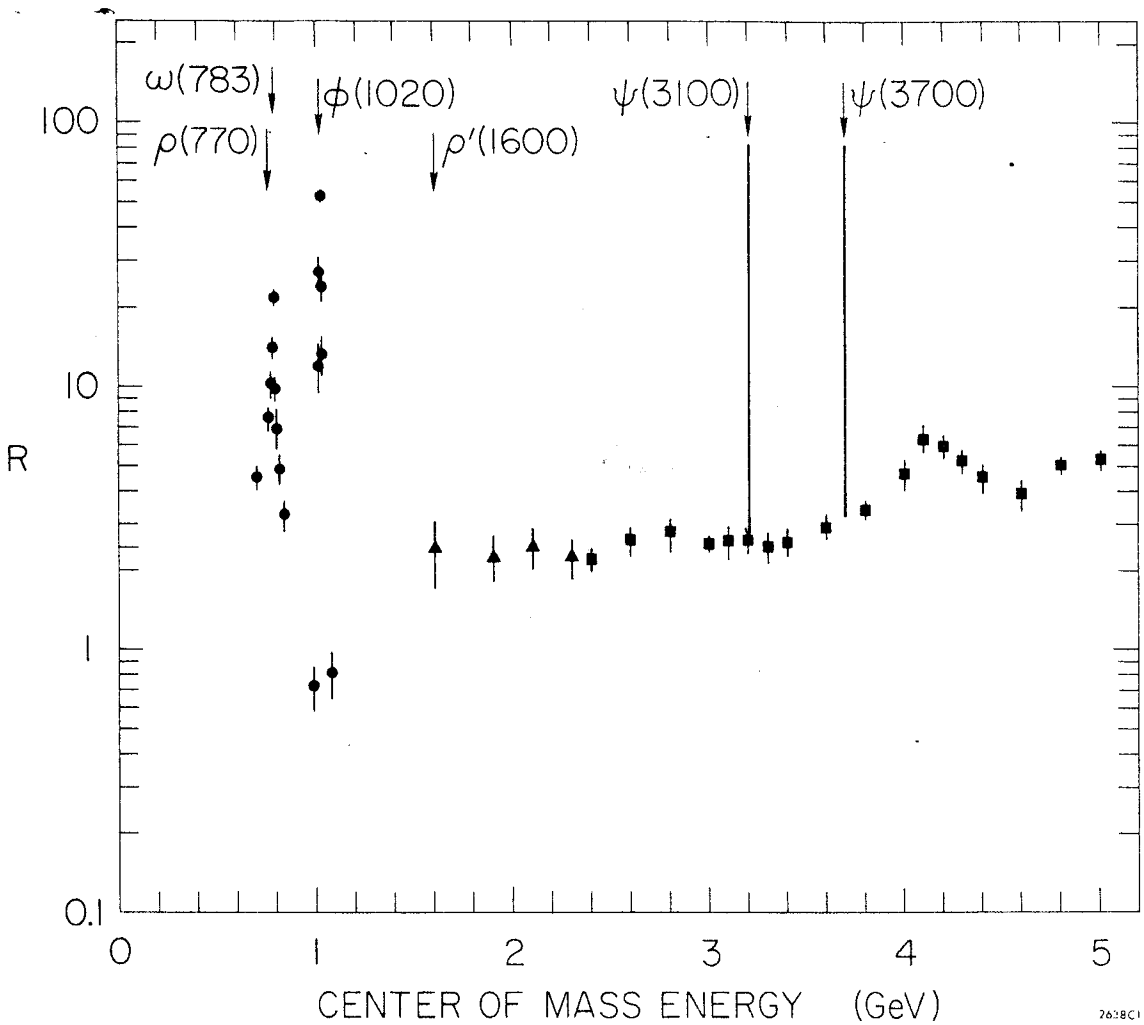
ω(783)
ρ(770)
φ(1020)
ρ′(1600)
ψ(3100)
ψ(3700)
100
10
1
0.1
R
0
1
2
3
4
5
CENTER OF MASS ENERGY (GeV)
2638C1

Fig. 65

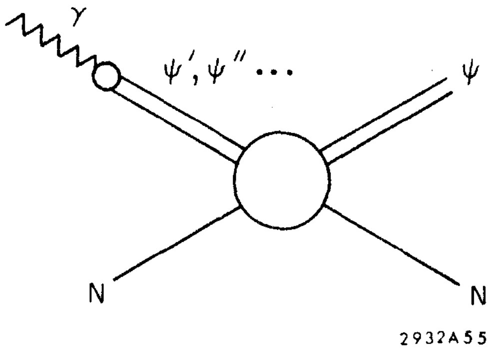

Fig. 66

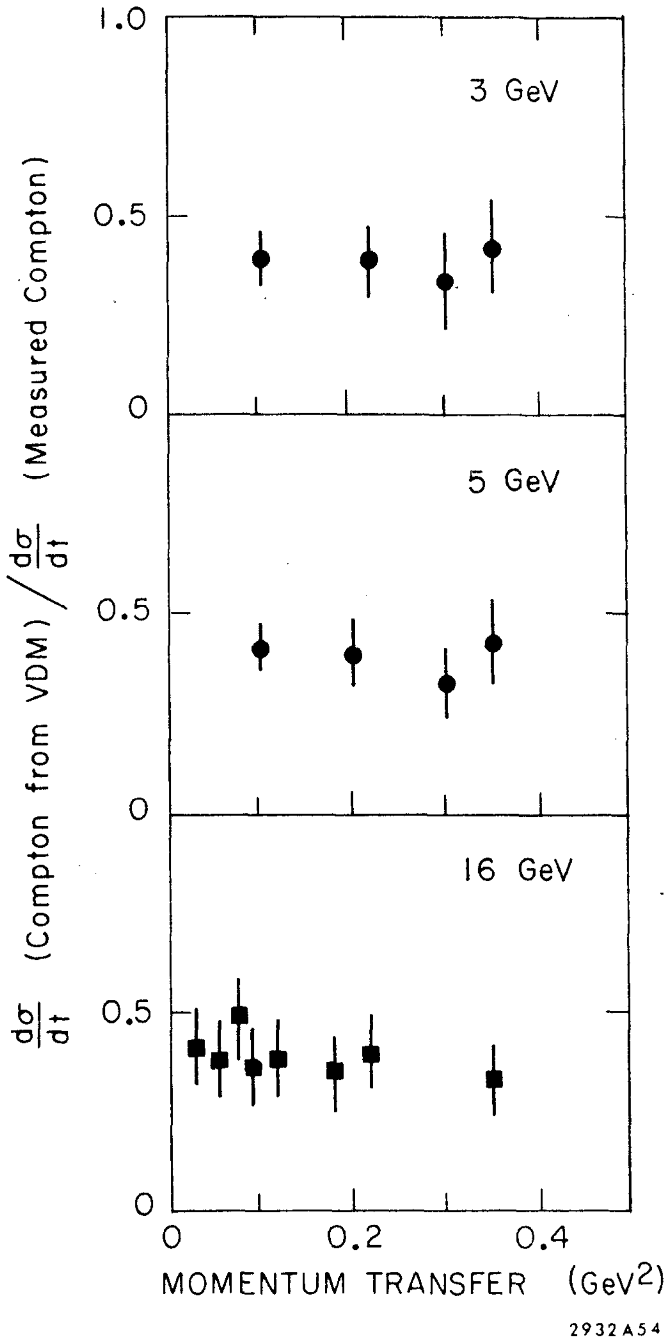

3 GeV
5 GeV
16 GeV
1.0
0.5
0
0.5
0
0.5
0
0
0.2
0.4
MOMENTUM TRANSFER (GeV2)
dσ/dt (Compton from VDM) / dσ/dt (Measured Compton)
2932A54

Fig. 67